Dynamic Consequences of Phenological Asynchrony in a Consumer–Resource Model

Sarah Abel

Thesis submitted to the University of Ottawa
in partial fulfillment of the requirements for the degree of
Master of Science Mathematics and Statistics*

Department of Mathematics and Statistics
Faculty of Science
University of Ottawa

*The M.Sc. program is a joint program with Carleton University, administered by the Ottawa-Carleton Institute of Mathematics and Statistics

Abstract

The relative phenology of interacting ecological populations directly influences their abilities to grow and persist. Differential phenological shifts, resulting in phenological asynchrony between interacting populations, can be detrimental to those that depend upon another species for survival (i.e., specialist consumers). There remains a lack of research regarding the long-term effects of phenological asynchrony on population dynamics. Given that phenological asynchrony is expected to become more prevalent with climate change, it is vital that we understand its consequences. This thesis contributes to our understanding of these long-term effects through the construction and analysis of a mathematical model. We derive a phenologically explicit "semi-discrete" model for a specialist consumer and its resource that overwinter in a dormant state. We observe that higher asynchrony has a stabilizing effect, but it increases the risk of consumer extinction. We show that for different consumer species, varying amounts of asynchrony result in the maximum long-term density.

Dedications

To my mom, dad, Megan and Willow, for always believing in me.

Acknowledgements

I would like to thank my supervisor Dr. Frithjof Lutscher for his excellent guidance and support throughout this thesis. I would also like to thank the University of Ottawa for their financial support.

Contents

List of Figures

List of Tables

Chapter 1

Introduction

This thesis is concerned with the effects that the relative timing of different species' life-cycle events have on the long-term dynamics of interacting ecological populations.

Phenology

Phenology is the timing of a species' most significant life-cycle events. Some examples of phenological events for a plant include germination, leaf emergence, flowering and seed production, as well as leaf senescence. For animals, like insects or birds, some examples include egg laying, egg hatching and migration, as well as entry into or exit from a period of dormancy. This thesis focuses on the aspects of phenology related to a period of dormancy.

Many species enter a dormant state in the winter to avoid unfavourable conditions and return to their active state in the spring when conditions become favourable again [13]. We call the period that a species is dormant its winter resting period (WRP). Species have evolved WRPs, as they directly increase species' survival [10, 13, 45]. In particular, they allow species to conserve energy, thereby reducing the risk of starvation when food supply is limited in the winter. Additionally, they reduce the risk of predation, since overwintering tends to take place in a protected shelter, like a cave or underground burrow. The two specific aspects of a species' phenology that we focus on are the immergence time and emergence time. The former is the time at which species transition into their dormant state, and the latter is the time at which they transition back into their active state.

A species' phenology directly influences its ability to grow and persist. The following examples demonstrate how harmful poor timing can be; see Iler et al. [17] and references therein for more. Leaf emergence that is too early can lead to frost-damaged leaves, which has been shown to result in plants with lower growth and survival rates compared with those that have later leaf emergence. Similarly, birds that hatch too early, and are thus exposed to colder temperatures, have been shown to have decreased survival rates and decreased amounts of offspring.

Changes to species' phenologies due to climate change are well documented [10, 17].

These observed phenological shifts are not unexpected given that the phenologies of species living in temperate climates are affected by temperature [12, 36], and climate change has increased the global surface temperature by about 1.09°C between 1850–1900 to 2011–2020 [18]. Climate change–induced phenological shifts can positively or negatively affect a species; see Iler et al. [17] and references therein. More specifically, phenological shifts may allow a species to maintain the climatic conditions that its life-cycle events occur under, even though the timing of the events has changed. However, since different components of climate (i.e., temperature and precipitation) are changing at different rates, phenological shifts in response to one component may still expose species to novel conditions.

The relative phenology of interacting populations directly influences each population's ability to grow and persist. For example, if a consumer reproduces far ahead of when its resource emerges from its WRP, then the consumer offspring may die from starvation due to the resource being unavailable for an extended period of time. If consumer reproduction occurs too far after its resource emerges, then the resource may again be unavailable (i.e., if the resource has already re-entered its WRP), or if there is resource available, it may be of poor quality. There is phenological synchrony when a phenological event of one species overlaps with that of an interacting species. Cushing [8] considered a consumer and its resource to have phenological synchrony if the consumer's most energetically demanding life-cycle event, which is typically assumed to be reproduction, occurs at the same time as peak resource availability. When phenological events do not overlap, there is phenological asynchrony. In theory, phenological synchrony is expected to be optimal for the consumer [8]. Additionally, the consumer is expected to suffer as the asynchrony increases, which our previous examples illustrated.

Interacting species may not experience climate change–induced phenological shifts at the same rate. To maintain phenological synchrony, the phenologies of some consumers have shifted in response to shifts in their resource's phenology [7, 34]. However, phenological asynchrony is expected to become more prevalent as a result of climate change and thus has the potential to disrupt evolved foodwebs [21].

Models for Interacting Ecological Populations

In this thesis, we study consumer–resource dynamics in the context of phenology. We model a specialist consumer that is a discrete breeder who reproduces once annually, and its resource who reproduces continuously. Generally speaking, specialist consumers are very selective over the resource species that they consume. Thus, phenological asynchrony can be especially detrimental to specialist consumers. We assume that both the consumer and its resource overwinter in a dormant state. Our model is phenologically explicit, as we include parameters for each species' emergence and immergence times. We were inspired by a select few existing models that can be grouped into two categories: (i) those that model phenology explicitly, and (ii) those that model consumers that are discrete breeders.

Models for Phenology

In the context of our work, the model by Revilla et al. [39] is the earliest relevant phenologically explicit model. Using a system of ordinary differential equations (ODEs), they modelled a consumer and resource that interact and reproduce continuously within each year. They assumed that offspring do not contribute to any consumer–resource interactions until they mature into adults in the following year. They incorporated phenology into their model through a time-dependent emergence distribution, according to which the new resource and consumer adults emerge each year. They measured phenological asynchrony as the difference between the dates of peak resource and peak consumer emergence. To study the effects of phenological asynchrony on the long-term dynamics, they varied the mean and width of the emergence distributions. They concluded that the consumer attains the highest abundances when it emerges slightly ahead of or after the resource, since asynchrony reduces the risk of resource overexploitation. Using the same general methods, they extended their two-species model to three-species community models. We discuss their model in more detail in Chapter 5.

Bewick et al. [3] used their phenologically explicit model to study the effects of phenological asynchrony on population dynamics. They modelled an annually reproducing consumer that can survive more than one year, taking into account consumer deaths that occur between years from overwintering. They assumed that the same amount of resources are available each year. The system of ODEs that govern their within-year dynamics are fairly similar in structure to Revilla et al.'s adult consumer and resource equations, except that Bewick et al. included consumer starvation explicitly. Bewick et al. also incorporated phenology into their model through emergence distributions, which generally had the same shape for both species. They measured phenological asynchrony as the displacement between the consumer's and resource's emergence distributions. To study the effects of phenological asynchrony, they shifted the displacement between the two distributions and observed any changes in the results. They demonstrated that the amount of asynchrony determines whether the consumer population goes extinct or displays stable, oscillatory or chaotic long-term dynamics.

In contrast to the previous two models, Simmonds et al. [42] studied the effects of phenological asynchrony on population persistence using an evolutionarily explicit integral projection model. They measured phenological asynchrony as the difference between great tit (consumer) hatch date and peak caterpillar (resource) abundance. They modelled these events so that their timing depends on the spring temperature. They simulated their model under different greenhouse-gas-emissions scenarios and observed how the phenological asynchrony and great tit population size were affected. Their results suggest that asynchrony will increase with climate change, thereby increasing the potential for great tit extinction.

Models for Consumers that are Discrete Breeders

In nature, there exist many examples of consumer–resource systems that involve a consumer that reproduces in discrete regular intervals (i.e., every spring) and a resource that reproduces continuously. Some examples for such systems include ungulates (consumer) and

vegetation (resource), ladybugs (consumer) and aphids (resource), as well as weasels (consumer) and voles (resource); see Pachepsky et al. [35] and references therein. These systems cannot be accurately modelled by a fully continuous or discrete system. To more accurately model the combination of continuous and discrete dynamics, Pachepsky et al. [35] derived a "semi-discrete" consumer–resource model. They used a system of ODEs to model the continuous within-year dynamics. They modelled the between-year dynamics using a system of difference equations to reflect the consumer's annual birth pulse event. Their impulsive ODE model is explicitly solvable and is capable of displaying a wide range of interesting dynamics. We present their model and its analysis in detail in Section 2.3.

We are aware of only two extensions of the model by Pachepsky et al. that are somewhat relevant in our context. Geng et al. [15] studied conditions for two consumers to coexist on a single resource. To add realism, they introduced a summer and a winter season. During the summer, the dynamics are as in Pachepsky et al.'s model; during the winter, each species decays. Hence, their winter season is essentially a WRP as introduced above. The consumer birth pulse occurs immediately after the winter season. The authors considered linear and nonlinear consumer reproduction. They found that coexistence of different consumers is possible only with nonlinear reproduction. They studied how consumer coexistence varies as the relative length of the summer and winter season changes.

In a follow-up paper, Geng and Lutscher [14] extended the model by Geng et al. to an arbitrary number of consumer species. They studied the coexistence conditions for communities of consumer species that feed on a single resource and found that at least twenty consumer species could coexist on a single resource.

In both of these works, the authors assumed that the consumer and resource species are active (summer) or dormant (winter) at the same time. We will model the case that the active and dormant periods of the year can differ between a consumer and its resource.

Our Objective and Motivation

Several authors have studied the effects of phenological asynchrony on population persistence [42], but few authors study its effects on other aspects of population dynamics [3]. In this thesis, we derive a novel phenologically explicit consumer–resource model that can be used to study the dynamic consequences of phenological (a-)synchrony. The phenological events that we focus on are the immergence and emergence times. We allow these times to differ between the consumer and resource, so that their WRPs and active seasons need not be synchronized. As was done by Geng et al. [15], as well as Geng and Lutscher [14], we use the semi-discrete model by Pachepsky et al. [35] as a framework for our model, since it reflects the discrete manner in which many consumer species reproduce.

Immergence and emergence times are expected to vary with climate change [10, 17], but there exists a general uncertainty regarding the long-term consequences of climate change–induced phenological shifts for populations of interacting species [21, 39]. The consumer–resource model that we will derive provides a means to better understand these consequences. By analyzing how varying degrees of phenological asynchrony affect the long-term consumer–

resource dynamics in our model, through changing the immergence and emergence times, we are able to form hypotheses with regards to the effects of climate change–induced phenological shifts.

The underlying question that we are studying is how the consumer–resource dynamics are affected by the timing of consumer–resource interactions. Thus, even though our model focuses on the aspects of phenology related to a species' WRP, our results can be interpreted more generally and are therefore transferrable to other aspects of phenology.

Thesis Outline

This thesis is organized as follows. In Chapter 2, we provide all necessary background information. We discuss continuous-time and discrete-time single-species models and consumer–resource models, as well as equilibrium points and their stability. We demonstrate how to transform a simple continuous-time model into a discrete-time model. Finally, we present in detail the model by Pachepsky et al. [35] and their results.

In Chapter 3, we give a detailed derivation and analysis of our explicitly solvable consumer–resource model. We nondimensionalize our impulsive ODE model and transform it into a fully discrete model. After making the simplifying assumption that both species share an immergence time, we determine all equilibrium points. We find explicit expressions for equilibrium points and analyze their stability, using numerical methods whenever necessary. We find transcritical bifurcations, Naimark–Sacker (Hopf) bifurcations and flip bifurcations.

In Chapter 4, we use two-parameter bifurcation diagrams and orbit diagrams to illustrate the effects that the interaction time and amount of phenological asynchrony have on the long-term dynamics and bifurcations. We discuss our results within the context of consumer–resource theory. We show that our model is capable of displaying stable coexistence, consumer–resource cycles and overcompensation cycles in the long term.

In Chapter 5, we use orbit diagrams to study the effects of phenological asynchrony on the asymptotic (long-term) densities. We analyze the level of asynchrony at which the asymptotic consumer density is maximized. Unlike Revilla et al. [39], we demonstrate that optimal asynchrony is dependent on parameter values.

In Chapter 6, we discuss our findings, ecological insights, model limitations and future directions of our research. In particular, we want to include climate change and evolution more explicitly into our model in the future.

Chapter 2

Background

The purpose of this chapter is to familiarize the reader with concepts necessary to understand the entirety of this thesis. We discuss single-species growth models, as well as consumer–resource models, in both continuous and discrete time. Additionally, we describe in detail the paper that greatly inspired our work.

2.1 Single-Species Growth Models

A population of a single species can grow as individuals are born and decay as individuals die. A variety of single-species growth models have been proposed to model this dynamic behaviour. These models can be divided into two categories: continuous-time models and discrete-time models. As implied by their names, continuous-time models track the population size in continuous time, whereas discrete-time models only record the size at discrete time intervals. In the former case, we use ordinary differential equations (ODEs) and in the latter, we use difference equations. Many books cover this basic material; we chose to follow Kot's [25] detailed descriptions of these models.

2.1.1 Continuous-Time Models

A continuous-time model is generally appropriate when modelling species that reproduce throughout the year with overlapping generations. We begin with describing the simplest continuous-time single-species growth model. The exponential growth equation is

$$\frac{\mathrm{d}F}{\mathrm{d}t} = rF, \tag{2.1.1}$$

where the independent variable t is time, which is considered continuous, and the dependent variable F is the population size, which is nonnegative. The parameter r is the per capita growth rate. It is equal to the difference between the population's per capita birth and death rates. When it is positive, the births outweigh the deaths, resulting in exponential growth.

When it is negative, the opposite is true, resulting in exponential decay. If it equals zero, then the births and deaths are balanced, resulting in a fixed population size.

Using an initial condition (IC) of $F(0)$, which we assume to be positive, we can solve (2.1.1) to get

$$F(t) = F(0)\,\mathrm{e}^{rt}. \tag{2.1.2}$$

An IC of zero leads to a population size of zero for all time. One major drawback of this model is its lack of realism. More specifically, if $r > 0$, there is nothing limiting the population size from growing to infinity.

A more realistic model is one where growth is density dependent. For example, as the population size increases, the amount of food per individual decreases, resulting in fewer births and greater deaths. To reflect this, we use a nonlinear ODE. A relatively simple model that reflects this density dependence is the logistic equation

$$\frac{\mathrm{d}F}{\mathrm{d}t} = rF\left(1 - \frac{F}{K}\right), \tag{2.1.3}$$

where t and F are the same as for the exponential growth equation (2.1.1). The intrinsic growth rate r is the growth rate when the population is at low densities, meaning that growth is not yet limited by density-dependent factors. We assume that $r > 0$. Furthermore, K is the population's carrying capacity, which is positive. If the population size is initially below (above) the carrying capacity, then it will grow (decay) until it reaches the carrying capacity. If the IC is close to zero, then the growth is almost exponential. The restriction that $r > 0$ ensures that the population size cannot grow if it is initially greater than the carrying capacity.

The explicit solution to the logistic equation (2.1.3) is

$$F(t) = \frac{K}{1 + \mathrm{e}^{-rt}\left(\frac{K}{F(0)} - 1\right)}. \tag{2.1.4}$$

We present details on the solution process in Subsection 2.1.3.

If we multiply the numerator and denominator in (2.1.4) by $F(0)$ to avoid dividing by it, we see that an IC of zero results in the population size being zero for all time. Similarly, an IC equal to the carrying capacity results in the population size being fixed at the carrying capacity. These special values of F are called *equilibrium points*. In general, if one were to start at an equilibrium point, then solutions will stay at that equilibrium point. Considering now the solution to the exponential growth equation (2.1.2), it is clear that for this model, the only equilibrium point is $F = 0$.

Each equilibrium point can be classified as *stable* or *unstable*. Generally speaking, if all solutions that start near an equilibrium point stay near that equilibrium point, then the equilibrium point is stable. Stable equilibrium points can be further classified as *locally asymptotically stable* if solutions converge to the equilibrium point. In contrast, if an equilibrium point is unstable, then there exists at least one IC close to it that will result in solutions moving away from the equilibrium point. Solutions of the logistic equation (2.1.3) with $r, K > 0$ converge to the carrying capacity for all $F(0) > 0$. Hence, the equilibrium

points $F = K$ and $F = 0$ are locally asymptotically stable and unstable, respectively. Solutions of the exponential growth equation (2.1.1) will grow to infinity if $r > 0$ and decay to zero if $r < 0$. Hence, the equilibrium point $F = 0$ is locally asymptotically stable if $r < 0$ and unstable if $r > 0$.

To make these concepts general, we consider the following general scalar, autonomous ODE:

$$\frac{\mathrm{d}F}{\mathrm{d}t} = g(F). \tag{2.1.5}$$

Definition 2.1.1. A value $F = F^*$ is an *equilibrium point* of (2.1.5) if

$$g(F^*) = 0. \tag{2.1.6}$$

Definition 2.1.2. Suppose that F^* is an equilibrium point of (2.1.5).

(i) The point F^* is *stable* if for every $\varepsilon > 0$, there exists a $\delta > 0$ such that if

$$|F(0) - F^*| < \delta, \tag{2.1.7}$$

then

$$|F(t) - F^*| < \varepsilon, \tag{2.1.8}$$

for all $t > 0$.

(ii) The point F^* is *unstable* if it is not stable, meaning that for at least one $\varepsilon > 0$, there exists a $\delta > 0$ and a value $F(0)$ such that if (2.1.7) holds, then (2.1.8) does not hold for all $t > 0$.

(iii) The point F^* is *locally asymptotically stable* if it is stable and if there exists an $\varepsilon > 0$ such that if

$$|F(0) - F^*| < \varepsilon, \tag{2.1.9}$$

then

$$\lim_{t\to\infty} |F(t) - F^*| = 0. \tag{2.1.10}$$

Proposition 2.1.3. An equilibrium point F^* of (2.1.5), with $g(\cdot)$ being a continuously differentiable function, is unstable if

$$g'(F^*) > 0, \tag{2.1.11}$$

and it is locally asymptotically stable if

$$g'(F^*) < 0. \tag{2.1.12}$$

A proof is provided by Kot [25].

2.1.2 Discrete-Time Models

A discrete-time model is generally appropriate for modelling species that reproduce at regular discrete intervals. Just like for the continuous-time models, growth can be density independent or density dependent. The simplest density-independent model is the linear difference equation

$$v_{n+1} = R_0 v_n, \tag{2.1.13}$$

where the independent variable $n = 0, 1, 2, \ldots$ denotes time and v_n is the population size at time n. The parameter R_0 combines year-to-year survival and reproduction, depending on the life cycle of the species modelled. This parameter is nonnegative and assumed to be the same for all individuals within the population. The population grows geometrically when $R_0 > 1$ and decays geometrically when $0 < R_0 < 1$. With an IC of v_0, which we assume to be positive, we can solve (2.1.13) to obtain

$$v_n = v_0 R_0^n. \tag{2.1.14}$$

If $v_0 = 0$, then the population size remains at zero for all time.

An example for a density-dependent model is the nonlinear Beverton–Holt model [2]:

$$v_{n+1} = \frac{R_0 v_n}{1 + \left(\frac{R_0 - 1}{K}\right) v_n}, \tag{2.1.15}$$

where R_0 is the same as for the linear difference equation (2.1.13) and $K > 0$ is the carrying capacity. As formulated, this model is only valid for $R_0 > 1$, since this ensures that the population size cannot grow if it is initially larger than the carrying capacity. The per capita number of offspring $(\frac{v_{n+1}}{v_n})$ is a decreasing function of v_n that approaches zero as v_n gets large. Using the IC $v_0 > 0$, the explicit solution to the Beverton–Holt model (2.1.15) is

$$v_n = \frac{K}{\left(\frac{K}{v_0} - 1\right) R_0^{-n} + 1}. \tag{2.1.16}$$

By multiplying the numerator and denominator in the above equation by v_0, we eliminate the division by it. If we set the IC to zero, then the population size is fixed at zero for all time. For this reason, we restrict $v_0 > 0$. Furthermore, an IC equal to the carrying capacity leads to a population size equal to the carrying capacity for all time.

Another density-dependent model is the Ricker model [40]:

$$v_{n+1} = v_n \, \mathrm{e}^{r\left(1 - \frac{v_n}{K}\right)}, \tag{2.1.17}$$

where $K > 0$ is still the carrying capacity and $r > 0$ is the intrinsic growth rate. We restrict r so that the population size cannot grow if it is initially larger than the carrying capacity. The per capita number of offspring $(\frac{v_{n+1}}{v_n})$ is a decreasing function of v_n, which approaches zero as v_n gets large. If the population size initially equals zero or the carrying capacity, then it will be fixed at that initial value for all time.

To define these concepts in general, we use the following general scalar, autonomous difference equation:

$$v_{n+1} = g(v_n). \tag{2.1.18}$$

Definition 2.1.4. A value $v_n = v^*$ is an *equilibrium point* of (2.1.18) if

$$v^* = g(v^*). \tag{2.1.19}$$

Definition 2.1.5. Suppose that v^* is an equilibrium point of (2.1.18).

(i) The point v^* is *stable* if for every $\varepsilon > 0$, there exists a $\delta > 0$ such that if

$$|v_0 - v^*| < \delta, \tag{2.1.20}$$

then

$$|v_n - v^*| < \varepsilon, \tag{2.1.21}$$

for all $n > 0$.

(ii) The point v^* is *unstable* if it is not stable, meaning that for at least one $\varepsilon > 0$, there exists a $\delta > 0$ such that if (2.1.20) holds, then (2.1.21) does not hold for all $n > 0$.

(iii) The point v^* is *locally asymptotically stable* if it is stable and if there exists an $\varepsilon > 0$ such that if

$$|v_0 - v^*| < \varepsilon, \tag{2.1.22}$$

then

$$\lim_{n\to\infty} |v_n - v^*| = 0. \tag{2.1.23}$$

Proposition 2.1.6. An equilibrium point v^* of (2.1.18), with $g(\cdot)$ being a continuously differentiable function is unstable if

$$|g'(v^*)| > 1, \tag{2.1.24}$$

and it is locally asymptotically stable if

$$|g'(v^*)| < 1. \tag{2.1.25}$$

For the linear difference equation (2.1.13), $v_n = 0$ is the only equilibrium point. If $0 < R_0 < 1$, then $v_n = 0$ is locally asymptotically stable, since solutions converge to zero. If $R_0 > 1$, then $v_n = 0$ is unstable, since solutions diverge to infinity. The equilibrium points for the Beverton–Holt model (2.1.15) and for the Ricker model (2.1.17) are both $v_n = 0$ and $v_n = K$. With the assumptions that $R_0 > 1$ and $K > 0$, solutions to the Beverton–Holt model converge to the carrying capacity. Hence, $v_n = 0$ is unstable and $v_n = K$ is locally asymptotically stable. With the assumption that $r, K > 0$, solutions to the Ricker model converge to the carrying capacity when $0 < r < 2$. In this case, $v_n = 0$ is unstable and $v_n = K$ is locally asymptotically stable. When $r > 2$, solutions do not converge to either of the two equilibrium points, so both are unstable.

2.1.3 From Continuous to Discrete

We can turn a continuous-time model into a discrete-time model by taking its solution map for a fixed time. We illustrate this process using the logistic equation (2.1.3). If we have the IC $F(0) > 0$, then we can find the exact solution to this initial value problem (IVP). One possible way to solve this IVP is to recognize that (2.1.3) is a Bernoulli differential equation. By multiplying each term by $-F^{-2}$ and letting $y = F^{-1}$, we can rewrite (2.1.3) as

$$\frac{\mathrm{d}y}{\mathrm{d}t} + ry = \frac{r}{K}. \tag{2.1.26}$$

This is a first-order non-homogeneous linear differential equation and can therefore be solved using an integrating factor. We obtain

$$y(t) = \mathrm{e}^{-rt}\left(\frac{1}{K}\int_0^t r\,\mathrm{e}^{rs}\,\mathrm{d}s + \frac{1}{F(0)}\right). \tag{2.1.27}$$

We use our substitution of $y = F^{-1}$ and get

$$F(t) = \frac{K}{1 + \mathrm{e}^{-rt}\left(\frac{K}{F(0)} - 1\right)}. \tag{2.1.28}$$

We now pick a fixed time $T > 0$, which we call a "year". We count the number of years by integers $n = 0, 1, 2, \ldots$ and denote the density at the beginning of year n by v_n. If $v_n = F(0)$ is the initial density in year n then $v_{n+1} = F(T^-)$ from (2.1.28) is the initial density in year $n + 1$.

Thus, the discrete map that relates v_n to v_{n+1} is

$$v_{n+1} = \frac{K}{1 + \mathrm{e}^{-rT}\left(\frac{K}{v_n} - 1\right)}. \tag{2.1.29}$$

Now, if we define $R_0 \equiv \mathrm{e}^{rT}$ and manipulate (2.1.29), we get

$$v_{n+1} = \frac{R_0 v_n}{1 + \frac{(R_0 - 1)}{K} v_n}, \tag{2.1.30}$$

which is the Beverton–Holt model (2.1.15). In this thesis, we will repeat this process for a more complicated consumer–resource model.

2.2 Consumer–Resource Models

The interaction between a consumer (predator) and its resource (prey) is one of the fundamental building blocks for ecological dynamics. Consumer–resource dynamics can be modelled in continuous or discrete time. In continuous time, the model consists of a system of ODEs; in discrete time, it consists of a system of difference equations.

2.2.1 Continuous-Time Models

Continuous-time models are generally appropriate for modelling consumer–resource systems with interactions between species and reproduction for both species that occur continuously. Arguably the most well known consumer–resource model is the Lotka–Volterra predator–prey model [27, 47]:

$$\frac{\mathrm{d}F}{\mathrm{d}t} = rF - aFC, \qquad \frac{\mathrm{d}C}{\mathrm{d}t} = qaFC - mC, \tag{2.2.1}$$

where the independent variable t is time, which is considered continuous. The dependent variables are F and C, which represent the prey and predator population size, respectively. The parameters r, a, q and m are the prey intrinsic growth rate, predator attack rate, predator conversion efficiency and predator death rate, respectively. We assume that all parameters are positive. The prey population grows exponentially when there are no predators, whereas the predator population decays exponentially when there are no prey. The functional response is the rate of prey consumption as a function of prey availability [1]. The Lotka–Volterra model has a linear functional response with slope a. As prey are consumed, they are converted into new predators. The numerical response is the change in the predator density as a function of the change in the prey density [1]. For the Lotka–Volterra model, the numerical response has a slope of q.

To reduce the number of parameters in the Lotka–Volterra model and simplify calculations, we nondimensionalize the model. Instead of minimizing the number of parameters, we nondimensionalize so that the equilibrium points of the resulting model are independent of the parameters. We introduce the dimensionless variables

$$f = \frac{F}{\hat{F}}, \qquad c = \frac{C}{\hat{C}}, \qquad s = \frac{t}{\hat{t}}, \tag{2.2.2}$$

which are the scaled prey population size, scaled predator population size and scaled time, respectively. We rewrite (2.2.1) as

$$\frac{df}{ds} = r\hat{t}f - a\hat{C}\hat{t}fc, \qquad \frac{dc}{ds} = qa\hat{F}\hat{t}fc - m\hat{t}c. \tag{2.2.3}$$

Choosing the units to be

$$\hat{F} = \frac{m}{qa}, \qquad \hat{C} = \frac{r}{a} \qquad \text{and} \qquad \hat{t} = 1 \tag{2.2.4}$$

results in the following nondimensional model:

$$\frac{df}{ds} = r(1-c)f, \qquad \frac{dc}{ds} = m(f-1)c. \tag{2.2.5}$$

We can generalize the notion of equilibrium points and their stability from Subsection 2.1.1, using a two-dimensional general system of autonomous ODEs

$$\frac{\mathrm{d}F}{\mathrm{d}t} = g(F, C), \qquad \frac{\mathrm{d}C}{\mathrm{d}t} = h(F, C), \tag{2.2.6}$$

but this can be extended to systems of higher dimensions. Analogous to Definition 2.1.1, an equilibrium point of (2.2.6) is a pair (F^*, C^*) that satisfies

$$g(F^*, C^*) = 0 = h(F^*, C^*). \tag{2.2.7}$$

To classify stability, we linearize about the equilibrium point. For the system (2.2.6), we obtain the Jacobian matrix

$$J = \begin{pmatrix} \frac{\partial g}{\partial F} & \frac{\partial g}{\partial C} \\ \frac{\partial h}{\partial F} & \frac{\partial h}{\partial C} \end{pmatrix}. \tag{2.2.8}$$

For a linear continuous-time model, solutions are of the form $\vec{v}\,\mathrm{e}^{\lambda t}$, where λ is an eigenvalue of the Jacobian matrix and $\vec{v}$ is the corresponding eigenvector. If the Jacobian matrix evaluated at the equilibrium point is

$$J(F^*, C^*) = \begin{pmatrix} J_{11} & J_{12} \\ J_{21} & J_{22} \end{pmatrix}, \tag{2.2.9}$$

then the eigenvalues are the solutions of the characteristic equation

$$\det \begin{pmatrix} J_{11} - \lambda & J_{12} \\ J_{21} & J_{22} - \lambda \end{pmatrix} = 0. \tag{2.2.10}$$

We can rewrite the equation using the determinant and trace of $J(F^*, C^*)$ as

$$\lambda^2 - \operatorname{Tr} J(F^*, C^*)\lambda + \det J(F^*, C^*) = 0. \tag{2.2.11}$$

Solving this quadratic equation, we obtain

$$\lambda_{1,2} = \frac{\operatorname{Tr} J(F^*, C^*) \pm \sqrt{(\operatorname{Tr} J(F^*, C^*))^2 - 4 \det J(F^*, C^*)}}{2}. \tag{2.2.12}$$

Analogous to Proposition 2.1.3, if both eigenvalues have negative real part, then the equilibrium point is locally asymptotically stable. If at least one eigenvalue has positive real part, then the equilibrium point is unstable. We can further classify the equilibrium points based on the particular combination of eigenvalues, which determine the behaviour of solutions near the equilibrium point; see Figure 2.1.

The equilibrium points of the nondimensional Lotka–Volterra model (2.2.5) are $(0, 0)$ and $(1, 1)$. The Jacobian matrix is

$$J = \begin{pmatrix} r(1-c) & -rf \\ mc & m(f-1) \end{pmatrix}. \tag{2.2.13}$$

At $(0, 0)$, the eigenvalues of the Jacobian are $\lambda_1 = r > 0$ and $\lambda_2 = -m < 0$. Therefore, $(0, 0)$ is a saddle point in the linearized and nonlinear systems. At $(1, 1)$, the eigenvalues of the Jacobian are $\lambda_{1,2} = \pm\sqrt{rm}i$, resulting in a center for the linearized system. Perturbations caused by the previously discarded nonlinear terms may result in eigenvalues for the nonlinear system with nonzero real part. Hence, the Lotka–Volterra model is structurally unstable. As explained in detail by Kot [25], it is possible to show graphically that $(1, 1)$ remains a center in the nonlinear system.

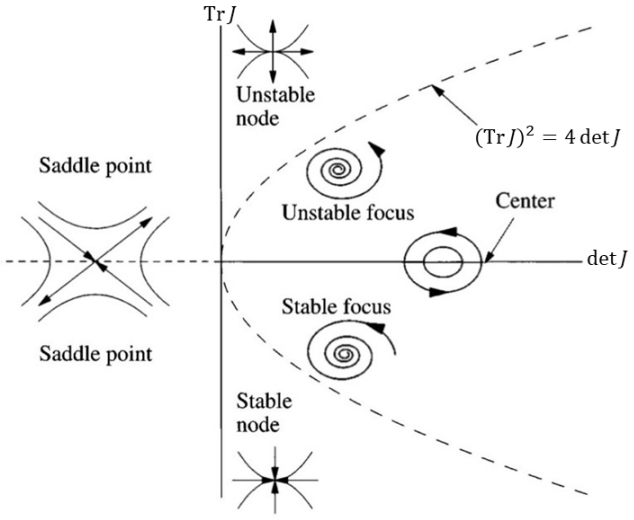

Figure 2.1: Classification of equilibrium points for continuous-time models in terms of the trace and determinant of $J(F^*, C^*)$. This plot is inspired by Kot [25].

The Lotka–Volterra model (2.2.1) can be adapted such that the resource grows logistically when the consumer is absent. Recalling the logistic equation (2.1.3), we have

$$\frac{\mathrm{d}F}{\mathrm{d}t} = rF\left(1 - \frac{F}{K}\right) - aFC, \qquad \frac{\mathrm{d}C}{\mathrm{d}t} = qaFC - mC. \tag{2.2.14}$$

All parameters are the same as in the classical Lotka–Volterra model. We assume again that all parameters are positive. This time, we nondimensionalize the model by selecting

$$\hat{F} = K, \qquad \hat{C} = \frac{r}{a}, \qquad \hat{t} = \frac{1}{r}, \tag{2.2.15}$$

resulting in

$$\frac{\mathrm{d}f}{\mathrm{d}s} = (1 - f - c)f, \qquad \frac{\mathrm{d}c}{\mathrm{d}s} = \beta(f - \varphi)c, \tag{2.2.16}$$

where $\beta = \frac{qaK}{r}$ and $\varphi = \frac{m}{qaK}$. This system has three equilibrium points: $(0,0), (1,0), (\varphi, 1-\varphi)$. For the coexistence equilibrium to exist, we require $\varphi \neq 1$. We determine the stability of each equilibrium point by linearizing about each one and analyzing the resulting eigenvalues. We summarize the results, but Kot [25] shows this analysis in detail. The eigenvalues of $J(0,0)$ are $\lambda_1 = 1$ and $\lambda_2 = -\beta\varphi$, so $(0,0)$ is a saddle point. The eigenvalues of $J(1,0)$ are $\lambda_1 = -1$ and $\lambda_2 = \beta(1-\varphi)$. If $\varphi > 1$, then $(1,0)$ is a stable node and if $\varphi < 1$, then it is a saddle point. The eigenvalues of $J(\varphi, 1-\varphi)$ are

$$\lambda_{1,2} = \frac{-\varphi \pm \sqrt{\varphi^2 - 4\beta\varphi(1-\varphi)}}{2}. \tag{2.2.17}$$

Referring to Figure 2.1, we see that if $\varphi > 1$, then $(\varphi, 1-\varphi)$ is a saddle point. If $\varphi < 1$, then $(\varphi, 1-\varphi)$ is either a stable node or a stable focus. If, in addition to the previous constraint, $\varphi > \frac{4\beta}{1+4\beta}$, then it is a stable node. If instead, $\varphi < \frac{4\beta}{1+4\beta}$, then it is a stable focus.

2.2.2 Discrete-Time Models

Discrete-time models are generally appropriate for modelling consumer–resource systems with interactions between species that occur over a short length of time and reproduction for both species that occurs at the same regular interval. Discrete-time models have been used a lot to study host–parasitoid dynamics. Unlike in continuous-time, events do not necessarily occur simultaneously in discrete-time models. As a result, the order in which events occur matters. As an example, Cobbold et al. [6] demonstrated that the timing of parasite emergence from its host affects the severity of host outbreaks. Perhaps the most famous host–parasitoid model is the Nicholson–Bailey model [32, 33]:

$$v_{n+1} = R_0 v_n \, \mathrm{e}^{-a w_n}, \qquad\qquad w_{n+1} = \ell v_n \big(1 - \mathrm{e}^{-a w_n}\big), \tag{2.2.18}$$

where the independent variable $n = 0, 1, 2, \ldots$ is time, which is measured in generations. The dependent variables v_n and w_n are the host and parasitoid population sizes in generation n, respectively; R_0 is the host net reproductive rate; a is the attack rate of the parasitoid; and ℓ is the number of parasitoid offspring per host. We assume that all parameters are positive. The probability that a host is not parasitized is equal to $\mathrm{e}^{-a w_n}$. It follows that $1 - \mathrm{e}^{-a w_n}$ is the probability that a host is parasitized.

We can generalize the notion of equilibrium points and their stability from Subsection 2.1.2, using a general two-dimensional system of autonomous difference equations

$$v_{n+1} = g(v_n, w_n), \qquad\qquad w_{n+1} = h(v_n, w_n), \tag{2.2.19}$$

but we can extend this to higher dimensions. Analogous to Definition 2.1.4, an equilibrium point of (2.2.19) is a pair (v^*, w^*) such that

$$v^* = g(v^*, w^*) \qquad \text{and} \qquad w^* = h(v^*, w^*). \tag{2.2.20}$$

To classify the stability of equilibrium points, we first linearize about the equilibrium point; i.e., we find the Jacobian matrix $J(v^*, w^*)$. Then we obtain the eigenvalues (λ) of J from the characteristic equation; see Subsection 2.2.1.

For a linear discrete-time model, solutions are of the form $\vec{v}\lambda^n$, where $\vec{v}$ is the corresponding eigenvector to λ. To analyze the stability of equilibrium points, we determine the modulus of λ. That is,

$$|\lambda| = \sqrt{\lambda \bar{\lambda}}, \tag{2.2.21}$$

where $\bar{\lambda}$ is the complex conjugate of λ. Analogous to Proposition 2.1.6, if both eigenvalues have modulus less than one, then the equilibrium point is locally asymptotically stable. In other words, both eigenvalues need to be within the unit circle in the complex plane. As in the continuous case, we can further classify the equilibrium points based on the particular combination of eigenvalues. For example, if both eigenvalues are real and one has modulus less than one, whereas the other has modulus greater than one, then the equilibrium point is a saddle point.

We can use the Jury test to determine whether all eigenvalues in a discrete-time model have modulus less than one [20]. For a two-dimensional system, the Jury conditions are

$$1 - \det J(v^*, w^*) > 0, \tag{2.2.22}$$
$$1 + \det J(v^*, w^*) - \operatorname{Tr} J(v^*, w^*) > 0, \tag{2.2.23}$$
$$1 + \det J(v^*, w^*) + \operatorname{Tr} J(v^*, w^*) > 0. \tag{2.2.24}$$

The equilibrium point (v^*, w^*) is stable if and only if all three Jury conditions are satisfied. If (2.2.22) is reversed, then there exists a complex pair of eigenvalues with modulus greater than one. When the inequality in (2.2.22) is replaced by an equality, a Naimark–Sacker (Hopf) bifurcation can occur, which leads to consumer–resource cycles. If (2.2.23) is reversed, then there is a real eigenvalue greater than one. When the inequality in (2.2.23) is replaced by an equality, a transcritical bifurcation can occur. At this transcritical bifurcation, two equilibrium points exchange stability. Lastly, if (2.2.24) is reversed, then there is a real eigenvalue less than negative one. When the inequality in (2.2.24) is replaced by an equality, a flip bifurcation can occur, which leads to two-cycles.

Considering again the Nicholson–Bailey model (2.2.18), the equilibrium points are $(0, 0)$ and

$$(v^*, w^*) = \left(\frac{R_0 \ln(R_0)}{a\ell(R_0 - 1)}, \frac{\ln(R_0)}{a} \right). \tag{2.2.25}$$

The former implies that both the host and parasitoid are extinct, and the latter implies that they coexist. We analyze stability in more detail than we did for continuous-time models, as we will use similar techniques throughout this thesis. The Jacobian matrix is

$$J = \begin{pmatrix} R_0 \, \mathrm{e}^{-aw_n} & -aR_0 v_n \, \mathrm{e}^{-aw_n} \\ \ell(1 - \mathrm{e}^{-aw_n}) & a\ell v_n \, \mathrm{e}^{-aw_n} \end{pmatrix}. \tag{2.2.26}$$

We have

$$J(0, 0) = \begin{pmatrix} R_0 & 0 \\ 0 & 0 \end{pmatrix}, \tag{2.2.27}$$

so the eigenvalues are $\lambda_1 = R_0$ and $\lambda_2 = 0$. If $R_0 > 1$, then $(0, 0)$ is a saddle point. If $R_0 < 1$, then it is locally asymptotically stable. The Jacobian matrix at (v^*, w^*) is

$$J(v^*, w^*) = \begin{pmatrix} 1 & \frac{-R_0 \ln(R_0)}{\ell(R_0 - 1)} \\ \ell(1 - \frac{1}{R_0}) & \frac{\ln(R_0)}{R_0 - 1} \end{pmatrix}. \tag{2.2.28}$$

We use the Jury test to assess stability. We have

$$\operatorname{Tr} J(v^*, w^*) = 1 + \frac{\ln(R_0)}{R_0 - 1}, \qquad \det J(v^*, w^*) = \frac{R_0 \ln(R_0)}{R_0 - 1}. \tag{2.2.29}$$

We determine that

$$\det J(v^*, w^*) - \operatorname{Tr} J(v^*, w^*) + 1 = \ln(R_0). \tag{2.2.30}$$

If $R_0 > 1$, then (2.2.23) holds. If $R_0 < 1$, then (v^*, w^*) is unstable. Next, we find that

$$\det J(v^*, w^*) + \operatorname{Tr} J(v^*, w^*) + 1 = 2 + \frac{(R_0 + 1) \ln(R_0)}{R_0 - 1}. \tag{2.2.31}$$

For $R_0 > 1$, (2.2.24) holds as well. Lastly, we analyze whether (2.2.22) also holds for $R_0 > 1$. We must show that

$$\underbrace{R_0 - 1 - R_0 \ln(R_0)}_{\equiv Z(R_0)} > 0. \tag{2.2.32}$$

Taking the derivative of the left-hand-side, we get

$$\frac{\mathrm{d}Z}{\mathrm{d}R_0} = -\ln(R_0). \tag{2.2.33}$$

For all $R_0 > 1$, the derivative is negative, meaning that $Z(R_0)$ is a decreasing function. We have

$$Z(1) = 0, \tag{2.2.34}$$

so $Z(R_0) < 0$ for all $R_0 > 1$. Therefore, not all three Jury conditions can be satisfied simultaneously. Assuming that $R_0 > 1$, (v^*, w^*) is unstable and the corresponding eigenvalues have nonzero imaginary parts. Hence, we expect consumer–resource cycles to occur.

2.3 The Pachepsky Model

A consumer–resource system that has both continuous and discrete behaviour cannot be accurately modelled by a fully continuous or discrete model. Instead, a "semi-discrete" model is required. The particular consumer–resource system that Pachepsky et al. [35] considered is one where the resource reproduces continuously, whereas the consumer reproduces in discrete regular intervals. In this section, we describe the semi-discrete consumer–resource model by Pachepsky et al. and provide a summary of their analysis and results.

2.3.1 Model Description

In the model by Pachepsky et al. [35], the consumer and resource interact continuously within a year but the consumer reproduces only once per year. Within each year, the resource grows logistically and is consumed by the consumer at a linear rate. The consumer decays exponentially and stores all energy accumulated through consumption. At the end of each year, any accumulated energy is used in its entirety for consumer reproduction. We refer to this event as the consumer birth pulse.

The length of a year is denoted by T; the time within a year is denoted by $t \in [0, T)$. The state variables are the resource density, F, the consumer density, C, and the amount of resource consumed per consumer, B. The system of ODEs that model the within-year dynamics are

$$\frac{\mathrm{d}F}{\mathrm{d}t} = rF\left(1 - \frac{F}{K}\right) - aFC, \qquad \frac{\mathrm{d}C}{\mathrm{d}t} = -mC, \qquad \frac{\mathrm{d}B}{\mathrm{d}t} = aF, \tag{2.3.1}$$

where r is the resource intrinsic growth rate, K is the resource carrying capacity, a is the consumer consumption rate and m is the consumer death rate.

The consumer birth pulse occurs when $t = T$ and is assumed to be instantaneous. The system of discrete equations that model the between-year dynamics are

$$F(T) = F(T^-), \qquad C(T) = [qB(T^-) + 1]C(T^-), \qquad B(T) = 0, \tag{2.3.2}$$

where $q > 0$ is the consumer conversion efficiency. The quantities after the birth pulse are used as the initial conditions (ICs) for the ODEs in the following year.

In the nondimensional model, each year is of length one and $s \in [0, 1)$ is the time within a year. Additionally, f, c and b are the scaled resource density, scaled consumer density and scaled amount of resource consumed per consumer, respectively. The within-year equations for the nondimensional model are

$$\frac{\mathrm{d}f}{\mathrm{d}s} = \rho f(1 - f) - \alpha f c, \qquad \frac{\mathrm{d}c}{\mathrm{d}s} = -\mu c, \qquad \frac{\mathrm{d}b}{\mathrm{d}s} = \alpha f, \tag{2.3.3}$$

where $\rho = rT$ is the scaled resource intrinsic growth rate, $\alpha = aqKT$ is the scaled consumer consumption rate and $\mu = mT$ is the scaled consumer death rate. The between-year equations for the nondimensional model are

$$f(1) = f(1^-), \qquad c(1) = [b(1^-) + 1]c(1^-), \qquad b(1) = 0. \tag{2.3.4}$$

We will refer to (2.3.3)–(2.3.4) as the Pachepsky model.

By selecting a time to record the densities at each year (the census time), it is possible to derive a discrete map that relates the resource density and consumer density at the census time of the current year to that of the next year. In doing so, the impulsive ODE model is transformed into a fully discrete model. We previously demonstrated how to do this for a simple single-species model; see Subsection 2.1.3. The authors selected the census time to be immediately following the consumer birth pulse. The integer n is used to denote the year. The initial densities for year n are $v_n = f(0)$ and $w_n = c(0)$. Since the amount of resource consumed per consumer is set to zero at the birth pulse, it does not require a separate variable in the discrete map. The solution map relating (v_{n+1}, w_{n+1}) to (v_n, w_n) is

$$\begin{aligned} v_{n+1} &= v_n \frac{\mathrm{e}^{\rho - \frac{\alpha w_n}{\mu}(1-\mathrm{e}^{-\mu})}}{\rho v_n \int_0^1 \mathrm{e}^{\rho t - \frac{\alpha w_n}{\mu}(1-\mathrm{e}^{-\mu t})}\,\mathrm{d}t + 1}, \\ w_{n+1} &= \left(\alpha v_n \int_0^1 \frac{\mathrm{e}^{\rho s - \frac{\alpha w_n}{\mu}(1-\mathrm{e}^{-\mu s})}}{\rho v_n \int_0^s \mathrm{e}^{\rho t - \frac{\alpha w_n}{\mu}(1-\mathrm{e}^{-\mu t})}\,\mathrm{d}t + 1}\,\mathrm{d}s + 1 \right) w_n e^{-\mu}. \end{aligned} \tag{2.3.5}$$

There exist up to three equilibrium points: the extinction state $(0, 0)$, the resource-only state $(1, 0)$ and the coexistence state (v, w). The components of the coexistence state are

$$v = \frac{1}{\rho} \frac{\mathrm{e}^{\frac{\rho}{\alpha}(\mathrm{e}^{\mu}-1)} - 1}{\int_0^1 \mathrm{e}^{\rho\left(s - (1 - \frac{\mathrm{e}^{\mu}-1}{\alpha})\frac{1-\mathrm{e}^{-\mu s}}{1-\mathrm{e}^{-\mu}}\right)}\,\mathrm{d}s} \qquad \text{and} \qquad w = \rho\mu \frac{1 - \frac{\mathrm{e}^{\mu}-1}{\alpha}}{\alpha(1 - \mathrm{e}^{-\mu})}. \tag{2.3.6}$$

The coexistence state is positive if $\mathrm{e}^{-\mu}(1 + \alpha) > 1$.

To analyze the stability of the equilibrium points, Pachepsky et al. performed a linear stability analysis. The matrix $J(0,0)$ has components $J_{12} = 0 = J_{21}$, so it is a diagonal matrix. Hence, the eigenvalues λ_1 and λ_2 are equal to J_{11} and J_{22}, respectively. They are

$$\lambda_1 = \mathrm{e}^{\rho} \qquad \text{and} \qquad \lambda_2 = \mathrm{e}^{-\mu}. \tag{2.3.7}$$

Since $\rho, \mu > 0$, we have $|\lambda_1| > 1$ and $|\lambda_2| < 1$. Therefore, $(0,0)$ is a saddle point.

The matrix $J(1,0)$ has component $J_{21} = 0$, so it is an upper triangular matrix. Thus, the eigenvalues λ_1 and λ_2 are again equal to J_{11} and J_{22}, respectively. They are

$$\lambda_1 = \mathrm{e}^{-\rho} \qquad \text{and} \qquad \lambda_2 = \mathrm{e}^{-\mu}(1+\alpha). \tag{2.3.8}$$

Since $\rho > 0$, we have $|\lambda_1| < 1$. Moreover, $|\lambda_2| < 1$ if and only if

$$\alpha < \mathrm{e}^{\mu} - 1. \tag{2.3.9}$$

Thus, $(1,0)$ is locally asymptotically stable if (2.3.9) holds. Otherwise, it is a saddle point.

To determine the stability of the coexistence state, Pachepsky et al. used the Jury test; see (2.2.22)–(2.2.24). If (2.2.23) holds, then (2.3.9) does not hold. Hence, the explicit expression for the transcritical bifurcation is (2.3.9), but with the inequality replaced by an equality. As the transcritical bifurcation is crossed, the states (v,w) and $(1,0)$ exchange stability. Pachepsky et al. called the transcritical bifurcation the consumer-extinction boundary, since it marks the boundary between consumer persistence and extinction. When the inequality in (2.2.22) is replaced by an equality, Pachepsky et al. called the expression the consumer–resource cycles boundary. When the same occurs for (2.2.24), Pachepsky et al. called the expression the overcompensation-cycles boundary. They used numerical methods to determine and plot the stability boundaries for (v,w).

2.3.2 Results

Figure 2.2 displays the two-parameter bifurcation plot for the coexistence state (v,w) in terms of the consumer consumption rate (α) and the consumer death rate (μ) with the resource intrinsic growth rate (ρ) fixed. As indicated by the blue consumer-extinction boundary, the consumer goes extinct for low values of α. Unsurprisingly, as the value of μ increases, the value of α required for the consumer to avoid extinction increases. The stable coexistence region, where all three Jury conditions are satisfied, is labelled within the plot.

The top left plot in Figure 2.3 illustrates the stable behaviour of solutions when the parameters selected are within this region. Instabilities arise for larger values of α. When the value of μ is small, the stable dynamics give way to consumer–resource cycles as the red consumer–resource cycles boundary is crossed; see the top right plot in Figure 2.3. When the value of μ is larger, the stable dynamics give way to overcompensation cycles as the black overcompensation-cycles boundary is crossed; see the bottom plot in Figure 2.3.

While both instabilities that occur for larger values of α result in solutions with cyclic behaviour, the two differ qualitatively. In consumer–resource cycles, population densities

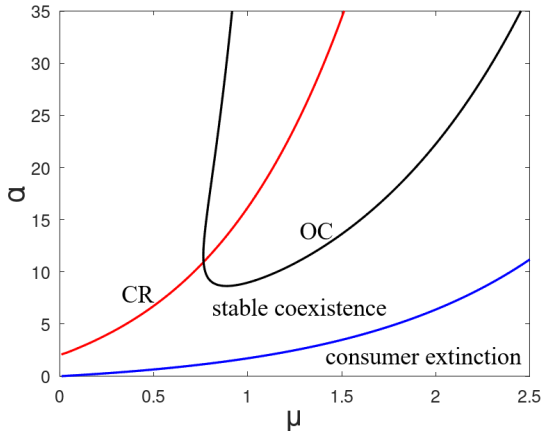

Figure 2.2: Bifurcation diagram for the Pachepsky model with $\rho = 20$. The blue curve is the consumer-extinction boundary. The red curve is the consumer–resource cycles boundary (CR). The black curve is the overcompensation-cycles boundary (OC).

increase and decrease gradually within each cycle. By contrast, in overcompensation cycles, population densities alternate between jumping up and down; see Figure 2.3.

One can calculate the period of emerging consumer–resource cycles by analyzing the eigenvalues at the bifurcation point. When the eigenvalues have nonzero imaginary part, they are given by

$$\lambda = \frac{1}{2}\operatorname{Tr} J(v,w) \pm \frac{1}{2}\sqrt{4\det J(v,w) - (\operatorname{Tr} J(v,w))^2}\; i. \tag{2.3.10}$$

Converting to polar form, we write λ in terms of the radius and θ, which is the angle in radians from the origin. On the consumer–resource cycles boundary, the radius is one, so we get

$$\lambda = \cos(\theta) + i\sin(\theta) = \mathrm{e}^{i\theta}. \tag{2.3.11}$$

Solutions in discrete time behave like λ^n [25]. We have that

$$\lambda^n = \mathrm{e}^{in\theta} = \cos(n\theta) + i\sin(n\theta). \tag{2.3.12}$$

Thus, the cycle period on the consumer–resource cycles boundary is

$$\text{period} = \frac{2\pi}{\theta}. \tag{2.3.13}$$

To solve for θ, we equate (2.3.10) and (2.3.11) to get

$$\theta = \cos^{-1}\left(\frac{1}{2}\operatorname{Tr} J(v,w)\right). \tag{2.3.14}$$

The cycle period on the consumer–resource cycles boundary in Figure 2.2 is shown in Figure 2.4. For each value of μ, a value of α was selected (not shown) such that the point

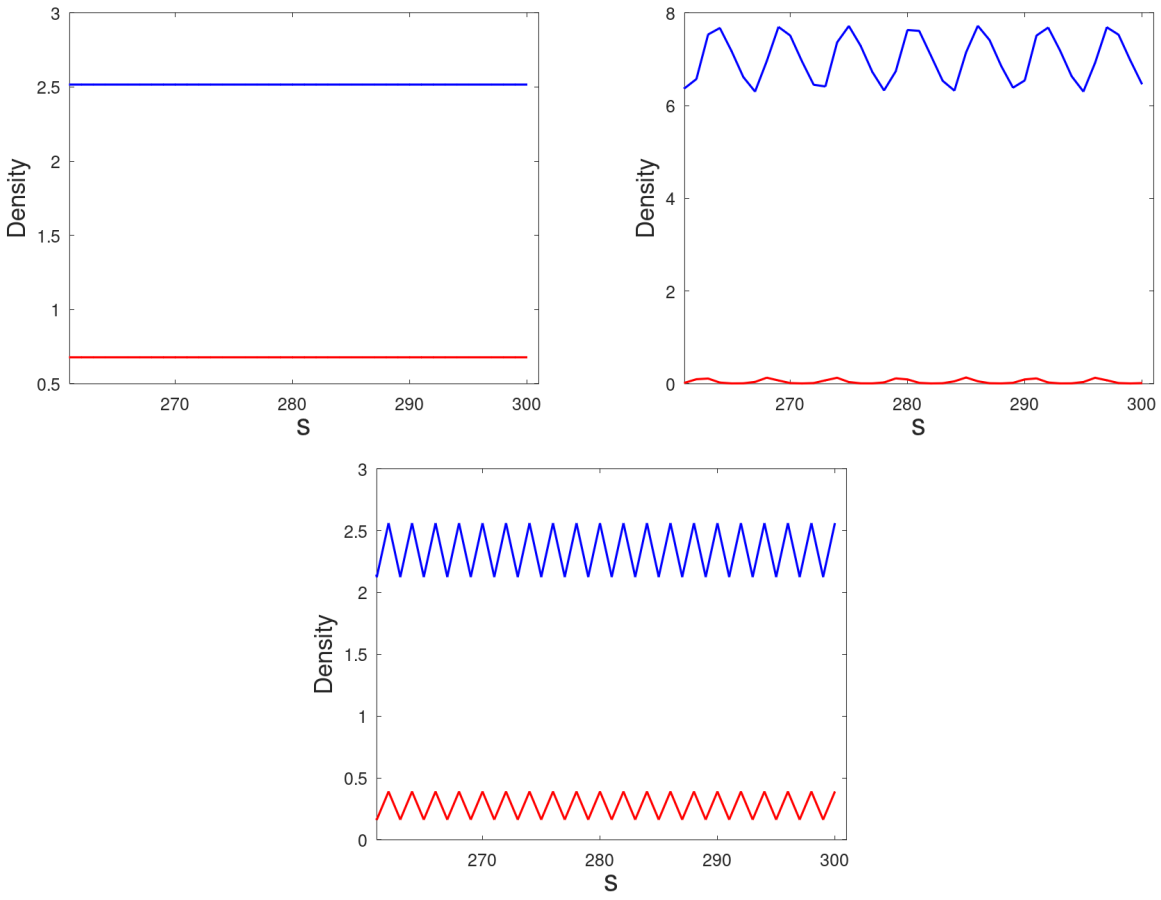

Figure 2.3: Possible behaviour of the Pachepsky model. The solid red (blue) line is the resource (consumer) density. Densities were recorded directly following the consumer birth pulse. In the top left plot, $\mu = 1.5$ and $\alpha = 10$. In the top right plot, $\mu = 0.1$ and $\alpha = 2.88$. In the bottom plot, $\mu = 0.81$ and $\alpha = 11$. In all plots, $\rho = 20$.

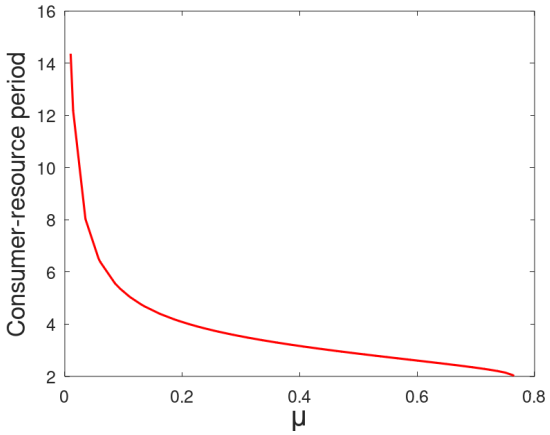

Figure 2.4: The cycle period on the consumer–resource cycles boundary for the Pachepsky model with $\rho = 20$.

(μ, α) remains on the consumer–resource cycles boundary. As the value of μ increases, the cycle period decreases to two. Two-cycles arise once the consumer–resource cycles boundary intersects with the overcompensation-cycles boundary.

A limitation of the Pachepsky model is that the consumer birth pulse is assumed to be instantaneous. Hence, Pachepsky et al. neglect the heterogeneity of individuals and instead essentially use an average or median birth pulse date for the consumer population. The Pachepsky model is thus suitable for modelling consumer populations with low heterogeneity, meaning that consumer reproduction occurs over a relatively small range of time (i.e., a few days or weeks) compared to the length of a year. As the heterogeneity of consumer individuals increases, the ability for the Pachepsky model to accurately model the consumer population decreases due to the above limiting assumption. Our model, which we will derive in Chapter 3, makes the same limiting assumption as the Pachepsky model.

In this chapter, we studied different single-species and consumer–resource models. Through analyzing these models, we have covered all of the necessary background information to understand our model derivation and analysis.

Chapter 3

The Model

In this chapter, we derive our consumer–resource model, which we will use to study the dynamic consequences of phenological asynchrony. We use an example that demonstrates how to solve our impulsive ODE model. We nondimensionalize our model and transform it into a discrete-time model. We end with a stability analysis.

3.1 Model Derivation

We model a specialist consumer and its resource that both enter a dormant state in the winter, called their winter resting period (WRP). When environmental conditions turn favourable in the spring, the species re-enter their active states [37]. The start of the WRP is called the *immergence time* and the end is called the *emergence time* [45]. These times are expected to change with climate change, but the shift in timing may not align for interacting species, resulting in phenological asynchrony [10, 17, 21]. We incorporate phenology into our model by explicitly including the immergence and emergence times for both species. We let the consumer and resource have different active and dormant periods of the year. In doing so, we are able to analyze the effects of phenological asynchrony on the consumer–resource dynamics.

We build on the model by Pachepsky et al. [35], but extend it such that it includes active and dormant periods for the consumer and resource, which are determined by their emergence and immergence times. The consumer and resource only interact when both are active. We model a consumer that is a discrete breeder who reproduces in a "birth pulse" at the consumer emergence time. In contrast, the resource is a continuous breeder who reproduces throughout its active season. When the resource is active, it grows logistically, and when it is dormant, it decays exponentially. Whether the consumer is active or dormant, it decays exponentially, but the rates at which it decays may differ. When the consumer and resource are both active, the consumer feeds on the resource at a linear rate and stores any energy accumulated. The accumulated energy is used in its entirety for reproduction when the consumer birth pulse occurs.

We denote the length of a year by T with $t \in [0, T)$ as the time within a year. We assume

that time equal to zero corresponds to January 1st. The emergence times of the consumer and resource are denoted by T_c and T_f, respectively; the corresponding immergence times by $\hat{T}_c$ and $\hat{T}_f$. We assume that there is a time period when both species are active simultaneously; i.e., $\min(\hat{T}_f, \hat{T}_c) > \max(T_f, T_c)$. Depending on the immergence and emergence times, we get four possible yearly scenarios; see Figure 3.1. Each scenario has a two-letter name, where the first letter indicates the species that emerges first and the second indicates the species that immerges first. The four scenarios are:

1. FC: Resource has an earlier emergence time and consumer has an earlier immergence time.
2. FF: Resource has earlier emergence and immergence times.
3. CC: Consumer has earlier emergence and immergence times.
4. CF: Consumer has an earlier emergence time and resource has an earlier immergence time.

We now present the equations for each of the distinct periods shown in Figure 3.1. Our model derivation closely follows the derivation by Pachepsky et al. [35], with the addition of the consumer and resource WRPs. We let F denote the resource density, C the consumer density and B the total amount of resource consumed per consumer. Our model variables and parameters, as well as their meanings, are summarized in Table 3.1.

The period when both the consumer and resource are dormant is shown in blue. When $0 \leq t < \min(T_f, T_c)$ or $\max(\hat{T}_f, \hat{T}_c) \leq t < T$, the system of ODEs is

$$\frac{\mathrm{d}F}{\mathrm{d}t} = -g_f F, \qquad \frac{\mathrm{d}C}{\mathrm{d}t} = -g_c C, \qquad \frac{\mathrm{d}B}{\mathrm{d}t} = 0, \tag{3.1.1}$$

where g_f and g_c are the death rates of the dormant resource and consumer, respectively.

The period when only the resource is active is shown in pink. When $T_f \leq t < T_c$ or $\hat{T}_c \leq t < \hat{T}_f$, the system of ODEs is

$$\frac{\mathrm{d}F}{\mathrm{d}t} = rF\left(1 - \frac{F}{K}\right), \qquad \frac{\mathrm{d}C}{\mathrm{d}t} = -g_c C, \qquad \frac{\mathrm{d}B}{\mathrm{d}t} = 0, \tag{3.1.2}$$

where r and K are the resource intrinsic growth rate and carrying capacity, respectively.

The period when only the consumer is active is shown in orange. When $T_c < t < T_f$ or $\hat{T}_f \leq t < \hat{T}_c$, the system of ODEs is

$$\frac{\mathrm{d}F}{\mathrm{d}t} = -g_f F, \qquad \frac{\mathrm{d}C}{\mathrm{d}t} = -mC, \qquad \frac{\mathrm{d}B}{\mathrm{d}t} = 0, \tag{3.1.3}$$

where m is the death rate of the active consumer.

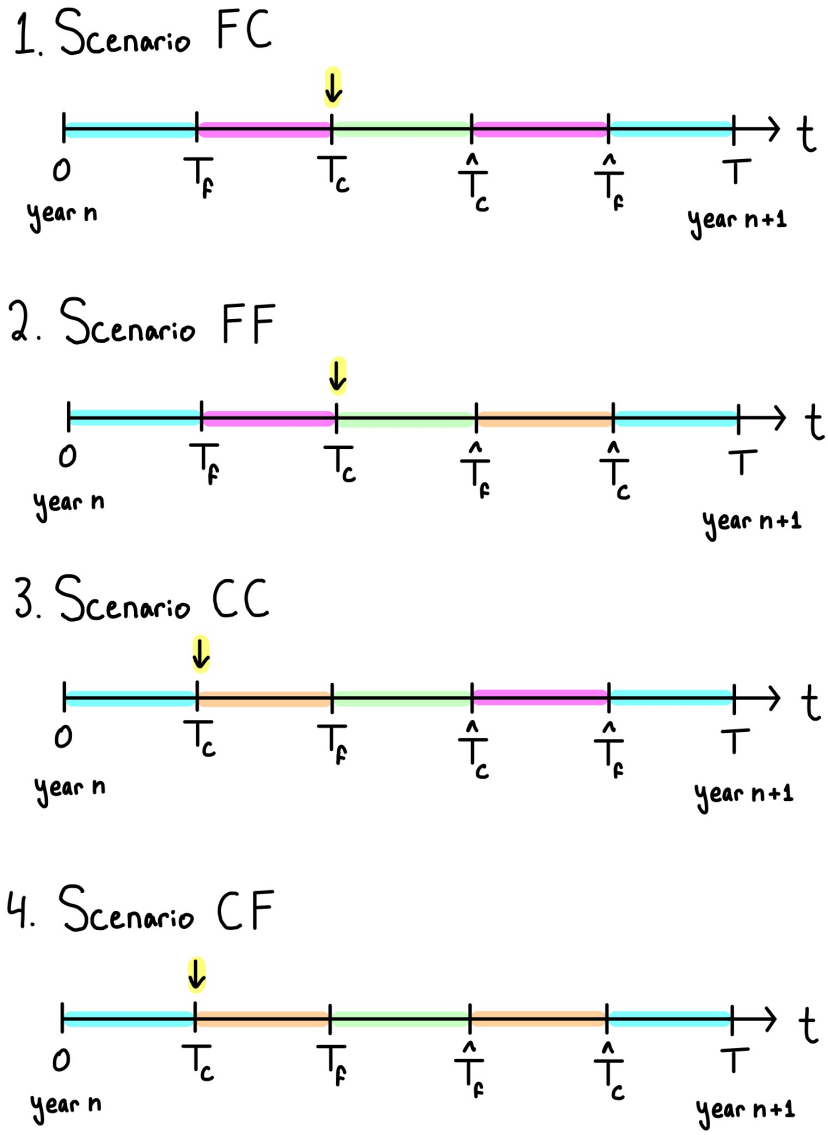

Figure 3.1: The four possible yearly scenarios. The blue period indicates the time when both the consumer and resource are dormant. The pink period indicates when only the resource is active. The orange period indicates when only the consumer is active. The green period indicates when both are active. These distinct periods of time do not overlap. The yellow arrow indicates the consumer birth pulse.

The period when both the consumer and resource are active is shown in green. In this period, we use the same system of ODEs as Pachepsky et al. [35]. When $\max(T_f, T_c) \le t < \min(\hat{T}_f, \hat{T}_c)$, the system of ODEs is

$$\frac{\mathrm{d}F}{\mathrm{d}t} = rF\left(1 - \frac{F}{K}\right) - aFC, \qquad \frac{\mathrm{d}C}{\mathrm{d}t} = -mC, \qquad \frac{\mathrm{d}B}{\mathrm{d}t} = aF, \tag{3.1.4}$$

where a is the consumer consumption rate.

Finally, the consumer birth pulse occurs at the consumer emergence time (T_c), as shown by the yellow arrow in Figure 3.1. When $t = T_c$, we have

$$F(T_c) = F(T_c^-), \qquad C(T_c) = [qB(T_c^-) + 1]C(T_c^-), \qquad B(T_c) = 0, \tag{3.1.5}$$

where q is the consumer conversion efficiency.

To complete the model description, we must define initial conditions (ICs) for each period. With the exception of when the consumer birth pulse occurs, all solutions are continuous, because the transition between periods is instantaneous. Therefore, when a period does not start directly following the consumer birth pulse, the ICs for the current period equal the final conditions from the preceding period. If a period does start directly following the consumer birth pulse, then its ICs are given by the expressions in (3.1.5).

The dimensional model is composed of (3.1.1)–(3.1.5). As we demonstrated in Subsection 2.1.3 with a simple single-species model, we can turn our impulsive ODE model into a discrete-time model by taking its solution map for a fixed time. The process of deriving the solution maps for our model is shown in Section 3.2 and Subsection 3.4.1.

3.2 Working Through an Example

We now solve our impulsive ODE model for Scenario FF; see Figure 3.1. The other three yearly scenarios follow similarly.

We begin with considering the first blue period ($0 \le t < T_f$), which is when both the consumer and resource are dormant. For this period, we solve (3.1.1), using the ICs $F(0)$, $C(0)$ and $B(0)$ to get

$$F(t) = F(0)\,\mathrm{e}^{-g_f t}, \qquad C(t) = C(0)\,\mathrm{e}^{-g_c t}, \qquad B(t) = B(0). \tag{3.2.1}$$

At the end of the first blue period, we have

$$F(T_f^-) = F(0)\,\mathrm{e}^{-g_f T_f}, \qquad C(T_f^-) = C(0)\,\mathrm{e}^{-g_c T_f}, \qquad B(T_f^-) = B(0). \tag{3.2.2}$$

Next, we consider the pink period ($T_f \le t < T_c$), which is when only the resource is active. For this period, we solve (3.1.2), using the ICs from (3.2.2). The resource equation in (3.1.2) is the logistic equation, which we showed how to solve in Subsection 2.1.3. We get

$$F(t) = \frac{K}{1 + \mathrm{e}^{r(T_f - t)}\left(\frac{K}{F(T_f)} - 1\right)}, \qquad C(t) = C(T_f)\,\mathrm{e}^{g_c(T_f - t)}, \qquad B(t) = B(T_f). \tag{3.2.3}$$

Variable	Definition	Units
t	time within a year	year
F	resource density	(resource amount)/area
C	consumer density	(consumer amount)/area
B	total amount of resource consumed per consumer	(resource amount)/(consumer amount)
Parameter	**Definition**	**Units**
T	length of a year	year
T_f	resource emergence time	year
T_c	consumer emergence time	year
$\hat{T}_f$	resource immergence time	year
$\hat{T}_c$	consumer immergence time	year
r	resource intrinsic growth rate	1/year
K	resource carrying capacity	(resource amount)/area
g_f	dormant resource death rate	1/year
a	consumer consumption rate	area/[(consumer amount)·year]
m	active consumer death rate	1/year
g_c	dormant consumer death rate	1/year
q	consumer conversion efficiency	(consumer amount)/(resource amount)

Table 3.1: Variables and parameters used in the dimensional model (3.1.1)–(3.1.5).

At the end of the pink period, we have

$$F(T_c^-) = \frac{K}{1 + \mathrm{e}^{r(T_f - T_c)}\left(\frac{K}{F(T_f)} - 1\right)}, \quad C(T_c^-) = C(T_f)\,\mathrm{e}^{g_c(T_f - T_c)}, \quad B(T_c^-) = B(T_f). \tag{3.2.4}$$

Now we consider the green period ($T_c < t < \hat{T}_f$), which is when both the consumer and resource are active. For this period, we solve (3.1.4). Since the consumer birth pulse occurs directly before the start of this period, the ICs are from (3.1.5). We solve the consumer equation in (3.1.4) and get

$$C(t) = C(T_c)\,\mathrm{e}^{m(T_c - t)}. \tag{3.2.5}$$

Substituting this into the resource equation in (3.1.4) yields

$$\frac{\mathrm{d}F}{\mathrm{d}t} = rF\left(1 - \frac{F}{K}\right) - aFC(T_c)\,\mathrm{e}^{m(T_c - t)}. \tag{3.2.6}$$

By recognizing that (3.2.6) is a Bernoulli differential equation, we can solve it in a similar way to how we solved the logistic equation in Subsection 2.1.3. By multiplying each term by $-F^{-2}$ and letting $y = F^{-1}$, we rewrite (3.2.6) as

$$\frac{\mathrm{d}y}{\mathrm{d}t} + (r - aC(T_c)\,\mathrm{e}^{m(T_c - t)})y = \frac{r}{K}. \tag{3.2.7}$$

This is a first-order non-homogeneous linear differential equation, which can be solved using an integrating factor. We obtain

$$y(t) = \mathrm{e}^{-rt-\frac{aC(T_c)}{m}\mathrm{e}^{m(T_c-t)}}\left(\frac{r}{K}\int_{T_c}^{t}\mathrm{e}^{rs+\frac{aC(T_c)}{m}\mathrm{e}^{m(T_c-s)}}\,\mathrm{d}s + \frac{\mathrm{e}^{rT_c+\frac{aC(T_c)}{m}}}{F(T_c)}\right). \tag{3.2.8}$$

We now use our substitution of $y = F^{-1}$ and get

$$F(t) = \frac{K\,\mathrm{e}^{rt+\frac{aC(T_c)}{m}(\mathrm{e}^{m(T_c-t)}-1)}}{r\int_{T_c}^{t}\mathrm{e}^{rs+\frac{aC(T_c)}{m}(\mathrm{e}^{m(T_c-s)}-1)}\,\mathrm{d}s + \frac{K\,\mathrm{e}^{rT_c}}{F(T_c)}}. \tag{3.2.9}$$

Lastly, we solve the equation for the consumed resource in (3.1.4) to get

$$B(t) = a\int_{T_c}^{t}F(s)\,\mathrm{d}s + B(T_c). \tag{3.2.10}$$

Using (3.2.5), (3.2.9), (3.2.10) and recalling that, as stated in (3.1.5), $B(T_c) = 0$, at the end of the green period, we have

$$F(\hat{T}_f^-) = \frac{K\,\mathrm{e}^{r\hat{T}_f+\frac{aC(T_c)}{m}(\mathrm{e}^{m(T_c-\hat{T}_f)}-1)}}{r\int_{T_c}^{\hat{T}_f}\mathrm{e}^{rs+\frac{aC(T_c)}{m}(\mathrm{e}^{m(T_c-s)}-1)}\,\mathrm{d}s + \frac{K\,\mathrm{e}^{rT_c}}{F(T_c)}},$$

$$C(\hat{T}_f^-) = C(T_c)\,\mathrm{e}^{m(T_c-\hat{T}_f)}, \tag{3.2.11}$$

$$B(\hat{T}_f^-) = a\int_{T_c}^{\hat{T}_f}\frac{K\,\mathrm{e}^{rt+\frac{aC(T_c)}{m}(\mathrm{e}^{m(T_c-t)}-1)}}{r\int_{T_c}^{t}\mathrm{e}^{rs+\frac{aC(T_c)}{m}(\mathrm{e}^{m(T_c-s)}-1)}\,\mathrm{d}s + \frac{K\,\mathrm{e}^{rT_c}}{F(T_c)}}\,\mathrm{d}t.$$

Next, we consider the orange period ($\hat{T}_f \le t < \hat{T}_c$), which is when only the consumer is active. For this period, we solve (3.1.3), using the ICs from (3.2.11). After solving, we get

$$F(t) = F(\hat{T}_f)\,\mathrm{e}^{g_f(\hat{T}_f-t)}, \qquad C(t) = C(\hat{T}_f)\,\mathrm{e}^{m(\hat{T}_f-t)}, \qquad B(t) = B(\hat{T}_f). \tag{3.2.12}$$

At the end of the orange period, we have

$$F(\hat{T}_c^-) = F(\hat{T}_f)\,\mathrm{e}^{g_f(\hat{T}_f-\hat{T}_c)}, \quad C(\hat{T}_c^-) = C(\hat{T}_f)\,\mathrm{e}^{m(\hat{T}_f-\hat{T}_c)}, \quad B(\hat{T}_c^-) = B(\hat{T}_f). \tag{3.2.13}$$

Finally, we consider the second blue period ($\hat{T}_c \le t < T$), which is when both the consumer and resource are dormant. For this period, we solve (3.1.1), using the ICs from (3.2.13). After solving, we get

$$F(t) = F(\hat{T}_c)\,\mathrm{e}^{g_f(\hat{T}_c-t)}, \qquad C(t) = C(\hat{T}_c)\,\mathrm{e}^{g_c(\hat{T}_c-t)}, \qquad B(t) = B(\hat{T}_c). \tag{3.2.14}$$

At the end of the second blue period, we have

$$F(T^-) = F(\hat{T}_c)\,\mathrm{e}^{g_f(\hat{T}_c - T)}, \qquad C(T^-) = C(\hat{T}_c)\,\mathrm{e}^{g_c(\hat{T}_c - T)}, \qquad B(T^-) = B(\hat{T}_c). \tag{3.2.15}$$

Recalling that with the exception of when the consumer birth pulse occurs, all solutions are continuous, we substitute (3.1.5), (3.2.2), (3.2.4), (3.2.11) and (3.2.13) into (3.2.15). This gives us explicit expressions for the resource density, consumer density and total amount of resource consumed per consumer at the end of the year for Scenario FF. The expressions in (3.2.15) are deceptively simple. When we make the required substitutions into (3.2.15) and simplify, we get

$$F(T^-) = \frac{K\,\mathrm{e}^{r\hat{T}_f + \frac{aC(0)}{m}[qB(0)+1]\,\mathrm{e}^{-g_cT_c}(\mathrm{e}^{m(T_c-\hat{T}_f)}-1) + g_f(\hat{T}_f - T)}}{r\int_{T_c}^{\hat{T}_f} \mathrm{e}^{rs + \frac{aC(0)}{m}[qB(0)+1]\,\mathrm{e}^{-g_cT_c}(\mathrm{e}^{m(T_c-s)}-1)}\,\mathrm{d}s + \mathrm{e}^{rT_c} + \mathrm{e}^{rT_f}\left(\frac{K\,\mathrm{e}^{g_fT_f}}{F(0)} - 1\right)},$$

$$C(T^-) = [qB(0)+1]C(0)\,\mathrm{e}^{m(T_c-\hat{T}_c) + g_c(\hat{T}_c - T_c - T)},$$

$$B(T^-) = \int_{T_c}^{\hat{T}_f} \frac{aK\,\mathrm{e}^{rt + \frac{aC(0)}{m}[qB(0)+1]\,\mathrm{e}^{-g_cT_c}(\mathrm{e}^{m(T_c-t)}-1)}}{r\int_{T_c}^{t} \mathrm{e}^{rs + \frac{aC(0)}{m}[qB(0)+1]\,\mathrm{e}^{-g_cT_c}(\mathrm{e}^{m(T_c-s)}-1)}\,\mathrm{d}s + \mathrm{e}^{rT_c} + \mathrm{e}^{rT_f}\left(\frac{K\,\mathrm{e}^{g_fT_f}}{F(0)} - 1\right)}\,\mathrm{d}t. \tag{3.2.16}$$

Figure 3.2 shows an example of a solution for Scenario FF over 200 years, with the last 5 years displayed. Throughout this thesis, the emergence and immergence times selected for simulations are always fractions with denominator 12. When the year is one unit long, which we will later achieve by nondimensionalizing the model (see Section 3.3), multiples of $\frac{1}{12}$ denote the months of the year. For example, $t = \frac{2}{12}$ is approximately March 1$^{\text{st}}$, since $t = 0$ is January 1$^{\text{st}}$.

In this section, we chose the ICs of the year to be given at $t = 0$. If we instead choose $t = T_c$, so that after one year, $t = T + T_c$, the explicit expressions for the solutions become simpler. We demonstrate this in Subsection 3.4.1. If we vary the time at which the ICs of the year are given (the census time), then we must transform the ICs accordingly to ensure that the two resulting systems are dynamically equivalent [28].

3.3 Nondimensionalization of the Model

We nondimensionalize our model to reduce the number of parameters, thereby simplifying our calculations. We introduce the dimensionless variables

$$f = \frac{F}{\hat{F}}, \qquad c = \frac{C}{\hat{C}}, \qquad b = \frac{B}{\hat{B}}, \qquad s = \frac{t}{\hat{t}}, \tag{3.3.1}$$

which are the scaled resource density, scaled consumer density, scaled total amount of resource consumed per consumer and scaled time within a year, respectively. We choose the

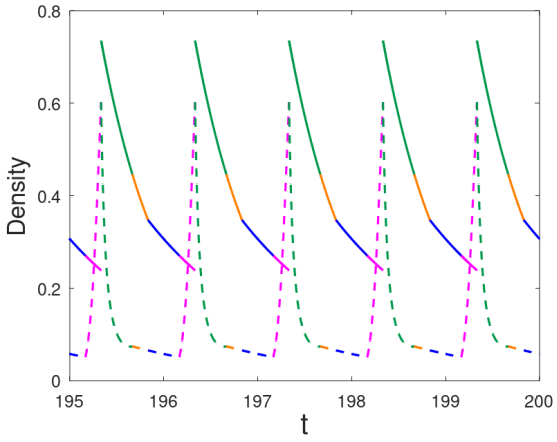

Figure 3.2: Example of a solution for Scenario FF. The colours correspond to those in Figure 3.1. The dashed (solid) line represents the resource (consumer) density. Time (t) is measured in years and the densities (F and C) are measured in resource or consumer amount per area. The parameters are $T_f = \frac{2}{12}$, $T_c = \frac{4}{12}$, $\hat{T}_f = \frac{8}{12}$, $\hat{T}_c = \frac{10}{12}$, $T = 1$, $a = 40$, $m = 1.5$, $g_f = 0.75 = g_c$, $r = 20$, $K = 1$, $q = 1$; see Table 3.1 for the units of the parameters.

units to be

$$\hat{F} = K, \qquad \hat{C} = Kq, \qquad \hat{B} = \frac{1}{q}, \qquad \hat{t} = T. \tag{3.3.2}$$

We now present the equations for the nondimensional model. The different variables and parameters, as well as their meanings, for the nondimensional model are shown in Table 3.2. Time equal to zero still corresponds to January 1$^{\text{st}}$, but a year is now of length one and $s \in [0, 1)$ is the time within a year. The scaled emergence and immergence times are

$$\tau_f = \frac{T_f}{T}, \qquad \tau_c = \frac{T_c}{T}, \qquad \hat{\tau}_f = \frac{\hat{T}_f}{T}, \qquad \hat{\tau}_c = \frac{\hat{T}_c}{T}. \tag{3.3.3}$$

The period when both the consumer and resource are dormant is shown in blue in Figure 3.1. In the nondimensional model, this occurs when $0 \leq s < \min(\tau_f, \tau_c)$ or $\max(\hat{\tau}_f, \hat{\tau}_c) \leq s < 1$. When this occurs, the system of ODEs is

$$\frac{\mathrm{d}f}{\mathrm{d}s} = -\gamma_f f, \qquad \frac{\mathrm{d}c}{\mathrm{d}s} = -\gamma_c c, \qquad \frac{\mathrm{d}b}{\mathrm{d}s} = 0, \tag{3.3.4}$$

where $\gamma_f = g_f T$ and $\gamma_c = g_c T$ are the scaled death rates of the dormant resource and consumer, respectively.

The period when only the resource is active is shown in pink. In the nondimensional model, this occurs when $\tau_f \leq s < \tau_c$ or $\hat{\tau}_c \leq s < \hat{\tau}_f$. When this occurs, the system of ODEs is

$$\frac{\mathrm{d}f}{\mathrm{d}s} = \rho f(1 - f), \qquad \frac{\mathrm{d}c}{\mathrm{d}s} = -\gamma_c c, \qquad \frac{\mathrm{d}b}{\mathrm{d}s} = 0, \tag{3.3.5}$$

where $\rho = rT$ is the scaled resource intrinsic growth rate.

The period when only the consumer is active is shown in orange. In the nondimensional model, this occurs when $\tau_c < s < \tau_f$ or $\hat{\tau}_f \leq s < \hat{\tau}_c$. When this occurs, the system of ODEs is

$$\frac{\mathrm{d}f}{\mathrm{d}s} = -\gamma_f f, \qquad \frac{\mathrm{d}c}{\mathrm{d}s} = -\mu c, \qquad \frac{\mathrm{d}b}{\mathrm{d}s} = 0, \tag{3.3.6}$$

where $\mu = mT$ is the scaled death rate of the active consumer.

The period when both the consumer and resource are active is shown in green. In the nondimensional model, this occurs when $\max(\tau_f, \tau_c) \leq s < \min(\hat{\tau}_f, \hat{\tau}_c)$. When this occurs, the system of ODEs is

$$\frac{\mathrm{d}f}{\mathrm{d}s} = \rho f(1-f) - \alpha f c, \qquad \frac{\mathrm{d}c}{\mathrm{d}s} = -\mu c, \qquad \frac{\mathrm{d}b}{\mathrm{d}s} = \alpha f, \tag{3.3.7}$$

where $\alpha = aqKT$ is the scaled consumer consumption rate.

The consumer birth pulse is shown as a yellow arrow in Figure 3.1. For the nondimensional model, this occurs when $s = \tau_c$. The discrete equations that model the consumer birth pulse are

$$f(\tau_c) = f(\tau_c^-), \qquad c(\tau_c) = [b(\tau_c^-) + 1]c(\tau_c^-), \qquad b(\tau_c) = 0. \tag{3.3.8}$$

The ICs for any periods that directly follow the consumer birth pulse are the equations in (3.3.8). Otherwise, the ICs for the current period equal the final conditions from the preceding period. The nondimensional model is composed of (3.3.4)–(3.3.8). We will continue to refer to ρ, α, μ, γ_c and γ_f as rates.

3.4 Analysis of the Model

3.4.1 Derivation of the Discrete Solution Maps

We transform our impulsive ODE model into a discrete-time model by taking its solution map for a fixed time. We demonstrated how to do this transformation for a simple single-species model in Subsection 2.1.3. We select a census time at which we record the densities each year. Our solution maps will relate the densities at the census time of one year to that of the next year. At the end of Section 3.2, we found complicated expressions for the solutions at the end of the year for Scenario FF. This demonstrates that a census time of zero can result in complicated solution maps. If we instead set the census time to be directly following the consumer birth pulse, the expressions become much simpler. This is because the amount of resource consumed per consumer is set to zero at the birth pulse, so it does not require a separate variable in the discrete map. Moving forward, we will use the nondimensional model (3.3.4)–(3.3.8) and set the census time to be immediately after the consumer birth pulse.

Variable	Definition	Defining expression
s	scaled time within a year	$s = t/T$
f	scaled resource density	$f = F/K$
c	scaled consumer density	$c = C/(Kq)$
b	scaled total amount of resource consumed per consumer	$b = qB$
Parameter	**Definition**	**Defining expression**
τ_f	scaled resource emergence time	$\tau_f = T_f/T$
τ_c	scaled consumer emergence time	$\tau_c = T_c/T$
$\hat{\tau}_f$	scaled resource immergence time	$\hat{\tau}_f = \hat{T}_f/T$
$\hat{\tau}_c$	scaled consumer immergence time	$\hat{\tau}_c = \hat{T}_c/T$
ρ	scaled resource intrinsic growth rate	$\rho = rT$
γ_f	scaled dormant resource death rate	$\gamma_f = g_f T$
α	scaled consumer consumption rate	$\alpha = aKqT$
μ	scaled active consumer death rate	$\mu = mT$
γ_c	scaled dormant consumer death rate	$\gamma_c = g_c T$

Table 3.2: Variables and parameters used in the nondimensional model (3.3.4)–(3.3.8).

For the nondimensional model, each year is one unit long and is represented by an integer n. We denote

$$v_n = f(\tau_c^+) \tag{3.4.1}$$

and

$$w_n = c(\tau_c^+) \tag{3.4.2}$$

as, respectively, the initial resource density and consumer density for year n.

We explicitly derive the solution map relating (v_{n+1}, w_{n+1}) to (v_n, w_n) for Scenario FF; see Figure 3.1. We begin with considering the green period ($\tau_c < s < \hat{\tau}_f$), which is when both the consumer and resource are active. For this period, we solve (3.3.7), with ICs (3.4.1)–(3.4.2) and

$$b(\tau_c^+) = 0. \tag{3.4.3}$$

After solving and simplifying, we get

$$\begin{aligned} f(s) &= \frac{v_n \, \mathrm{e}^{\rho(s-\tau_c)+\frac{\alpha w_n}{\mu}(\mathrm{e}^{\mu(\tau_c-s)}-1)}}{\rho v_n \int_{\tau_c}^{s} \mathrm{e}^{\rho(t-\tau_c)+\frac{\alpha w_n}{\mu}(\mathrm{e}^{\mu(\tau_c-t)}-1)} \, \mathrm{d}t + 1}, \\ c(s) &= w_n \, \mathrm{e}^{\mu(\tau_c-s)}, \\ b(s) &= \alpha \int_{\tau_c}^{s} f(t) \, \mathrm{d}t + b(\tau_c). \end{aligned} \tag{3.4.4}$$

At the end of the green period, we have

$$f(\hat{\tau}_f^-) = \frac{v_n \, \mathrm{e}^{\rho(\hat{\tau}_f - \tau_c) + \frac{\alpha w_n}{\mu}(\mathrm{e}^{\mu(\tau_c - \hat{\tau}_f)} - 1)}}{\rho v_n \int_{\tau_c}^{\hat{\tau}_f} \mathrm{e}^{\rho(t-\tau_c) + \frac{\alpha w_n}{\mu}(\mathrm{e}^{\mu(\tau_c - t)} - 1)} \, \mathrm{d}t + 1},$$

$$c(\hat{\tau}_f^-) = w_n \, \mathrm{e}^{\mu(\tau_c - \hat{\tau}_f)}, \tag{3.4.5}$$

$$b(\hat{\tau}_f^-) = \alpha v_n \int_{\tau_c}^{\hat{\tau}_f} \frac{\mathrm{e}^{\rho(s-\tau_c) + \frac{\alpha w_n}{\mu}(\mathrm{e}^{\mu(\tau_c - s)} - 1)}}{\rho v_n \int_{\tau_c}^{s} \mathrm{e}^{\rho(t-\tau_c) + \frac{\alpha w_n}{\mu}(\mathrm{e}^{\mu(\tau_c - t)} - 1)} \, \mathrm{d}t + 1} \, \mathrm{d}s.$$

Next, we consider the orange period ($\hat{\tau}_f \le s < \hat{\tau}_c$), which is when only the consumer is active. For this period, we solve (3.3.6), using the ICs from (3.4.5), and get

$$f(s) = f(\hat{\tau}_f) \, \mathrm{e}^{\gamma_f(\hat{\tau}_f - s)}, \qquad c(s) = c(\hat{\tau}_f) \, \mathrm{e}^{\mu(\hat{\tau}_f - s)}, \qquad b(s) = b(\hat{\tau}_f). \tag{3.4.6}$$

At the end of the orange period, we have

$$f(\hat{\tau}_c^-) = f(\hat{\tau}_f) \, \mathrm{e}^{\gamma_f(\hat{\tau}_f - \hat{\tau}_c)}, \qquad c(\hat{\tau}_c^-) = c(\hat{\tau}_f) \, \mathrm{e}^{\mu(\hat{\tau}_f - \hat{\tau}_c)}, \qquad b(\hat{\tau}_c^-) = b(\hat{\tau}_f). \tag{3.4.7}$$

Now we consider the blue period ($\hat{\tau}_c \le s < \tau_f + 1$), which is when both the consumer and resource are dormant. For this period, we solve (3.3.4), using the ICs from (3.4.7). At the end of the blue period, we have

$$\begin{aligned} f((\tau_f + 1)^-) &= f(\hat{\tau}_c) \, \mathrm{e}^{\gamma_f(\hat{\tau}_c - \tau_f - 1)}, \\ c((\tau_f + 1)^-) &= c(\hat{\tau}_c) \, \mathrm{e}^{\gamma_c(\hat{\tau}_c - \tau_f - 1)}, \\ b((\tau_f + 1)^-) &= b(\hat{\tau}_c). \end{aligned} \tag{3.4.8}$$

Next, we consider the pink period ($\tau_f + 1 \le s < \tau_c + 1$), which is when only the resource is active. For this period, we solve (3.3.5), using the ICs from (3.4.8), and get

$$f(s) = \frac{1}{1 + \mathrm{e}^{\rho(\tau_f + 1 - s)}\left(\frac{1}{f(\tau_f + 1)} - 1\right)}, \quad c(s) = c(\tau_f + 1) \, \mathrm{e}^{\gamma_c(\tau_f + 1 - s)}, \quad b(s) = b(\tau_f + 1). \tag{3.4.9}$$

At the end of the pink period, we have

$$\begin{aligned} f((\tau_c + 1)^-) &= \frac{1}{1 + \mathrm{e}^{\rho(\tau_f - \tau_c)}\left(\frac{1}{f(\tau_f + 1)} - 1\right)}, \\ c((\tau_c + 1)^-) &= c(\tau_f + 1) \, \mathrm{e}^{\gamma_c(\tau_f - \tau_c)}, \\ b((\tau_c + 1)^-) &= b(\tau_f + 1). \end{aligned} \tag{3.4.10}$$

Finally, we consider the yellow arrow. This is the consumer birth pulse. At this time, we use (3.3.8), but with $s = \tau_c + 1$. The solution map relating (v_{n+1}, w_{n+1}) to (v_n, w_n) for Scenario FF is

$$\begin{aligned} v_{n+1} &= \frac{1}{1 + \mathrm{e}^{\rho(\tau_f - \tau_c)} \left[\frac{\rho v_n \int_{\tau_c}^{\hat{\tau}_f} \mathrm{e}^{\rho(t-\tau_c) + \frac{\alpha w_n}{\mu}(\mathrm{e}^{\mu(\tau_c - t)} - 1)} \, \mathrm{d}t + 1}{v_n \, \mathrm{e}^{\rho(\hat{\tau}_f - \tau_c) + \frac{\alpha w_n}{\mu}(\mathrm{e}^{\mu(\tau_c - \hat{\tau}_f)} - 1) + \gamma_f(\hat{\tau}_f - \tau_f - 1)}} - 1 \right]}, \\ w_{n+1} &= \left[\alpha v_n \int_{\tau_c}^{\hat{\tau}_f} \frac{\mathrm{e}^{\rho(s-\tau_c) + \frac{\alpha w_n}{\mu}(\mathrm{e}^{\mu(\tau_c - s)} - 1)}}{\rho v_n \int_{\tau_c}^{s} \mathrm{e}^{\rho(t-\tau_c) + \frac{\alpha w_n}{\mu}(\mathrm{e}^{\mu(\tau_c - t)} - 1)} \, \mathrm{d}t + 1} \, \mathrm{d}s + 1 \right] \\ &\quad \times w_n \, \mathrm{e}^{\mu(\tau_c - \hat{\tau}_c) + \gamma_c(\hat{\tau}_c - \tau_c - 1)}. \end{aligned} \tag{3.4.11}$$

We use similar methods to get the solution maps for the other three scenarios depicted in Figure 3.1. For Scenario FC ($\tau_f < \tau_c$ and $\hat{\tau}_c < \hat{\tau}_f$), we obtain the solution map

$$\begin{aligned} v_{n+1} &= \frac{E}{E + \mathrm{e}^{\rho(\tau_f - \tau_c)} \left[1 + \mathrm{e}^{\rho(\hat{\tau}_c - \hat{\tau}_f)} \left(\frac{\rho v_n \int_{\tau_c}^{\hat{\tau}_c} \mathrm{e}^{\rho(t-\tau_c) + \frac{\alpha w_n}{\mu}(\mathrm{e}^{\mu(\tau_c - t)} - 1)} \, \mathrm{d}t + 1}{v_n \, \mathrm{e}^{\rho(\hat{\tau}_c - \tau_c) + \frac{\alpha w_n}{\mu}(\mathrm{e}^{\mu(\tau_c - \hat{\tau}_c)} - 1)}} - 1 \right) - E \right]}, \\ w_{n+1} &= \left[\alpha v_n \int_{\tau_c}^{\hat{\tau}_c} \frac{\mathrm{e}^{\rho(s-\tau_c) + \frac{\alpha w_n}{\mu}(\mathrm{e}^{\mu(\tau_c - s)} - 1)}}{\rho v_n \int_{\tau_c}^{s} \mathrm{e}^{\rho(t-\tau_c) + \frac{\alpha w_n}{\mu}(\mathrm{e}^{\mu(\tau_c - t)} - 1)} \, \mathrm{d}t + 1} \, \mathrm{d}s + 1 \right] \\ &\quad \times w_n \, \mathrm{e}^{\mu(\tau_c - \hat{\tau}_c) + \gamma_c(\hat{\tau}_c - \tau_c - 1)}, \end{aligned} \tag{3.4.12}$$

where $E = \mathrm{e}^{\gamma_f(\hat{\tau}_f - \tau_f - 1)}$. For Scenario CC ($\tau_c < \tau_f$ and $\hat{\tau}_c < \hat{\tau}_f$), we obtain the solution map

$$\begin{aligned} v_{n+1} &= \frac{\mathrm{e}^{\gamma_f(\hat{\tau}_f - \tau_c - 1)}}{1 + \mathrm{e}^{\rho(\hat{\tau}_c - \hat{\tau}_f)} \left[\frac{\rho v_n \int_{\tau_f}^{\hat{\tau}_c} \mathrm{e}^{\rho(t-\tau_f) + \frac{\alpha w_n}{\mu} \mathrm{e}^{\mu(\tau_c - \tau_f)}(\mathrm{e}^{\mu(\tau_f - t)} - 1) + \gamma_f(\tau_c - \tau_f)} \, \mathrm{d}t + 1}{v_n \, \mathrm{e}^{\rho(\hat{\tau}_c - \tau_f) + \frac{\alpha w_n}{\mu} \mathrm{e}^{\mu(\tau_c - \tau_f)}(\mathrm{e}^{\mu(\tau_f - \hat{\tau}_c)} - 1) + \gamma_f(\tau_c - \tau_f)}} - 1 \right]}, \\ w_{n+1} &= \left[\alpha v_n \int_{\tau_f}^{\hat{\tau}_c} \frac{\mathrm{e}^{\rho(s-\tau_f) + \frac{\alpha w_n}{\mu} \mathrm{e}^{\mu(\tau_c - \tau_f)}(\mathrm{e}^{\mu(\tau_f - s)} - 1) + \gamma_f(\tau_c - \tau_f)}}{\rho v_n \int_{\tau_f}^{s} \mathrm{e}^{\rho(t-\tau_f) + \frac{\alpha w_n}{\mu} \mathrm{e}^{\mu(\tau_c - \tau_f)}(\mathrm{e}^{\mu(\tau_f - t)} - 1) + \gamma_f(\tau_c - \tau_f)} \, \mathrm{d}t + 1} \, \mathrm{d}s + 1 \right] \\ &\quad \times w_n \, \mathrm{e}^{\mu(\tau_c - \hat{\tau}_c) + \gamma_c(\hat{\tau}_c - \tau_c - 1)}. \end{aligned} \tag{3.4.13}$$

For Scenario CF ($\tau_c < \tau_f$ and $\hat{\tau}_f < \hat{\tau}_c$), we obtain the solution map

$$\begin{aligned} v_{n+1} &= \frac{v_n \, \mathrm{e}^{\rho(\hat{\tau}_f - \tau_f) + \frac{\alpha w_n}{\mu} \mathrm{e}^{\mu(\tau_c - \tau_f)}(\mathrm{e}^{\mu(\tau_f - \hat{\tau}_f)} - 1) + \gamma_f(\hat{\tau}_f - \tau_f - 1)}}{\rho v_n \int_{\tau_f}^{\hat{\tau}_f} \mathrm{e}^{\rho(t-\tau_f) + \frac{\alpha w_n}{\mu} \mathrm{e}^{\mu(\tau_c - \tau_f)}(\mathrm{e}^{\mu(\tau_f - t)} - 1) + \gamma_f(\tau_c - \tau_f)} \, \mathrm{d}t + 1}, \\ w_{n+1} &= \left[\alpha v_n \int_{\tau_f}^{\hat{\tau}_f} \frac{\mathrm{e}^{\rho(s-\tau_f) + \frac{\alpha w_n}{\mu} \mathrm{e}^{\mu(\tau_c - \tau_f)}(\mathrm{e}^{\mu(\tau_f - s)} - 1) + \gamma_f(\tau_c - \tau_f)}}{\rho v_n \int_{\tau_f}^{s} \mathrm{e}^{\rho(t-\tau_f) + \frac{\alpha w_n}{\mu} \mathrm{e}^{\mu(\tau_c - \tau_f)}(\mathrm{e}^{\mu(\tau_f - t)} - 1) + \gamma_f(\tau_c - \tau_f)} \, \mathrm{d}t + 1} \, \mathrm{d}s + 1 \right] \\ &\quad \times w_n \, \mathrm{e}^{\mu(\tau_c - \hat{\tau}_c) + \gamma_c(\hat{\tau}_c - \tau_c - 1)}. \end{aligned} \tag{3.4.14}$$

3.4.2 Stability Analysis

We find the equilibrium points of the solution maps from Subsection 3.4.1 and analyze their stability. Since considering all four scenarios would be repetitive, we simplify the model by setting the immergence times of the consumer and resource equal. This results in Scenario FC being equivalent to Scenario FF, as well as Scenario CC being equivalent to Scenario CF. We make this specific simplification because emergence times have received far more attention in the literature than immergence times. This is likely due to the difficulty associated with determining accurate immergence times [10]. We denote the shared immergence time by $\hat{\tau}$. There are now three cases to consider: the consumer has an earlier emergence time, the resource has an earlier emergence time, or they have the same emergence time. We can combine the latter case with either of the two former cases by simply setting $\tau_f = \tau_c$. Since the calculations are simpler when the consumer emerges first, we will consider the following two cases: (i) the consumer has either an earlier or the same emergence time as the resource ($\tau_c \leq \tau_f$), or (ii) the resource has an earlier emergence time ($\tau_c > \tau_f$).

3.4.2.1 Case (i): $\tau_c \leq \tau_f$

We begin with the case where the consumer emergence time is earlier or the same as that of the resource; i.e., Scenarios CC and CF. When $\hat{\tau}_f = \hat{\tau} = \hat{\tau}_c$, the solution maps for Scenarios CC (3.4.13) and CF (3.4.14) both equal

$$v_{n+1} = \frac{v_n \, \mathrm{e}^{\rho(\hat{\tau} - \tau_f) + \frac{\alpha w_n}{\mu} \mathrm{e}^{\mu(\tau_c - \tau_f)}(\mathrm{e}^{\mu(\tau_f - \hat{\tau})} - 1) + \gamma_f(\hat{\tau} - \tau_f - 1)}}{\rho v_n \int_{\tau_f}^{\hat{\tau}} \mathrm{e}^{\rho(t-\tau_f) + \frac{\alpha w_n}{\mu} \mathrm{e}^{\mu(\tau_c - \tau_f)}(\mathrm{e}^{\mu(\tau_f - t)} - 1) + \gamma_f(\tau_c - \tau_f)} \, \mathrm{d}t + 1}, \tag{3.4.15}$$

$$\begin{aligned} w_{n+1} &= \left[\alpha v_n \int_{\tau_f}^{\hat{\tau}} \frac{\mathrm{e}^{\rho(s-\tau_f) + \frac{\alpha w_n}{\mu} \mathrm{e}^{\mu(\tau_c - \tau_f)}(\mathrm{e}^{\mu(\tau_f - s)} - 1) + \gamma_f(\tau_c - \tau_f)}}{\rho v_n \int_{\tau_f}^{s} \mathrm{e}^{\rho(t-\tau_f) + \frac{\alpha w_n}{\mu} \mathrm{e}^{\mu(\tau_c - \tau_f)}(\mathrm{e}^{\mu(\tau_f - t)} - 1) + \gamma_f(\tau_c - \tau_f)} \, \mathrm{d}t + 1} \, \mathrm{d}s + 1 \right] \\ &\quad \times w_n \, \mathrm{e}^{\mu(\tau_c - \hat{\tau}) + \gamma_c(\hat{\tau} - \tau_c - 1)}. \end{aligned} \tag{3.4.16}$$

There exist up to three equilibrium points: when both species are extinct $(0, 0)$, when only the resource is present $(\tilde{v}_c, 0)$, and when the species coexist (v_c, w_c). We require

$\tilde{v}_c, v_c, w_c > 0$. We find explicit expressions for all equilibrium points and analyze their stability.

To find an explicit expression for $\tilde{v}_c$, we set $v_{n+1} = \tilde{v}_c = v_n$ and $w_n = 0$ in (3.4.15). After integrating and simplifying, we obtain

$$\tilde{v}_c = \frac{\mathrm{e}^{\rho(\hat{\tau}-\tau_f)+\gamma_f(\hat{\tau}-\tau_c-1)} - \mathrm{e}^{\gamma_f(\tau_f-\tau_c)}}{\mathrm{e}^{\rho(\hat{\tau}-\tau_f)} - 1}. \tag{3.4.17}$$

We get that $\tilde{v}_c > 0$ if and only if

$$\rho > \frac{\gamma_f(\tau_f - \hat{\tau} + 1)}{\hat{\tau} - \tau_f}. \tag{3.4.18}$$

To find an explicit expression for (v_c, w_c), we set $v_{n+1} = v_c = v_n$ and $w_{n+1} = w_c = w_n$ in (3.4.15)–(3.4.16). We first determine the expression for v_c in terms of w_c:

$$v_c = \frac{\mathrm{e}^{\rho(\hat{\tau}-\tau_f)+\frac{\alpha w_c}{\mu}\mathrm{e}^{\mu(\tau_c-\tau_f)}(\mathrm{e}^{\mu(\tau_f-\hat{\tau})}-1)+\gamma_f(\hat{\tau}-\tau_f-1)} - 1}{\rho\int_{\tau_f}^{\hat{\tau}} \mathrm{e}^{\rho(t-\tau_f)+\frac{\alpha w_c}{\mu}\mathrm{e}^{\mu(\tau_c-\tau_f)}(\mathrm{e}^{\mu(\tau_f-t)}-1)+\gamma_f(\tau_c-\tau_f)}\,\mathrm{d}t}. \tag{3.4.19}$$

Using (3.4.16), we find that

$$\frac{\mathrm{e}^{\mu(\hat{\tau}-\tau_c)+\gamma_c(\tau_c-\hat{\tau}+1)} - 1}{\alpha} = \int_{\tau_f}^{\hat{\tau}} \frac{\mathrm{e}^{\rho(s-\tau_f)+\frac{\alpha w_c}{\mu}\mathrm{e}^{\mu(\tau_c-\tau_f)}(\mathrm{e}^{\mu(\tau_f-s)}-1)+\gamma_f(\tau_c-\tau_f)}}{\rho\int_{\tau_f}^{s} \mathrm{e}^{\rho(t-\tau_f)+\frac{\alpha w_c}{\mu}\mathrm{e}^{\mu(\tau_c-\tau_f)}(\mathrm{e}^{\mu(\tau_f-t)}-1)+\gamma_f(\tau_c-\tau_f)}\,\mathrm{d}t + \frac{1}{v_c}}\,\mathrm{d}s \tag{3.4.20}$$

$$= \frac{1}{\rho}\ln\left(v_c\rho\int_{\tau_f}^{\hat{\tau}} \mathrm{e}^{\rho(t-\tau_f)+\frac{\alpha w_c}{\mu}\mathrm{e}^{\mu(\tau_c-\tau_f)}(\mathrm{e}^{\mu(\tau_f-t)}-1)+\gamma_f(\tau_c-\tau_f)}\,\mathrm{d}t + 1\right). \tag{3.4.21}$$

Substituting (3.4.19) into (3.4.21) and simplifying, it follows that

$$w_c = \mu\frac{\rho\left(\frac{\mathrm{e}^{\mu(\hat{\tau}-\tau_c)+\gamma_c(\tau_c-\hat{\tau}+1)}-1}{\alpha} + \tau_f - \hat{\tau}\right) + \gamma_f(\tau_f + 1 - \hat{\tau})}{\alpha\,\mathrm{e}^{\mu(\tau_c-\tau_f)}\left(\mathrm{e}^{\mu(\tau_f-\hat{\tau})} - 1\right)}. \tag{3.4.22}$$

This explicit expression for w_c can be substituted into (3.4.19), to get

$$v_c = \frac{\mathrm{e}^{\rho\tau_f+\gamma_f(\tau_f-\tau_c)}\left(\mathrm{e}^{\rho\left(\frac{\mathrm{e}^{\mu(\hat{\tau}-\tau_c)+\gamma_c(\tau_c-\hat{\tau}+1)}-1}{\alpha}\right)} - 1\right)}{\rho\int_{\tau_f}^{\hat{\tau}} \exp\left(\rho\left(t + \left[\frac{\mathrm{e}^{\mu(\hat{\tau}-\tau_c)+\gamma_c(\tau_c-\hat{\tau}+1)}-1}{\alpha} + \tau_f - \hat{\tau} + \frac{\gamma_f}{\rho}(\tau_f + 1 - \hat{\tau})\right]\frac{\left(\mathrm{e}^{\mu(\tau_f-t)}-1\right)}{\left(\mathrm{e}^{\mu(\tau_f-\hat{\tau})}-1\right)}\right)\right)\mathrm{d}t}. \tag{3.4.23}$$

To assess the stability of the equilibrium points, we find the Jacobian matrix associated with (3.4.15)–(3.4.16) at each equilibrium point. The Jacobian matrix evaluated at a point (v^*, w^*) is

$$J(v^*, w^*) = \begin{pmatrix} J_{11} & J_{12} \\ J_{21} & J_{22} \end{pmatrix}. \tag{3.4.24}$$

When evaluating $J(v^*, w^*)$, we use Maple® to simplify calculations.

We begin by analyzing the stability of $(0,0)$. The matrix $J(0,0)$ has components $J_{12} = 0 = J_{21}$, so it is a diagonal matrix. The eigenvalues λ_1 and λ_2 are therefore equal to J_{11} and J_{22}, respectively. They are

$$\lambda_1 = \mathrm{e}^{\rho(\hat{\tau}-\tau_f)+\gamma_f(\hat{\tau}-\tau_f-1)} \qquad \text{and} \qquad \lambda_2 = \mathrm{e}^{\mu(\tau_c-\hat{\tau})+\gamma_c(\hat{\tau}-\tau_c-1)}. \tag{3.4.25}$$

We have that $|\lambda_1| > 1$ if and only if

$$\rho > \frac{\gamma_f(\tau_f - \hat{\tau} + 1)}{\hat{\tau} - \tau_f}. \tag{3.4.26}$$

The exponent in the expression for λ_2 is negative, so $|\lambda_2| < 1$. Hence, $(0,0)$ is locally asymptotically stable if the inequality in (3.4.26) is reversed, and it is a saddle point if (3.4.26) holds. However, if $\tilde{v}_c > 0$, then $(0,0)$ must be a saddle point, since (3.4.26) is equivalent to (3.4.18).

Next, we analyze the stability of $(\tilde{v}_c, 0)$. The matrix $J(\tilde{v}_c, 0)$ has component $J_{21} = 0$, so it is an upper triangular matrix. The eigenvalues λ_1 and λ_2 are thus equal to J_{11} and J_{22}, respectively. They are

$$\lambda_1 = \mathrm{e}^{\rho(\tau_f-\hat{\tau})+\gamma_f(\tau_f-\hat{\tau}+1)} \tag{3.4.27}$$

and

$$\begin{aligned}\lambda_2 = \mathrm{e}^{\mu(\tau_c-\hat{\tau})+\gamma_c(\hat{\tau}-\tau_c-1)} \Bigg[1 + \alpha\Big(\mathrm{e}^{\rho\hat{\tau}+\gamma_f(\hat{\tau}-\tau_c-1)} - \mathrm{e}^{\rho\tau_f+\gamma_f(\tau_f-\tau_c)} \Big) \\ \times \int_{\tau_f}^{\hat{\tau}} \frac{\mathrm{e}^{\rho s}}{\mathrm{e}^{\rho\hat{\tau}+\gamma_f(\hat{\tau}-\tau_c-1)}\big(\mathrm{e}^{\rho s} - \mathrm{e}^{\rho\tau_f}\big) + \mathrm{e}^{\rho\tau_f+\gamma_f(\tau_f-\tau_c)}\big(\mathrm{e}^{\rho\hat{\tau}} - \mathrm{e}^{\rho s}\big)} \,\mathrm{d}s \Bigg].\end{aligned} \tag{3.4.28}$$

We have that $|\lambda_1| < 1$ if and only if

$$\rho > \frac{\gamma_f(\tau_f - \hat{\tau} + 1)}{\hat{\tau} - \tau_f}. \tag{3.4.29}$$

Since (3.4.29) is equivalent to (3.4.18), the condition for $\tilde{v}_c > 0$, we always have that $|\lambda_1| < 1$.

Considering (3.4.28), we have that

$$\int_{\tau_f}^{\hat{\tau}} \frac{\mathrm{e}^{\rho s}}{\mathrm{e}^{\rho\hat{\tau}+\gamma_f(\hat{\tau}-\tau_c-1)}\big(\mathrm{e}^{\rho s} - \mathrm{e}^{\rho\tau_f}\big) + \mathrm{e}^{\rho\tau_f+\gamma_f(\tau_f-\tau_c)}\big(\mathrm{e}^{\rho\hat{\tau}} - \mathrm{e}^{\rho s}\big)} \,\mathrm{d}s \tag{3.4.30}$$

$$= \frac{\ln\left(\frac{\mathrm{e}^{\gamma_f(\hat{\tau}-\tau_f-1)}\left(\mathrm{e}^{2\rho\hat{\tau}} - \mathrm{e}^{\rho(\hat{\tau}+\tau_f)}\right)}{\mathrm{e}^{\rho(\hat{\tau}+\tau_f)} - \mathrm{e}^{2\rho\tau_f}} \right)}{\rho\Big(\mathrm{e}^{\rho\hat{\tau}+\gamma_f(\hat{\tau}-\tau_c-1)} - \mathrm{e}^{\rho\tau_f+\gamma_f(\tau_f-\tau_c)} \Big)}. \tag{3.4.31}$$

In the preceding integral, $s \in [\tau_f, \hat{\tau}]$, so

$$\mathrm{e}^{\rho s} - \mathrm{e}^{\rho\tau_f} \geq 0 \qquad \text{and} \qquad \mathrm{e}^{\rho\hat{\tau}} - \mathrm{e}^{\rho s} \geq 0. \tag{3.4.32}$$

It is not possible for both conditions in (3.4.32) to equal zero simultaneously, so the denominator of the integrand is positive; i.e.,

$$e^{\rho\hat{\tau}+\gamma_f(\hat{\tau}-\tau_c-1)}(e^{\rho s}-e^{\rho\tau_f})+e^{\rho\tau_f+\gamma_f(\tau_f-\tau_c)}(e^{\rho\hat{\tau}}-e^{\rho s})>0. \tag{3.4.33}$$

Additionally, the numerator of the integrand is obviously positive. Hence, the integrand is a positive function, which implies that (3.4.31) is positive. If

$$\rho\hat{\tau}+\gamma_f(\hat{\tau}-\tau_c-1)>\rho\tau_f+\gamma_f(\tau_f-\tau_c), \tag{3.4.34}$$

then the denominator of (3.4.31) is positive. We can rewrite (3.4.34) as

$$\rho>\frac{\gamma_f(\tau_f-\hat{\tau}+1)}{\hat{\tau}-\tau_f}. \tag{3.4.35}$$

Since (3.4.35) is equivalent to (3.4.18), the condition for $\tilde{v}_c>0$, we must always have that the denominator of (3.4.31) is positive. Therefore, the numerator of (3.4.31) must be positive; i.e.,

$$\ln\left(\frac{e^{\gamma_f(\hat{\tau}-\tau_f-1)}\left(e^{2\rho\hat{\tau}}-e^{\rho(\hat{\tau}+\tau_f)}\right)}{e^{\rho(\hat{\tau}+\tau_f)}-e^{2\rho\tau_f}}\right)>0. \tag{3.4.36}$$

We can rewrite (3.4.28) using (3.4.31) as

$$\lambda_2=e^{\mu(\tau_c-\hat{\tau})+\gamma_c(\hat{\tau}-\tau_c-1)}\left[1+\frac{\alpha}{\rho}\ln\left(\frac{e^{\gamma_f(\hat{\tau}-\tau_f-1)}\left(e^{2\rho\hat{\tau}}-e^{\rho(\hat{\tau}+\tau_f)}\right)}{e^{\rho(\hat{\tau}+\tau_f)}-e^{2\rho\tau_f}}\right)\right]. \tag{3.4.37}$$

We get that $|\lambda_2|<1$ if and only if

$$\alpha<\frac{e^{\mu(\hat{\tau}-\tau_c)+\gamma_c(\tau_c-\hat{\tau}+1)}-1}{\frac{1}{\rho}\ln\left(\frac{e^{\gamma_f(\hat{\tau}-\tau_f-1)}\left(e^{2\rho\hat{\tau}}-e^{\rho(\hat{\tau}+\tau_f)}\right)}{e^{\rho(\hat{\tau}+\tau_f)}-e^{2\rho\tau_f}}\right)}. \tag{3.4.38}$$

We know that $|\lambda_1|<1$, so if (3.4.38) holds, then $(\tilde{v}_c,0)$ is locally asymptotically stable. If instead, $|\lambda_2|>1$, then $(\tilde{v}_c,0)$ is a saddle point.

The expressions for the eigenvalues associated with studying the stability of (v_c,w_c) are complicated, so we instead use the Jury test, which, in this case, requires the use of numerical methods. We described the Jury test in detail in Subsection 2.2.2, so we omit some of the finer details here. The Jury conditions are (2.2.22)–(2.2.24). The equilibrium point (v_c,w_c) is stable if and only if all three Jury conditions hold. If (2.2.23) is an equality, then (v_c,w_c) loses stability though a transcritical bifurcation. For (2.2.23) to hold, we must have that (3.4.38) does not hold. Therefore, the transcritical bifurcation can be written explicitly as (3.4.38), but with the inequality replaced by an equality. As the transcritical bifurcation is crossed, (v_c,w_c) and $(\tilde{v}_c,0)$ exchange stability. We call the transcritical bifurcation the consumer-extinction boundary, since it marks the difference between the consumer persisting or not. If instead, (2.2.22) is an equality, then (v_c,w_c) becomes unstable in a Naimark–Sacker (Hopf) bifurcation, which leads to consumer–resource cycles. We call this the consumer–resource

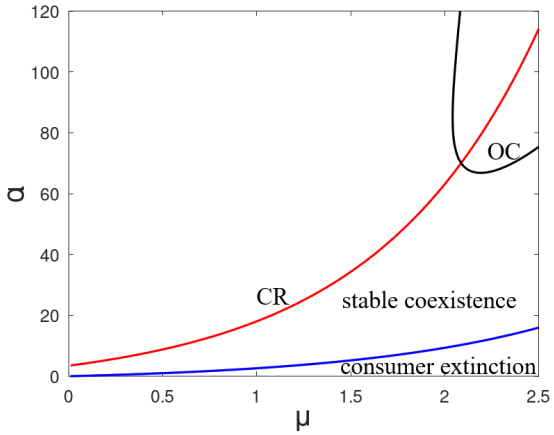

Figure 3.3: Bifurcation diagram for early consumer emergence. The blue curve is the consumer-extinction boundary. The red curve is the consumer–resource cycles boundary (CR). The black curve is the overcompensation-cycles boundary (OC). The parameters are $\tau_f = \frac{3}{12}$, $\tau_c = 0$, $\hat{\tau} = \frac{10}{12}$, $\gamma_f = \frac{\mu}{2} = \gamma_c$ and $\rho = 20$.

cycles boundary. If (2.2.24) is an equality, then stability is lost in a flip bifurcation, which leads to two-cycles. We call this the overcompensation-cycles boundary.

To use the Jury test, we code $J(v_c, w_c)$ in Octave, using the `trapz` and `cumtrapz` functions to numerically integrate wherever necessary via the trapezoidal method [1]. We select two parameters to vary and fix all others, so that we can create a two-parameter bifurcation diagram that illustrates the stability of the coexistence state. For each combination of parameter values, we evaluate $J(v_c, w_c)$. We then use its trace and determinant to evaluate the left-hand-sides of (2.2.22) and (2.2.24). When the former is equal to zero, we are on the consumer–resource cycles boundary. The same for the latter implies that we are on the overcompensation-cycles boundary. To illustrate these boundaries, we use a contour plot. We also plot the consumer-extinction boundary using our explicit expression. An example of a resulting bifurcation diagram with $\tau_c \leq \tau_f$, is displayed in Figure 3.3. All three Jury conditions are satisfied within the indicated stable coexistence region. Our model, like the Pachepsky model (2.3.3)–(2.3.4), can display stable coexistence, consumer–resource cycles and overcompensation cycles. We illustrated each type of behaviour using the Pachepsky model in Figure 2.3. Our model produces qualitatively equivalent results to theirs for each type of behaviour. In fact, with $\tau_c = 0 = \tau_f$ and $\hat{\tau}_c = 1 = \hat{\tau}_f$, our model is equivalent to their model. By making these changes to τ_c, τ_f, $\hat{\tau}_c$ and $\hat{\tau}_f$, the bifurcations shown in Figure 3.3 shift such that the resulting bifurcation diagram is exactly Figure 2.2. Thus, we can recreate the exact results shown in Figure 2.3 using our model.

We can calculate the cycle period on the consumer–resource cycles boundary. In Sub-

[1] To create all of the bifurcation diagrams, consumer–resource period plots and Figure 2.3, we partitioned the interval of integration into 500 evenly spaced points. To create all of the orbit diagrams, we instead partitioned the interval of integration into 100 evenly spaced points. We observed very small differences in the resulting figure, typically less than 1%, when we reduced the number of points from 500 to 100.

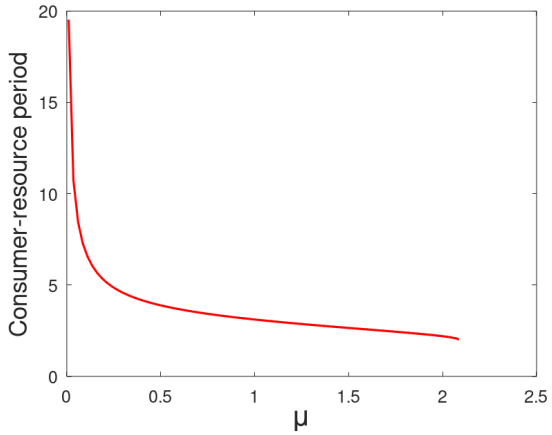

Figure 3.4: The cycle period on the consumer–resource cycles boundary. All parameters are the same as in Figure 3.3.

section 2.3.2, we showed that, in general, this period is calculated using (2.3.13). Figure 3.4 displays the cycle period on the consumer–resource cycles boundary from Figure 3.3. For each value of μ, a value of α is selected such that the point (μ, α) lies on the red curve from Figure 3.3. We chose to display the cycle period as a function of μ, since the corresponding bifurcation diagram is also displayed in this way. Figure 3.4 shows that the cycle period is a decreasing function of μ. For the parameters selected, it equals two when $\mu \approx 2.1$.

3.4.2.2 Case (ii): $\tau_c > \tau_f$

We now consider the case where the resource emergence time is earlier than that of the consumer; i.e., Scenarios FF and FC. The general process for finding equilibrium points and analyzing their stability is the same as in Case (i), so we omit the details here. When $\hat{\tau}_f = \hat{\tau} = \hat{\tau}_c$, the solution maps for Scenarios FF (3.4.11) and FC (3.4.12) both equal

$$v_{n+1} = \frac{v_n}{v_n + \mathrm{e}^{\rho(\tau_f - \tau_c)}\left[\dfrac{\rho v_n \int_{\tau_c}^{\hat{\tau}} \mathrm{e}^{\rho(t-\tau_c)+\frac{\alpha w_n}{\mu}(\mathrm{e}^{\mu(\tau_c - t)}-1)}\,\mathrm{d}t + 1}{\mathrm{e}^{\rho(\hat{\tau}-\tau_c)+\frac{\alpha w_n}{\mu}(\mathrm{e}^{\mu(\tau_c-\hat{\tau})}-1)+\gamma_f(\hat{\tau}-\tau_f-1)}} - v_n\right]}, \tag{3.4.39}$$

$$w_{n+1} = \left[\alpha v_n \int_{\tau_c}^{\hat{\tau}} \frac{\mathrm{e}^{\rho(s-\tau_c)+\frac{\alpha w_n}{\mu}(\mathrm{e}^{\mu(\tau_c - s)}-1)}}{\rho v_n \int_{\tau_c}^{s} \mathrm{e}^{\rho(t-\tau_c)+\frac{\alpha w_n}{\mu}(\mathrm{e}^{\mu(\tau_c - t)}-1)}\,\mathrm{d}t + 1}\,\mathrm{d}s + 1\right] w_n\, \mathrm{e}^{\mu(\tau_c - \hat{\tau})+\gamma_c(\hat{\tau}-\tau_c-1)}. \tag{3.4.40}$$

There are again up to three equilibrium points: when both species are extinct $(0, 0)$, when only the resource is present $(\tilde{v}_f, 0)$, and when the species coexist (v_f, w_f). We require $\tilde{v}_f, v_f, w_f > 0$. We can find an explicit expression for $(\tilde{v}_f, 0)$, but not for (v_f, w_f).

To find an explicit expression for $\tilde{v}_f$, we set $v_{n+1} = \tilde{v}_f = v_n$ and $w_{n+1} = 0 = w_n$ in

(3.4.39). We integrate and simplify to get

$$\tilde{v}_f = \frac{1}{1 + \mathrm{e}^{\rho(\hat{\tau}+\tau_f-\tau_c)}\left(\frac{1-\mathrm{e}^{\gamma_f(\hat{\tau}-\tau_f-1)}}{\mathrm{e}^{\rho\hat{\tau}+\gamma_f(\hat{\tau}-\tau_f-1)}-\mathrm{e}^{\rho\tau_f}}\right)}. \tag{3.4.41}$$

We have that $\tilde{v}_f > 0$ if and only if

$$\rho > \frac{\gamma_f(\tau_f - \hat{\tau} + 1)}{\hat{\tau} - \tau_f}. \tag{3.4.42}$$

We set $v_{n+1} = v_f = v_n$ and $w_{n+1} = w_f = w_n$ in (3.4.39)–(3.4.40). We obtain an expression for v_f in terms of w_f:

$$v_f = \frac{1 - \mathrm{e}^{\rho(\tau_f-\hat{\tau})+\frac{\alpha w_f}{\mu}\left(1-\mathrm{e}^{\mu(\tau_c-\hat{\tau})}\right)+\gamma_f(\tau_f-\hat{\tau}+1)}}{1 + \mathrm{e}^{\rho(\tau_f-\tau_c)}\left[\frac{\rho\int_{\tau_c}^{\hat{\tau}} \mathrm{e}^{\rho t+\frac{\alpha w_f}{\mu}(\mathrm{e}^{\mu(\tau_c-t)}-1)}\,\mathrm{d}t}{\mathrm{e}^{\rho\hat{\tau}+\frac{\alpha w_f}{\mu}(\mathrm{e}^{\mu(\tau_c-\hat{\tau})}-1)+\gamma_f(\hat{\tau}-\tau_f-1)}} - 1\right]}. \tag{3.4.43}$$

Using (3.4.40), we determine that

$$\frac{\mathrm{e}^{\mu(\hat{\tau}-\tau_c)+\gamma_c(\tau_c-\hat{\tau}+1)} - 1}{\alpha} = \frac{1}{\rho}\ln\left(v_f\rho\int_{\tau_c}^{\hat{\tau}} \mathrm{e}^{\rho(t-\tau_c)+\frac{\alpha w_f}{\mu}(\mathrm{e}^{\mu(\tau_c-t)}-1)}\,\mathrm{d}t + 1\right). \tag{3.4.44}$$

Substituting (3.4.43) into (3.4.44) does not simplify the equation enough for us to determine an explicit expression for w_f. We therefore use numerical methods to determine the coexistence state. We bring both terms in (3.4.44) to the same side, replace v_f with (3.4.43), and use the `fzero` function in Octave to find the roots of the function, thereby solving for w_f. We calculate v_f by substituting the calculated value of w_f into (3.4.43). We use the `trapz` and `cumtrapz` functions to numerically integrate wherever necessary via the trapezoidal method. Our stability analysis follows closely to that of Case (i). We determine that $(0, 0)$ is either locally asymptotically stable or a saddle point. However, if $\tilde{v_f} > 0$, then $(0, 0)$ must be a saddle point due to (3.4.42). Furthermore, $(\tilde{v_f}, 0)$ is locally asymptotically stable if and only if

$$\alpha < \frac{\mathrm{e}^{\mu(\hat{\tau}-\tau_c)+\gamma_c(\tau_c-\hat{\tau}+1)} - 1}{\frac{1}{\rho}\ln\left(\frac{\mathrm{e}^{\gamma_f(\hat{\tau}-\tau_f-1)}\left(\mathrm{e}^{2\rho\hat{\tau}}-\mathrm{e}^{\rho(\hat{\tau}+\tau_f)}\right)}{\mathrm{e}^{\gamma_f(\hat{\tau}-\tau_f-1)}\left(\mathrm{e}^{\rho(\hat{\tau}+\tau_c)}-\mathrm{e}^{\rho(\hat{\tau}+\tau_f)}\right)-\mathrm{e}^{\rho(\tau_f+\tau_c)}+\mathrm{e}^{\rho(\hat{\tau}+\tau_f)}}\right)}. \tag{3.4.45}$$

If the inequality in (3.4.45) is reversed, then $(\tilde{v}_f, 0)$ is a saddle point. A transcritical bifurcation exists when the inequality in (3.4.45) is replaced by an equality. As the transcritical boundary is crossed, the stability of $(\tilde{v}_f, 0)$ and (v_f, w_f) exchange. As in Case (i), we use numerical methods to study the stability of (v_f, w_f) using the Jury test. We are able to produce two-parameter bifurcation diagrams and plots that illustrate the cycle period on the consumer–resource cycles boundary, like we did in Case (i). We demonstrate this in Section 4.4. The coexistence state can be stable or unstable. If it is unstable, then we may observe consumer–resource cycles or overcompensation cycles.

Comparing Cases (i) ($\tau_c \leq \tau_f$) and (ii) ($\tau_c > \tau_f$), we observe the same types of equilibrium points, which are the extinction state, the resource-only state, and the coexistence state. However, the expressions for the latter two states differ between the cases. No matter who emerges first, we determine an explicit expression for the resource-only state and the same condition under which its resource density is positive; i.e., (3.4.18) and (3.4.42) are identical. In Case (i), we determine an explicit expression for the coexistence state, but the same is not possible in Case (ii). The qualitative behaviour of the two systems are the same, but the stability boundaries differ. In both cases, the only stability boundary that we have an explicit expression for is the consumer-extinction boundary.

In this chapter, we derived our semi-discrete consumer–resource model that depends explicitly on each species' phenology. Using a detailed example, we illustrated how to solve our dimensional model. We nondimensionalized our model and derived the discrete solution maps of it, thereby transforming it into a fully discrete model. We ended this chapter with analyzing the stability of the resulting model. In the next chapter, we use bifurcation diagrams and period plots, like Figures 3.3 and 3.4, to observe how phenological shifts affect the long-term dynamics.

Chapter 4

Dynamics and Bifurcations

In this chapter, we analyze how changes in phenology (i.e., phenological shifts) affect bifurcations and the long-term consumer–resource dynamics in our model. In some consumer–resource systems, phenological shifts can disrupt the phenological synchrony, resulting in phenological asynchrony. We first consider the case where phenological synchrony is maintained and then when it is not. We place our results into the context of consumer–resource theory, which we briefly review at the beginning.

4.1 Instabilities in Discrete Consumer–Resource Models

The stability of consumer–resource or predator–prey systems has been a focus of study in theoretical ecology since at least the 1970s, with works by Rosenzweig and MacArthur [41] on the importance of having a nonlinear functional response, as well as the work by May [29] on the stability of discrete-time systems. Discrete-time consumer–resource models contain an implicit delay that prohibits the consumer from responding instantaneously to changes in the resource density [4, 25]. This is known as delayed density dependence, as species densities may surpass equilibrium values before being regulated by negative feedback. If the resulting oscillations about the equilibrium values are damped, then eventually solutions stabilize at the equilibrium values. If they are permanent, then we observe unstable behaviour, like consumer–resource cycles or overcompensation cycles. The principle of interaction strength states that, in general, consumer–resource interactions are more likely to destabilize as the consumer consumption rate increases relative to the consumer death rate, whereas the opposite stabilizes the interactions [30]. We previously transformed our impulsive ODE model into a discrete-time model and demonstrated that it is capable of displaying the previously described range of dynamic behaviour; see Subsection 3.4.2.

The strength of the numerical response is a distinguishing factor between overcompensation cycles and consumer–resource cycles. In Subsection 2.2.1, we defined the numerical response, which is the change in the consumer density as a function of the change in the resource density [1]. A strong numerical response implies that changes in the resource density will affect the consumer density. Overcompensation cycles exist when the consumer

density can quickly increase above the equilibrium value in one year and then crash below it in the following year due to delayed density dependence. Therefore, overcompensation cycles require a strong numerical response. Consumer–resource cycles exist when the increase and decrease in the consumer density are more gradual, hence requiring a weaker numerical response.

The parameters in our model that most influence the strength of the numerical response are the consumer consumption rate (α) and the active consumer death rate (μ). The consumer consumption rate is positively correlated with the consumer density, where larger values of α result in larger increases in the density. In contrast, the active consumer death rate is negatively correlated with the consumer density, where larger values of μ result in larger decreases in the density. Therefore, larger values of α and μ generally increase the strength of the numerical response. In the following sections of this chapter, we will frequently refer to the principle of interaction strength, as well as the strength of the numerical response.

Throughout this chapter, we assume that μ is larger than the dormant consumer and resource death rates (γ_c and γ_f), since winter resting periods (WRPs) have been shown to directly increase survival [10, 45]. Furthermore, we fix the scaled resource intrinsic growth rate (ρ) to 20 so that generally the resource can support the consumer and that we observe interesting dynamics. Additionally, it is within the range that Pachepsky et al. [35] considered biologically reasonable.

4.2 Effects of the Active Season Length with Synchrony

We associate longer summers and shorter winters with climate change, since temperature is expected to continue to increase [18]. In our model, the summer can be represented by the length of time when both species are active, which we will henceforth refer to as the active season length; see the green period in Figure 3.1. Thus, the ongoing effects of climate change are expected to increase the active season length. In this section, we vary the active season length to analyze its effects on the stability of the coexistence state. To focus our attention on the active season length only, we assume that there is phenological synchrony between the consumer and its resource. This assumption is not unrealistic, as climate change–induced phenological shifts do not always result in phenological asynchrony in nature [7]. A similar question was previously studied by Geng et al. [15]. They focused on understanding whether two consumer species can coexist on one resource, whereas we are interested in studying the coexistence of one consumer species and its resource, as well as the long-term dynamic behaviour.

In this section, we assume that the dormant resource and consumer death rates are both half of the active consumer death rate; i.e., $\gamma_f = \frac{\mu}{2} = \gamma_c$. We fix the resource and consumer emergence times at zero; i.e., $\tau_f = 0 = \tau_c$. To impose phenological synchrony, we assume that they also have the same immergence time; i.e., $\hat{\tau}_f = \hat{\tau} = \hat{\tau}_c$. We vary $\hat{\tau}$ to change the active season length. As $\hat{\tau}$ increases, the active season length increases and the length of the WRP decreases. When $\hat{\tau} = 1$, our model is equivalent to the Pachepsky model

(2.3.3)–(2.3.4), as the WRP is of length zero and the active season is of length one.

To study the stability of the coexistence state, using our nondimensional model, we create two-parameter bifurcation diagrams in terms of α and μ for varying values of $\hat{\tau}$; see Figure 4.1. The overcompensation-cycles boundary exists outside of the parameter ranges in the top left plot. As the active season length increases, we observe the following: All stability boundaries shift down, implying that consumer extinction becomes less likely and the region of stable coexistence in parameter space decreases. Additionally, the overcompensation-cycles boundary shifts left, indicating that instabilities are more likely to arise as overcompensation cycles when the active season length is longer, whereas consumer–resource cycles are more likely when it is shorter.

The mechanism behind the qualitative behaviour of the consumer-extinction boundary is that longer active season lengths provide the resource with more time to grow and the consumer with more time to consume. As a result, smaller values of α are required for the consumer to avoid extinction. The qualitative behaviours of the cycles boundaries are explained by longer active season lengths increasing the number of consumer–resource interactions, as well as the probability that the consumer dies in one year, since $\mu > \gamma_c$. Hence, to maintain the strength of the numerical response, the values of α and μ must decrease as the active season length increases.

Figure 4.2 displays the cycle period on the consumer–resource cycles boundary as a function of μ. For all $\hat{\tau}$, the cycle period is a decreasing function of μ, since larger values of μ increase the strength of the numerical response. For a given value of μ, the cycle period decreases as $\hat{\tau}$ increases. This is explained by the numerical response increasing in strength as $\hat{\tau}$ increases.

We illustrate the asymptotic (long-term) densities in the orbit diagrams in Figure 4.3. As indicated by the black dashed line in each bifurcation diagram in Figure 4.1, when creating the orbit diagrams, we fixed $\alpha = 10$. We ran simulations using different values of μ. Once transients had died out, we plotted the resource and consumer densities at the census time each year as red and blue points, respectively. Figure 4.3 demonstrates how the stability of the coexistence state changes as parameter values cross the different stability boundaries. For values of μ where the black dashed line in Figure 4.1 is in the stable coexistence region, we see a stable steady state in Figure 4.3. When it is above the red curve in Figure 4.1, we observe consumer–resource cycles in Figure 4.3, where the asymptotic densities oscillate. When it is above the black curve in Figure 4.1, we see overcompensation cycles in Figure 4.3, where the asymptotic densities "flip" between two values. When it is below the blue curve in Figure 4.1, only the resource persists, and we stop plotting.

In the first row of Figure 4.3, the coexistence state for each value of μ is stable. In the second row, we observe consumer–resource cycles when μ is small, but for larger values of μ, we observe only stable coexistence states. In the third row, as μ increases, we first observe consumer–resource cycles, then stable coexistence states, then overcompensation cycles, followed again by stable coexistence states. The orbit diagrams illustrate our previous observation, which is that increasing the active season length has a destabilizing effect on the system, while decreasing it has a stabilizing effect.

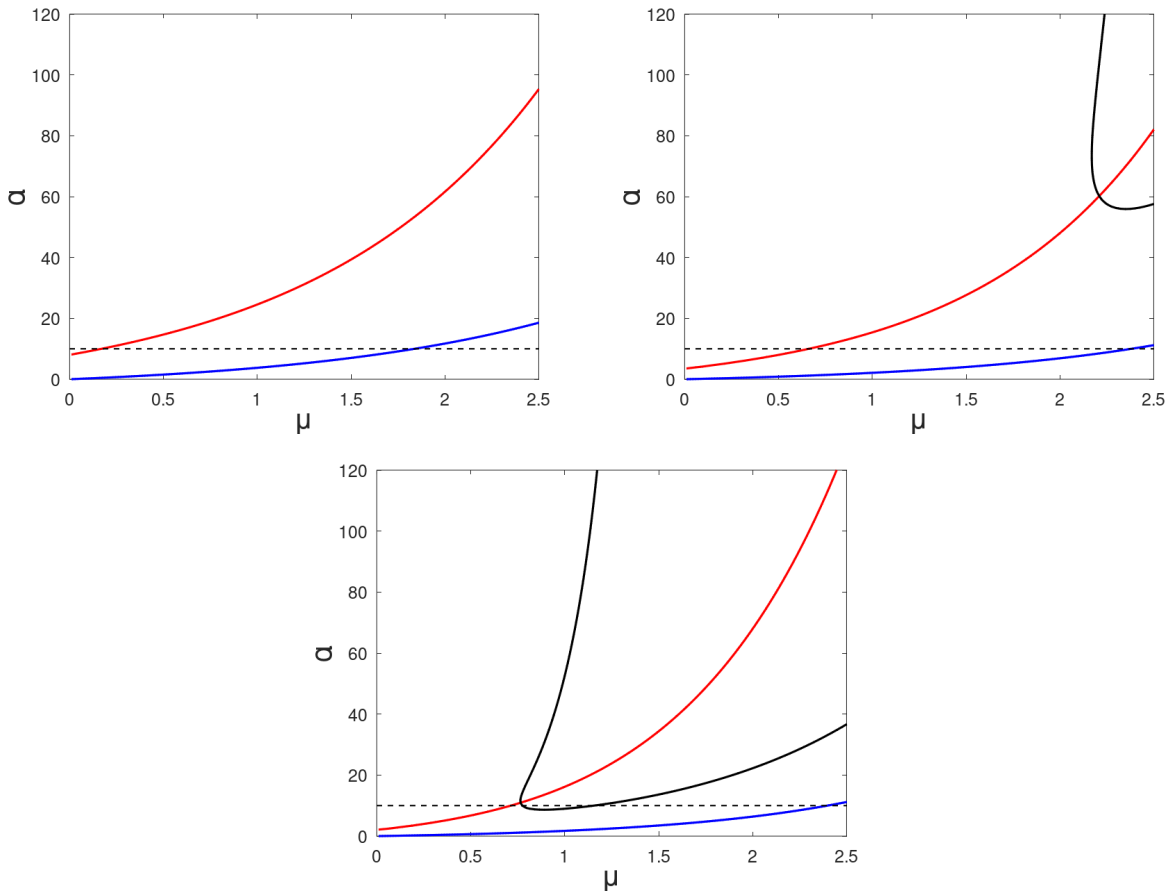

Figure 4.1: Bifurcation diagrams for different active season lengths. The blue curve is the consumer-extinction boundary. The red curve is the consumer–resource cycles boundary. The black curve is the overcompensation-cycles boundary. In the top left plot, $\hat{\tau} = \frac{3}{12}$. In the top right plot, $\hat{\tau} = \frac{7}{12}$. In the bottom plot, $\hat{\tau} = 1$. In all plots, $\tau_f = 0 = \tau_c$, $\gamma_f = \frac{\mu}{2} = \gamma_c$ and $\rho = 20$.

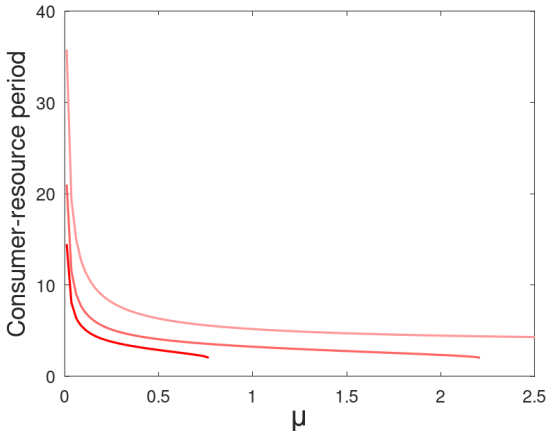

Figure 4.2: The cycle period on the consumer–resource cycles boundary for different active season lengths. The three curves correspond to $\hat{\tau} = \frac{3}{12}, \frac{7}{12}, 1$. Darker colours indicate increasing values of $\hat{\tau}$. All other parameters are the same as in Figure 4.1.

4.3 Effects of Climate Change on the Immergence Time

Several species have evolved WRPs to minimize the effects of harsh winter conditions, like cold temperatures and lack of food availability [13]. As climate change continues to increase temperatures, we expect winter conditions to become more favourable. As a result, later immergence times have been observed in nature. For example, a population of European hedgehogs (*Erinaceus europaeus*) in Denmark had later immergence times during years with particularly mild fall and winter conditions, since their food remained available later into the year than usual [38]. We previously varied the shared immergence time in Section 4.2 when we studied the effects of the active season length. In this section, we illustrate our results more explicitly in terms of $\hat{\tau}$ to explore how changing it will affect the long-term dynamics.

As in Section 4.2, we set $\tau_f = 0 = \tau_c$, but we fix $\gamma_f = 0 = \gamma_c$. Although this choice for the dormant death rates is unrealistic, it allows us to easily compare our results with the results by Pachepsky et al. [35], as their model did not include a WRP; see Section 2.3. We assume that the shared active season length is at least one month long, so $\hat{\tau} \in [\frac{1}{12}, 1]$. If $\hat{\tau}$ is equal to one, then our model simplifies to exactly the Pachepsky model (2.3.3)–(2.3.4).

We illustrate the asymptotic densities for varying $\hat{\tau}$ in Figure 4.4. For each value of $\hat{\tau}$, we ran simulations, and once transients had died out, we plotted the resource and consumer densities at the census time each year as red and blue points, respectively. Additionally, we use a solid black curve to illustrate the average of the asymptotic densities and a solid cyan curve to illustrate the analytically obtained equilibrium values for each value of $\hat{\tau}$. If a value of $\hat{\tau}$ results in a stable coexistence state, then the red/blue point, the black curve and the cyan curve are impossible to distinguish, since their values are all equal.

The selected values of μ and α from each row of Figure 4.4 were previously used to demonstrate the possible dynamic behaviour of the Pachepsky model; see Figure 2.3. We

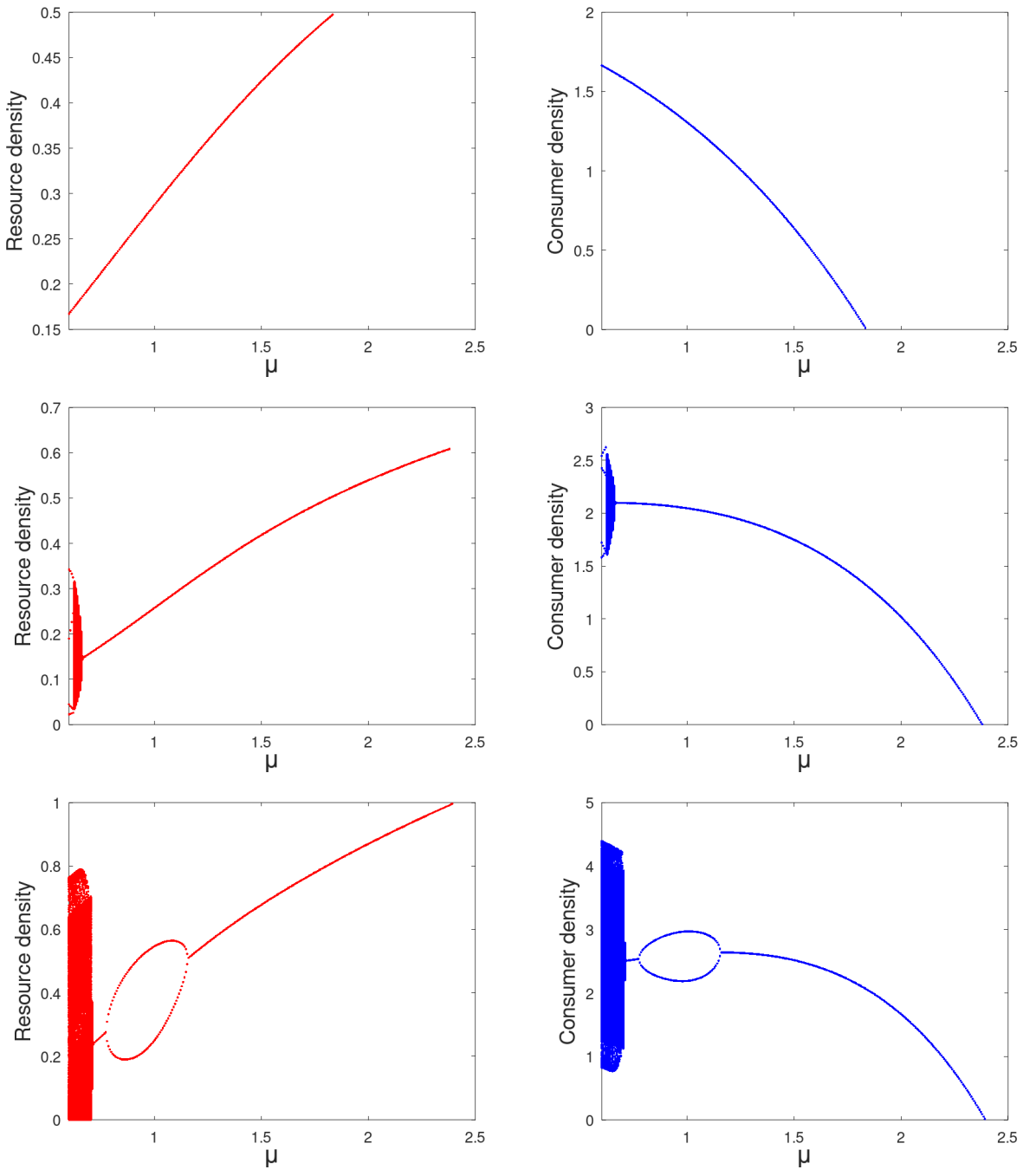

Figure 4.3: Asymptotic densities in terms of μ for different active season lengths. The red (blue) points are the simulated long-term resource (consumer) density. In the first row, $\hat{\tau} = \frac{3}{12}$. In the second row, $\hat{\tau} = \frac{7}{12}$. In the third row, $\hat{\tau} = 1$. In all plots, $\alpha = 10$. All other parameters are the same as in Figure 4.1.

illustrated that the Pachepsky model with (μ, α) equal to $(1.5, 10)$, $(0.1, 2.88)$ and $(0.81, 11)$ produced stable long-term dynamics, consumer–resource cycles and overcompensation cycles, respectively. The same behaviours are also illustrated in Figure 4.4 when $\hat{\tau}$ is equal to one. Figure 4.4 clearly demonstrates our main conclusion from Section 4.2, which is that smaller values of $\hat{\tau}$ (shorter active season lengths) stabilize the system and larger values (longer active season lengths) tend to destabilize the system. Independent of the values of μ and α, the average long-term densities of both the consumer and resource increase as $\hat{\tau}$ increases. This is explained by longer active season lengths increasing the time that the resource has to grow and the consumer has to consume.

In this section, we assumed that both the consumer and resource respond in the same way to climate change and that it only effects the active season length by changing $\hat{\tau}$. Given that climate change is expected to increase the active season length, we expect that stable consumer–resource systems could be destabilized in the future. As a result, densities may fluctuate between being abundant in some years and scarce in others. The mechanism behind this change in behaviour is that longer active season lengths increase the number of consumer–resource interactions. Hence, for a given value of α, the numerical response increases in strength as the active season length increases. Although we expect to observe fewer stable consumer–resource systems with climate change, we expect the average consumer and resource densities to increase. Climate change almost certainly affects more than just the shared active season length. Depending on the specific system, other consequences of climate change need to be considered to see whether the results change.

4.4 Effects of One Species Emerging Earlier

Phenological asynchrony between interacting species has been observed as a consequence of climate change, and it is hypothesized that it will become more prevalent as temperatures continue to increase [21]. In nature, earlier emergence times have been frequently observed as a result of warmer temperatures [10, 34]. In this section, we analyze how phenological asynchrony affects the stability of the coexistence state by shifting one species' emergence time to earlier dates, while maintaining a fixed active season length. We consider two cases: (i) the consumer emerges first ($\tau_c < \tau_f$) and (ii) the resource emerges first ($\tau_c > \tau_f$).

For the purpose of this section, we chose the following parameter values: $\gamma_f = \frac{\mu}{2} = \gamma_c$ and $\hat{\tau} = \frac{10}{12}$. Additionally, we fixed the emergence time of the later emerging species to $\frac{3}{12}$. As a result, the active season is always $\frac{7}{12}$ units long.

4.4.1 Case (i): Consumer emerges first

The stability of the coexistence state for increasingly early consumer emergence times is illustrated in the left plot in Figure 4.5. It displays the resulting two-parameter bifurcation diagram in terms of α and μ for each value of τ_c. As the consumer emerges earlier, we observe the following: All stability boundaries shift up, indicating that consumer extinction becomes

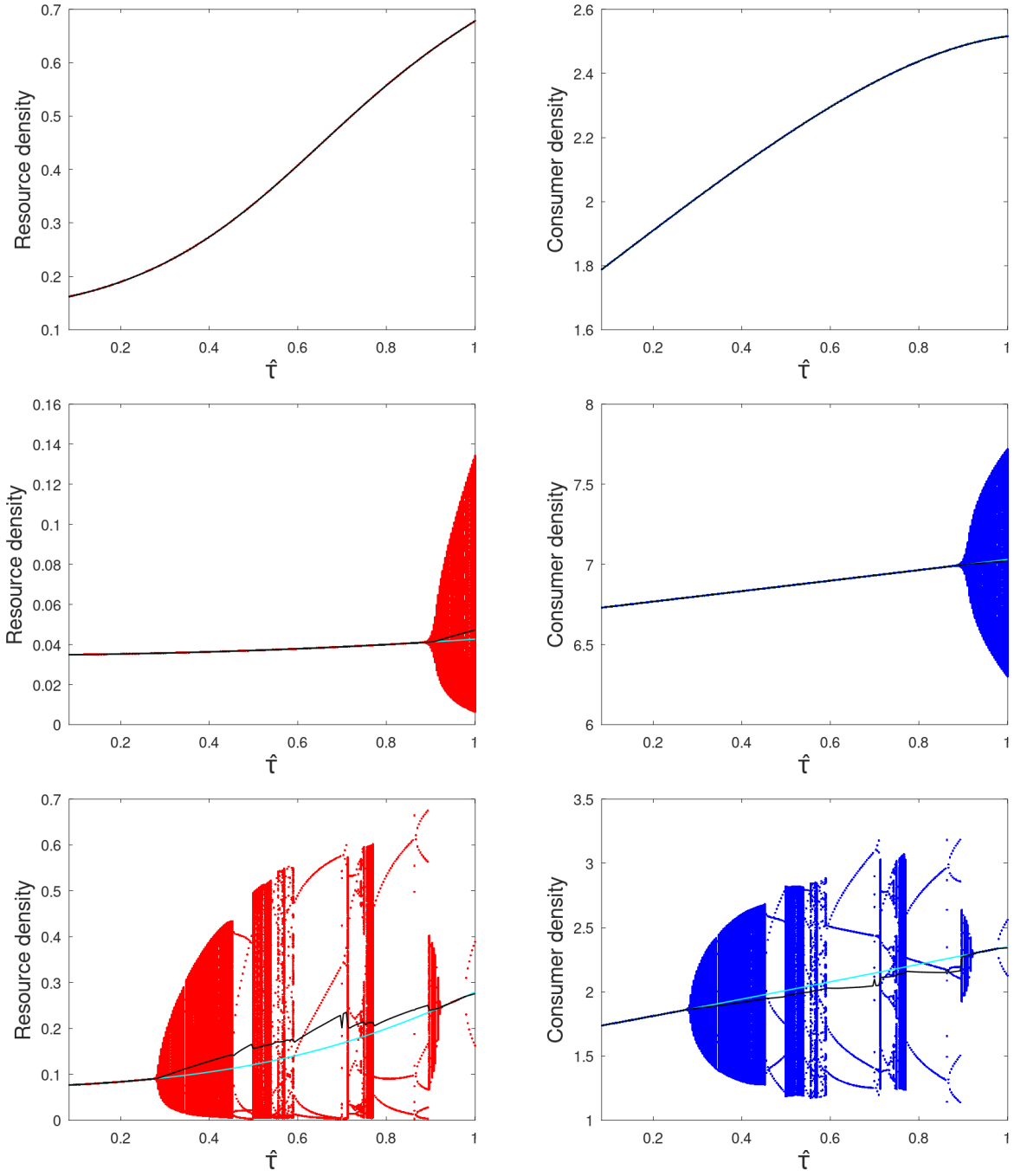

Figure 4.4: Asymptotic densities in terms of $\hat{\tau}$ for different active season lengths. The red (blue) points are the simulated long-term resource (consumer) density. The solid black curves correspond to the respective averages. The solid cyan curves correspond to the analytically obtained equilibrium densities. In the first row, $\mu = 1.5$ and $\alpha = 10$. In the second row $\mu = 0.1$ and $\alpha = 2.88$. In third row, $\mu = 0.81$ and $\alpha = 11$. In all plots, $\tau_f = 0 = \tau_c, \gamma_f = 0 = \gamma_c$ and $\rho = 20$.

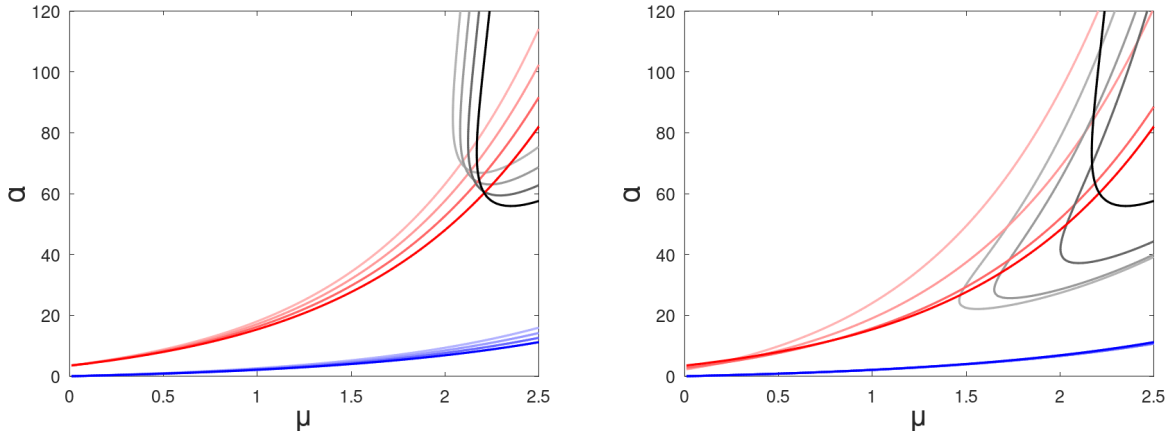

Figure 4.5: Bifurcation diagrams for varying early emergence times. For descriptions of the red, blue and black curves, see Figure 4.1. In the left plot, $\tau_f = \frac{3}{12}$ and $\tau_c = 0, \frac{1}{12}, \frac{2}{12}, \frac{3}{12}$. In the right plot, $\tau_c = \frac{3}{12}$ and $\tau_f = 0, \frac{1}{12}, \frac{2}{12}, \frac{3}{12}$. Darker colours indicate increasing values of τ_c (left) and τ_f (right). In all plots $\hat{\tau} = \frac{10}{12}, \gamma_f = \frac{\mu}{2} = \gamma_c$ and $\rho = 20$.

more likely, whereas instabilities become less likely. Furthermore, the overcompensation-cycles boundary shifts left, which implies that instabilities arising as overcompensation cycles become more likely.

We explain the previously observed effects as follows: As the consumer emerges earlier, the probability that the consumer dies in one year increases, since $\mu > \gamma_c$. As a result, larger values of α are required for the consumer to avoid extinction. According to the principle of interaction strength, to maintain an interaction strength that destabilizes the system, the value of α must increase as the probability of consumer death increases. Hence, larger values of α are required to observe unstable behaviour as the consumer emerges earlier. Lastly, smaller values of μ are required to maintain the strength of the numerical response as the probability of consumer death increases. Thus, overcompensation cycles arise for smaller values of μ as the consumer emerges earlier.

The left plot in Figure 4.6 displays the cycle period on the consumer–resource cycles boundary as a function of μ on a log scale. We scaled the vertical axis to make the differences between curves more visible. The overall shape of the curves are the same as in Figure 4.2. For a given value of μ, the cycle period decreases as τ_c decreases. This is explained by the numerical response increasing in strength as τ_c decreases.

4.4.2 Case (ii): Resource emerges first

The stability of the coexistence state for increasingly early resource emergence times is illustrated in the right plot in Figure 4.5. It displays the two-parameter bifurcation diagram in terms of α and μ for each value of τ_f. As the resource emerges earlier, we observe the following: The overcompensation-cycles boundary and the consumer-extinction boundary

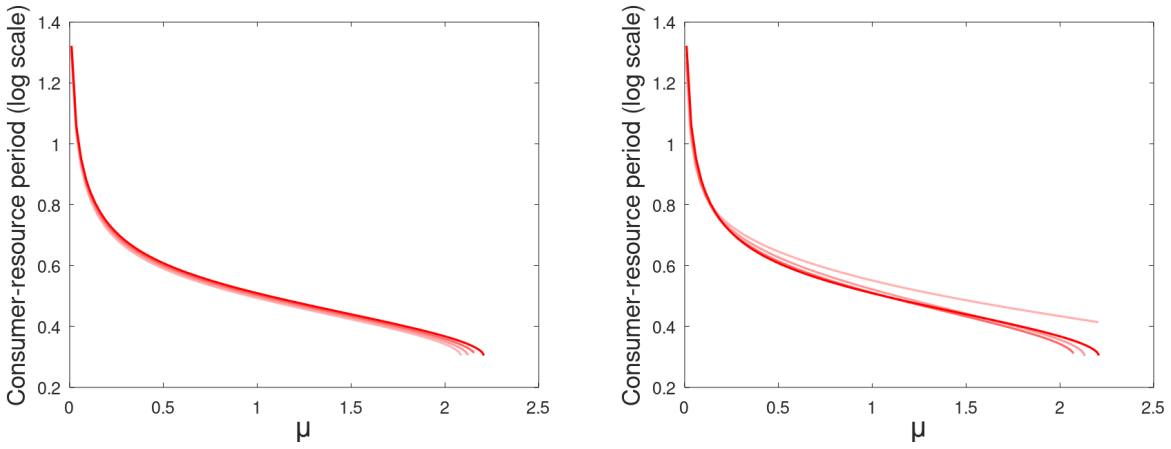

Figure 4.6: The cycle period on the consumer–resource cycles boundary on a log scale for varying early emergence times. The parameter values for the left (right) plot are the same as in the left (right) plot in Figure 4.5. Darker colours indicate increasing values of τ_c (left) and τ_f (right).

shift down; see the enlarged plot of the consumer-extinction boundary in Figure 4.7 (left). The consumer–resource cycles boundary shifts down when μ is small; see the enlarged plot in Figure 4.7 (right). When μ is larger, it shifts up instead. Furthermore, the overcompensation-cycles boundary shifts left.

We explain the previously observed behaviours as follows: The resource has more time to grow independently when it emerges earlier, resulting in larger resource densities at the consumer emergence time. This implies that lower values of α are required for the consumer to avoid extinction as the resource emerges earlier. It also implies that the resource density at the consumer emergence time becomes less dependent on the dynamics in the year prior. In other words, the more time that the resource has to grow without risk of consumption, the more the two species decouple. As a result, our discrete-time consumer–resource model becomes more like a discrete-time single-species model for the consumer, and hence is less prone to display consumer–resource cycles. To obtain consumer–resource cycles, the interaction strength has to be sufficiently large. Therefore, the value of α required to observe consumer–resource cycles tends to increase as the resource emerges earlier. The only situation where this result does not hold is when the value of μ is small.

For smaller values of μ, there is greater risk of the consumer overexploiting the resource. Therefore, even if the resource emerges early, the resource density at the consumer emergence time remains dependent on the dynamics in the year prior. If the coexistence state can be destabilized for small values of μ, then we must observe consumer–resource cycles. Overcompensation cycles are not possible in this case, since the consumer survives with high probability, and hence the consumer density can not decay quickly from one year to the next. As the resource emerges earlier, smaller values of α are required to maintain the strength of the numerical response. Thus, when μ is very small, consumer–resource cycles arise for smaller values of α as the resource emerges earlier. In the case where μ is not small, the

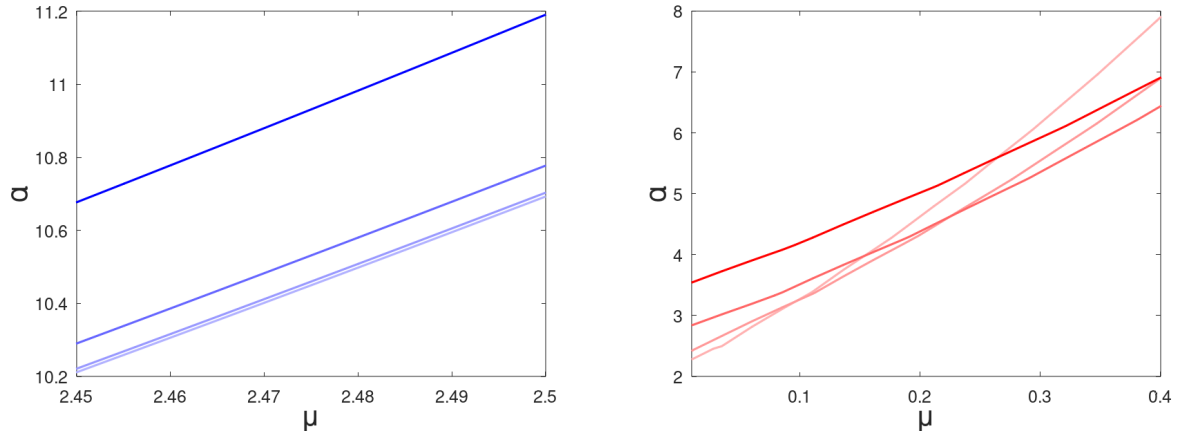

Figure 4.7: Enlarged consumer-extinction boundary (left) and consumer–resource cycles boundary (right) from the right plot in Figure 4.5. Darker colours indicate increasing values of τ_f.

same behaviour is observed but for the overcompensation-cycles boundary. According to the principle of interaction strength, to maintain an unstable system as the value of α decreases, μ must also decrease. Hence, overcompensation cycles arise for smaller values of μ as the resource emerges earlier.

The right plot in Figure 4.6 displays the cycle period on the consumer–resource cycles boundary as a function of μ on a log scale. We scaled the vertical axis to make the differences between curves more visible. The overall shape of the curves are the same as in Figure 4.2. The behaviour with respect to τ_f is not monotone.

Rather than decreasing τ_f, another way to increase the resource density is to consider a fast growing resource, which was studied by Pachepksy et al. [35]. They observed that large resource intrinsic growth rates (ρ) effectively reduce their model to a single-species model for the consumer. As a result, their model with increasing ρ and our model with decreasing τ_f, display qualitatively equivalent dynamic behaviour for the consumer–resource cycles boundary and the overcompensation-cycles boundary.

Comparing Cases (i) ($\tau_c < \tau_f$) and (ii) ($\tau_c > \tau_f$), decreasing τ_c or τ_f have opposite effects on the consumer-extinction boundary, but similar effects on the consumer–resource cycles boundary; see Figure 4.5. Both cause the consumer–resource cycles boundary to shift up, hence stabilizing the system. The overcompensation-cycles boundary shifts up for decreasing τ_c, but shifts down for decreasing τ_f. In this way, smaller τ_c stabilizes the system, whereas smaller τ_f destabilizes it. In the subsequent section, we consider the case where the active season length is no longer fixed.

4.5 Effects of the Active Season Length with Asynchrony

Although earlier emergence times are a frequently observed consequence of climate change, delays in emergence times are still possible [10]. For instance, delayed emergence times were observed for a population of wild female Columbian ground squirrels (*Urocitellus columbianus*) in Canada [26]. In this section, we fix the resource emergence time and vary the consumer emergence time, but unlike in Section 4.4, the active season length decreases as the consumer emerges increasingly later than the resource.

For the purpose of this section, we chose the following parameter values: $\gamma_f = \frac{\mu}{2} = \gamma_c$, $\hat{\tau} = \frac{10}{12}$, $\tau_f = \frac{3}{12}$ and $\tau_c \in [0, \frac{9}{12}]$. According to Pachepsky et al. [35], the maximum biologically reasonable value of μ is two. We previously analyzed the case where $\tau_c \leq \tau_f$ in Subsection 4.4.1; see Figure 4.5 (left). We now analyze the case where $\tau_c > \tau_f$.

The stability of the coexistence state for increasingly late consumer emergence times, when $\tau_c > \tau_f$, is displayed in the left plot in Figure 4.8. When $\tau_c = \frac{7}{12}$, the overcompensation-cycles boundary exists outside of the parameter ranges. As the consumer emerges later, we observe the following: For biologically reasonable values of μ, all of the stability boundaries shift up; see the enlarged plot of the consumer–extinction boundary in Figure 4.8 (right). Additionally, the overcompensation-cycles boundary shifts right, implying that instabilities become increasingly likely to arise as consumer–resource cycles. The cycle period on the consumer–resource cycles boundary increases as the consumer emerges later (not shown).

We explain the previously observed behaviours as follows: Shorter active season lengths decrease the amount of time that the consumer can consume the resource. As a result, larger values of α are required to maintain the strength of the numerical response. Thus, larger values of α are required for the consumer to avoid extinction or for instabilities to arise as the consumer emerges later. Furthermore, the probability that the consumer dies in one year decreases as the consumer emerges later, since $\mu > \gamma_c$. Hence, larger values of μ are also required to maintain the strength of the numerical response. This explains why overcompensation cycles arise for increasing μ as the consumer emerges later.

We combine the results from Figures 4.5 and 4.8 (both left) into one plot. We varied $\tau_c \in [0, \frac{9}{12}]$ and selected four values of μ. The result is a two-parameter bifurcation diagram in terms of α and the difference in emergence times $(\tau_c - \tau_f)$; see Figure 4.9. There are four red and four blue curves (one for each value of μ). There are only two black curves, which correspond to the two largest values of μ selected, since overcompensation cycles do not exist for smaller values of μ; see Figures 4.5 and 4.8 (both left). An advantage of displaying the results in this way is that it is easier to visualize how phenological asynchrony affects the stability of the coexistence state. When $\tau_c = \tau_f$, we have phenological synchrony, otherwise we have asynchrony. Figure 4.9 demonstrates that the system stabilizes and the risk of consumer extinction increases as the asynchrony $(\tau_c - \tau_f)$ increases in either direction. The mechanism behind this result is that higher asynchrony decreases the number of consumer–resource interactions.

In this chapter, we studied the effects of phenological shifts on bifurcations and the long-term dynamics. We first considered the case where phenological synchrony is maintained, but the active season length varies. After that, we analyzed the case where phenological shifts

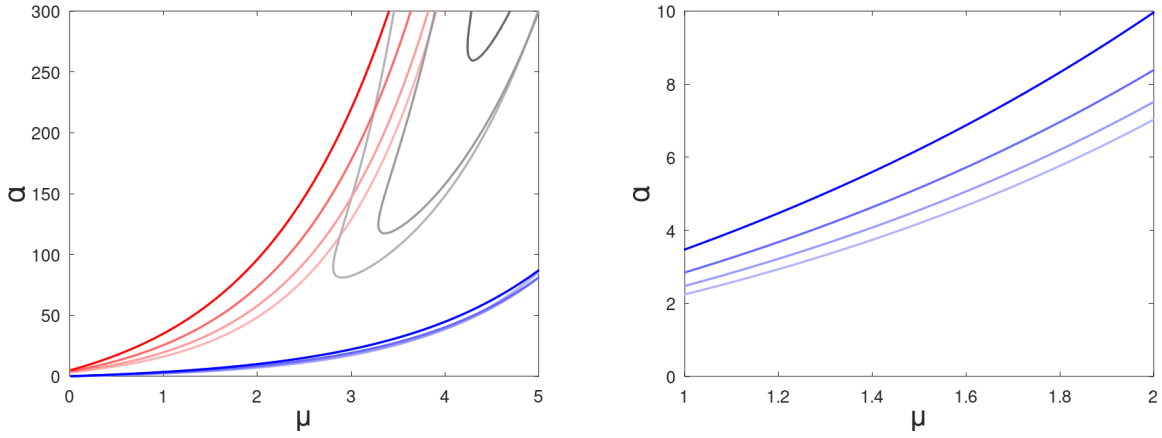

Figure 4.8: Bifurcation diagram for varying late consumer emergence times. For descriptions of the red, blue and black curves, see Figure 4.1. The consumer–extinction boundary is enlarged on the right. The parameters are $\tau_c = \frac{4}{12}, \frac{5}{12}, \frac{6}{12}, \frac{7}{12}$, $\tau_f = \frac{3}{12}$, $\hat{\tau} = \frac{10}{12}$, $\gamma_f = \frac{\mu}{2} = \gamma_c$ and $\rho = 20$. Darker colours indicate increasing values of τ_c.

increase phenological asynchrony. Initially, we did not let the active season length vary as the asynchrony increased. Finally, we demonstrated that we can use one bifurcation diagram to display the effects of asynchrony in both directions on the stability of the coexistence state. We will use this type of diagram again when we consider the effects of asynchrony on the asymptotic consumer density in Chapter 5.

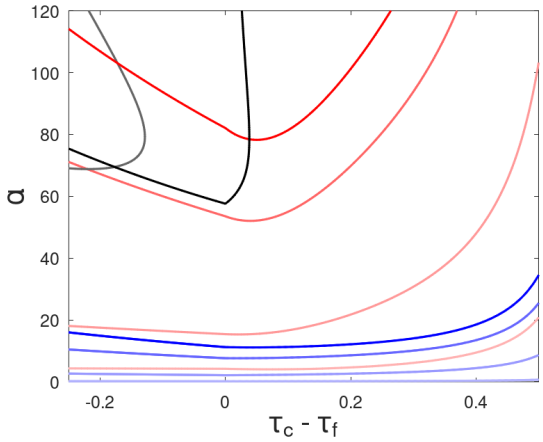

Figure 4.9: Bifurcation diagram in terms of the difference in emergence times. For descriptions of the red, blue and black curves, see Figure 4.1. The parameters are $\mu = 0.1, 1, 2.1, 2.5$, $\tau_f = \frac{3}{12}$, $\hat{\tau} = \frac{10}{12}$, $\gamma_f = \frac{\mu}{2} = \gamma_c$ and $\rho = 20$. Darker colours indicate increasing values of μ.

Chapter 5

Maximizing Consumer Density

In this chapter, we ask the question: what consumer and resource emergence times maximize the asymptotic (long-term) consumer density? We interpret our results within the context of phenological synchrony/asynchrony. We consider the phenologically explicit consumer–resource model by Revilla et al. [39] in terms of the match–mismatch hypothesis. We begin with the necessary background information.

5.1 Phenology and the Match–Mismatch Hypothesis

A species' phenology is the timing of its most significant life-cycle events. For interacting species, their relative phenology plays a critical role in each population's growth and persistence. As an example, orange-tip butterflies (*Anthocharis cardamines*) select their host plant based on the plant's phenological stage [43]. When phenological events of interacting species coincide, there is phenological synchrony; otherwise, there is phenological asynchrony. It is well documented that the phenologies of species living in temperate climates are affected by temperature [12, 36]. Since climate change is expected to cause phenological shifts, it risks disturbing the phenological synchrony between interacting species and hence has the potential to disrupt evolved foodwebs [17, 21].

The match–mismatch hypothesis (MMH) provides insight into how consumer–resource relationships may be affected by climate change. The MMH was initially proposed as a way to understand the effect of the timing of fish larvae (consumer) production, relative to peak plankton (resource) production [8]. According to the MMH, consumer growth is optimized if there is phenological synchrony between the timing of peak consumer energetic demand and peak resource availability. The apparent simplicity of the MMH is deceiving, as it contains many assumptions that make testing the MMH difficult [22, 23].

We summarize the explicit and implicit assumptions of the MMH, which Kharouba and Wolkovich [23] discussed in detail. The first explicit assumption is that consumer growth must be mainly influenced by the resource. It is also explicitly assumed that there is a limited time period where the consumer and resource interactions result in optimal consumer growth. To know when there is match (phenological synchrony) or mismatch (phenological

asynchrony) between the consumer and its resource, it is implicitly assumed that we know what the most energetically demanding consumer life-cycle event is, as well as when it occurs. Additionally, it is implicitly assumed that we choose a measure for the consumer growth that accurately reflects the consumer's ability to reproduce and survive. As examples, we can use density, body mass, number of recruits, offspring survival per year, etc. Lastly, so that the first explicit assumption is satisfied, it is implicitly assumed that the consumer is a resource specialist.

Several researchers have tested at least some aspect of the MMH. As an example, one empirical study observed that the factors that enable the recruitment success of blue mussel (*Mytilus edulis*) are in agreement with the MMH [44]. In particular, it was observed that phenological synchrony between the timing of blue mussel recruitment and peak high-quality resource abundance increased blue mussel recruitment success. Theoretical research related to the MMH has advanced over time. For example, Nakazawa and Doi [31] created minimal three-species community models to extend the MMH to community contexts. As pointed out by Revilla et al. [39], the models by Nakazawa and Doi are most suitable for species with multiple overlapping generations within a year. Their work inspired Revilla et al. to create a two-species model, as well as three-species community models, to test the MMH for more common types of species, which are those who require time to mature before contributing to any ecological interactions. Since they test the MMH in a very elaborate way, we will describe Revilla et al.'s two-species model, as well as their results in detail, so that we can later compare our results with theirs.

5.2 The Revilla Model

Assuming that the most energetically demanding consumer life-cycle event is reproduction, the MMH suggests that consumer growth is optimized when there is synchrony between the timing of consumer reproduction and peak resource availability [8]. Furthermore, it suggests that consumer growth decreases as phenological asynchrony increases. Revilla et al. [39] created a phenologically explicit consumer–resource model to test this aspect of the MMH.

5.2.1 Model Description

Revilla et al. [39] modelled a consumer and resource that each require time to mature into adults before they can interact with one another. This scenario is common in nature where offspring are produced as eggs or seeds. Like Pachepsky et al. [35], they created a semi-discrete model with continuous within-year dynamics and discrete between-year dynamics.

Revilla et al. assumed that both the consumer adults and resource adults decay exponentially within each year. They assumed that consumer adults can only consume resource adults. This consumption occurs at a linear rate, and any resource consumed is continuously converted into new consumer offspring. The rate at which the resource adults continuously reproduce is limited by intraspecific competition. Although offspring are inactive during the

year, they decay exponentially. Between years, any remaining adults from the previous year die and all remaining offspring mature.

Each year is 365 days long, and t denotes the time within a year. The system of ODEs that model the within-year dynamics are

$$\begin{aligned} \frac{\mathrm{d}F}{\mathrm{d}t} &= p_f(t)j_f - m_f F - aFC, & \frac{\mathrm{d}C}{\mathrm{d}t} &= p_c(t)j_c - m_c C, \\ \frac{\mathrm{d}J_f}{\mathrm{d}t} &= \frac{rF}{1+hF} - d_f J_f, & \frac{\mathrm{d}J_c}{\mathrm{d}t} &= qaFC - d_c J_c, \end{aligned} \tag{5.2.1}$$

where F and J_f are densities of the resource adults and resource offspring, respectively, and C and J_c are the densities of the consumer adults and consumer offspring, respectively. We define parameters for species i, where $i = f$ stands for the resource and $i = c$ for the consumer. The matured individuals emerge as adults throughout the year according to distributions $p_i(t)$, which were assumed to be normal distributions with mean $\bar{T}_i$ and standard deviation σ_i. The density of matured individuals available at the beginning of the year is j_i. The adult death rate is m_i and the offspring death rate is d_i. The parameters r, h, a and q are the resource intrinsic growth rate, the resource intraspecific competition coefficient, the consumer consumption rate and the consumer conversion efficiency, respectively.

The number of adults emerging in the following year is equal to the number of offspring remaining at the end of the previous year. Using an additional subscript to indicate the year, from year n to year $n+1$, the between-year equations are

$$j_{f,n+1} = J_{f,n}(365), \qquad j_{c,n+1} = J_{c,n}(365). \tag{5.2.2}$$

At the beginning of each year, there are no active adults or offspring. Hence, the initial conditions (ICs) are

$$F(0) = 0, \qquad C(0) = 0, \qquad J_f(0) = 0, \qquad J_c(0) = 0. \tag{5.2.3}$$

We will refer to (5.2.1)–(5.2.3) as the Revilla model.

Although the authors selected parameter values arbitrarily, their choices were somewhat restricted. They selected values of adult death rates, m_f and m_c, that ensured that the average adult lifespan of both species was less than one month. To ensure that a substantial number of offspring survive until the end of the year, they assumed that offspring death rates were much smaller than adult death rates; i.e., $d_f \ll m_f$ and $d_c \ll m_c$. To simplify matters, the authors assumed that $m_f = m_c$ and $d_f = d_c$.

To study which emergence times maximize the asymptotic consumer density and to test the MMH, Revilla et al. fixed the mean emergence time of the resource and varied that of the consumer such that $\bar{T}_f = 180$ and $\bar{T}_c \in [80, 280]$. They say that there is phenological synchrony when $\bar{T}_c = \bar{T}_f$; otherwise, there is phenological asynchrony. The degree of asynchrony was measured as $\bar{T}_c - \bar{T}_f$. Using (5.2.2)–(5.2.3), Revilla et al. numerically integrated (5.2.1) for each value of $\bar{T}_c$ and recorded the asymptotic densities of the consumer and resource.

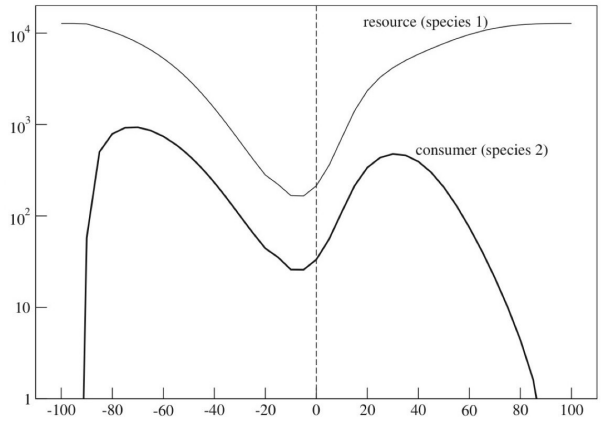

Figure 5.1: Asymptotic densities in terms of the amount of phenological asynchrony ($\bar{T}_c - \bar{T}_f$) for the Revilla model. This plot is taken directly from Revilla et al. [39].

5.2.2 Results

Revilla et al. [39] plotted the asymptotic densities in terms of the amount of phenological asynchrony; see Figure 5.1. The consumer density (thick black curve) displays a bimodal pattern that is maximized when there is intermediate asynchrony, either positive or negative. It achieves a global maximum when the asynchrony is negative ($\bar{T}_c < \bar{T}_f$). The consumer goes extinct when the asynchrony is too high (either positive or negative). The consumer density has a local minimum when the asynchrony is low; i.e., when it is close to synchrony. We generally expect a lower consumer density to result in a higher resource density, but this is not the case for the Revilla model when there is low asynchrony. The resource density (thin black curve) displays an "exploitation valley", where the density is minimized when there is low asynchrony (near synchrony) and maximized when there is high asynchrony.

The results above only partially agree with the MMH. Revilla et al. chose consumer density as the measure for consumer growth. Therefore, the MMH suggests that an increase in phenological synchrony should benefit the consumer by increasing consumer density. In the Revilla model, this is true when there is high asynchrony. However, when there is intermediate asynchrony, the consumer density decreases as the synchrony increases. Revilla et al. explain this discrepancy by overexploitation.

Overexploitation occurs when the consumer consumes the resource at a rate that prevents the resource from recovering fully. The risk of overexploitation is highest when there is phenological synchrony, since the interaction time between the two species is maximized. Low asynchrony thus results in low asymptotic densities for both species. Asynchrony reduces the risk of overexploitation. For example, if the consumer emerges ahead of the resource ($\bar{T}_c < \bar{T}_f$), then some consumers die before the resource emerges. If the consumer emerges after the resource ($\bar{T}_c > \bar{T}_f$), then the resource density increases, since the resource has time to reproduce independently of the consumer. If the asynchrony is too high, then the two species have little to no time to interact, leading to consumer extinction and resource abundance. Therefore, the largest asymptotic consumer densities are achieved when there

is intermediate asynchrony. Earlier emerging consumer species have more time to reproduce and consume the resource, so negative intermediate asynchrony is most beneficial to the consumer. Overall, Revilla et al. showed that the effect of asynchrony on consumer density is strongly influenced by overexploitation, which the MMH overlooks.

5.3 Phenological Asynchrony in Our Model

Following Revilla et al. [39], we analyze the effects of phenological asynchrony on the long-term dynamics in our nondimensional model (3.3.4)–(3.3.8). We focus on two aspects: (i) the stability of the coexistence equilibrium point, and (ii) the asymptotic consumer density for different consumer consumption rates (α). We compare results for consumer species that only differ in their winter mortality (γ_c). In Subsection 5.3.1, we select a higher value of γ_c; in Subsection 5.3.2, we select a lower value. We measure the amount of phenological asynchrony as the difference between the consumer and resource emergence times; i.e., $\tau_c - \tau_f$. When the emergence times are equal, we have phenological synchrony.

Unless stated otherwise, all simulations in this section were run with the following parameter values:

$$\rho = 20, \qquad \hat{\tau} = \frac{10}{12}, \qquad \tau_f = \frac{5}{12}, \qquad \tau_c \in \left[0, \frac{9}{12}\right], \qquad \mu = 1.55, \qquad \gamma_f = 0.775. \tag{5.3.1}$$

We use the above resource intrinsic growth rate (ρ) so that generally the resource can support the consumer and so that we observe interesting dynamics. Also, it is within the range that Pachepsky et al. [35] considered biologically reasonable. We use a later resource emergence time (τ_f) than we did in Sections 4.4 and 4.5, because a larger amount of asynchrony between the earliest emerging consumer and its resource leads to more interesting results. We use the above maximum consumer emergence time (τ_c) so that the minimum active season length, which is the time when both species are active, is one month ($\frac{1}{12}$). The active consumer death rate (μ) selected makes the similarities and differences between qualitative results clear and it is within the range that Pachepsky et al. [35] considered biologically reasonable. Winter resting periods (WRPs) have been shown to directly increase survival [10, 45]. Therefore, we assume that the value of μ is always greater than the dormant resource and consumer death rates (γ_f and γ_c). We verify that the qualitative results that we obtain in Subsections 5.3.1 and 5.3.2 are robust with respect to changes in μ.

5.3.1 Higher Consumer Winter Mortality

We consider a consumer that has relatively high winter mortality ($\gamma_c = \frac{\mu}{2}$) and use a bifurcation diagram, which we display in terms of the amount of phenological asynchrony and α, to see where the coexistence state is stable; see Figure 5.2. In the given parameter ranges, there is no overcompensation-cycles boundary. The coexistence equilibrium is stable between the red and blue curves.

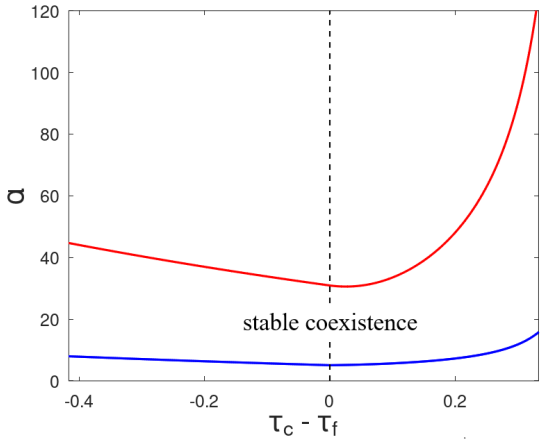

Figure 5.2: Bifurcation diagram in terms of the amount of phenological asynchrony. The blue (red) curve corresponds to the consumer-extinction boundary (consumer–resource cycles boundary). The parameters are $\gamma_c = 0.775$ and those listed in (5.3.1).

Both the consumer–resource cycles boundary and the consumer-extinction boundary achieve a global minimum when the asynchrony is low, and they are maximized when the asynchrony is high. The global maximum of both boundaries is achieved when the asynchrony is positive. The mechanism behind these observations is that increasing asynchrony decreases the number of consumer–resource interactions, which enhances stability but also increases the risk of consumer extinction. When $\tau_c < \tau_f$, the active season length is fixed at $\hat{\tau} - \tau_f$, but when $\tau_c > \tau_f$, it is of length $\hat{\tau} - \tau_c$. Positive asynchrony more effectively reduces the number of interactions, since the active season length decreases as τ_c increases.

Analogous to Figure 5.1, in Figures 5.3 and 5.4, we plot the asymptotic density of the resource (left) and consumer (right) in terms of the amount of asynchrony for different values of α. All equilibrium points shown in Figure 5.3 are locally asymptotically stable, since the selected values of α are within the stable coexistence region of Figure 5.2. This is not the case for Figure 5.4, which also displays unstable equilibrium points. To create Figure 5.4, we ran simulations using different values of $\tau_c - \tau_f$. Once transients had died out, we plotted the resource and consumer densities at the census time each year as red and blue points, respectively. For each value of $\tau_c - \tau_f$, we also plotted the average of the asymptotic densities (solid black curve) and the analytically obtained equilibrium values (solid cyan curve). If a value of $\tau_c - \tau_f$ results in a stable coexistence state, then the red/blue point, the black curve and the cyan curve are impossible to distinguish, since their values are all equal.

For values of α just above the consumer-extinction boundary, synchrony is optimal for the consumer; see the red curve in Figure 5.3. As the value of α increases, the consumer density increases and the optimal density occurs at increasing asynchrony, specifically when the consumer emerges later than the resource; see the orange curve. As the value of α continues to increase, the still-increasing consumer distribution becomes bimodal and the optimal density continues to occur at increasing asynchrony; see the yellow and green curves. For large values of α, the consumer density decreases again, optimal density arises for even

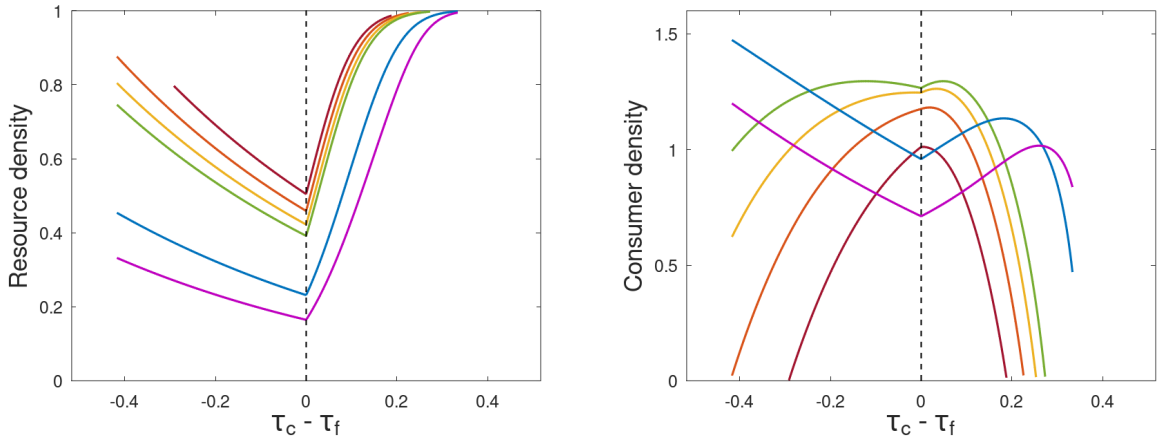

Figure 5.3: Asymptotic densities in terms of the amount of phenological asynchrony. The six curves correspond to $\alpha = 7, 8, 9, 10, 20, 30$. The order of the colours in the rainbow indicate increasing values of α (red is the minimum value and purple is the maximum). The other parameters are $\gamma_c = 0.775$ and those listed in (5.3.1).

larger asynchrony and the distribution remains bimodal; see the blue and purple curves. The resource shows the expected behaviour in Figure 5.3. More specifically, increasing consumption (α) decreases the resource density and the distributions display an exploitation valley, where perfect synchrony has the lowest resource density.

Once the value of α is large enough to cause instabilities, we observe consumer–resource cycles when there is low asynchrony; see Figure 5.4. As the value of α increases, higher degrees of asynchrony are required to maintain the stability of the coexistence state. However, the average densities continue to display the previously described behaviour. In particular, the average resource density distributions display an exploitation valley, whereas the average consumer density distributions achieve local maximums for increasing degrees of asynchrony as the value of α increases. In summary, the resource distributions are qualitatively equivalent for all α, but the qualitative behaviour of the consumer distributions change with α. Hence, the differences observed in the consumer distributions seem to arise from consumers interacting with one another, rather than with the resource.

The mechanism behind the observed behaviour is overexploitation. As explained in Subsection 5.2.2 and demonstrated by the exploitation valley in the resource distributions, the risk of overexploitation is highest when there is synchrony, and the risk decreases as the asynchrony increases. Additionally, the risk of overexploitation increases as consumption (α) increases. For low values of α, the risk is negligible, so the consumer distributions are unimodal and are maximized when the asynchrony is low. For larger values of α, overexploitation causes the consumer distributions to become bimodal and eventually decrease. The asymptotic consumer density is minimized when overexploitation occurs. As the value of α increases, higher asynchrony is required to avoid overexploitation. For the parameters we checked, the larger the value of α, the more likely that the asymptotic consumer density is globally maximized when the asynchrony is negative ($\tau_c < \tau_f$). This is because earlier

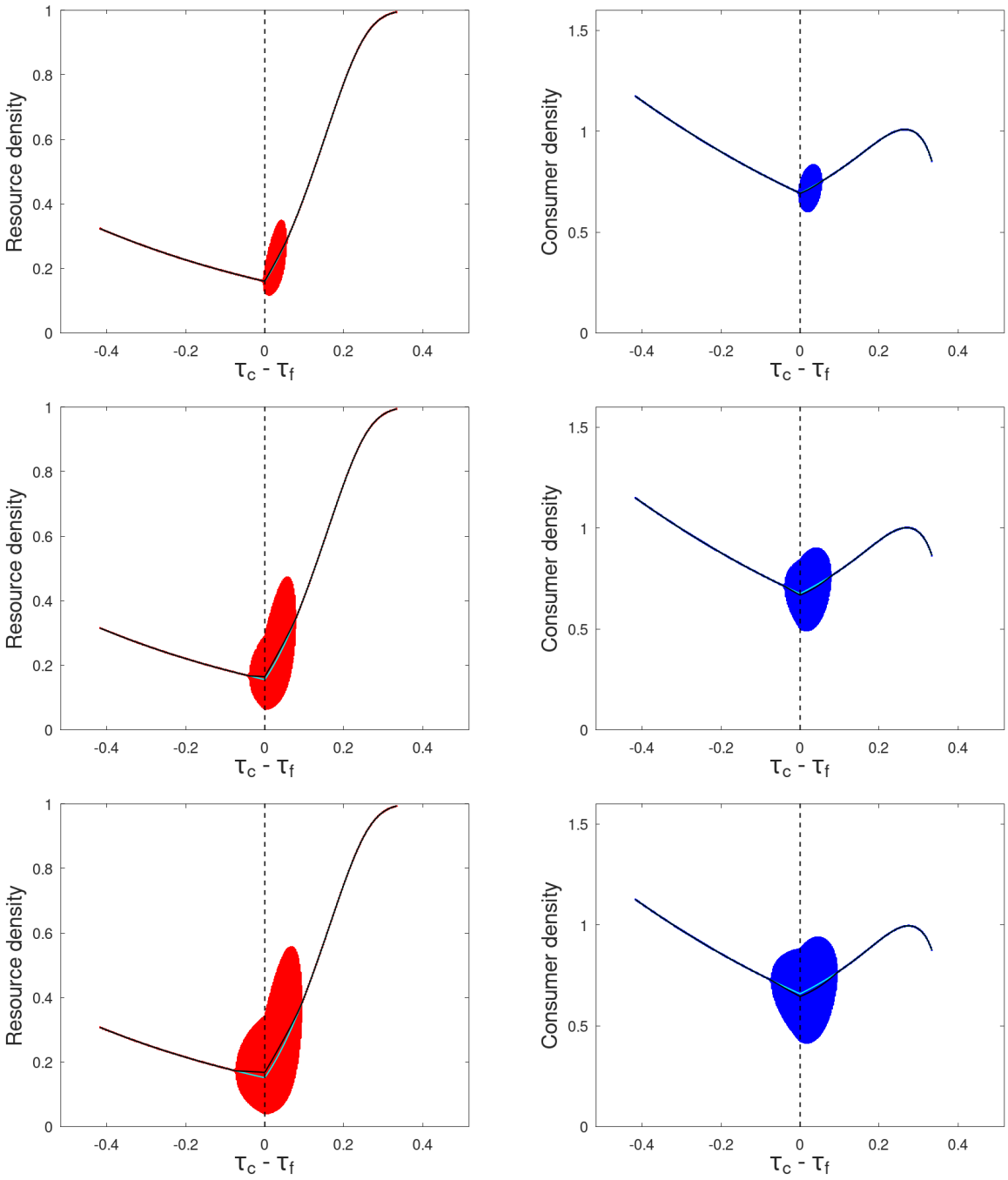

Figure 5.4: Asymptotic densities in terms of the amount of phenological asynchrony. The red (blue) points are the simulated long-term resource (consumer) density. The solid black curves correspond to the respective averages. The solid cyan curves correspond to the analytically obtained equilibrium densities. In the first, second, and third rows, $\alpha = 31, 32, 33$, respectively. The other parameters are $\gamma_c = 0.775$ and those listed in (5.3.1).

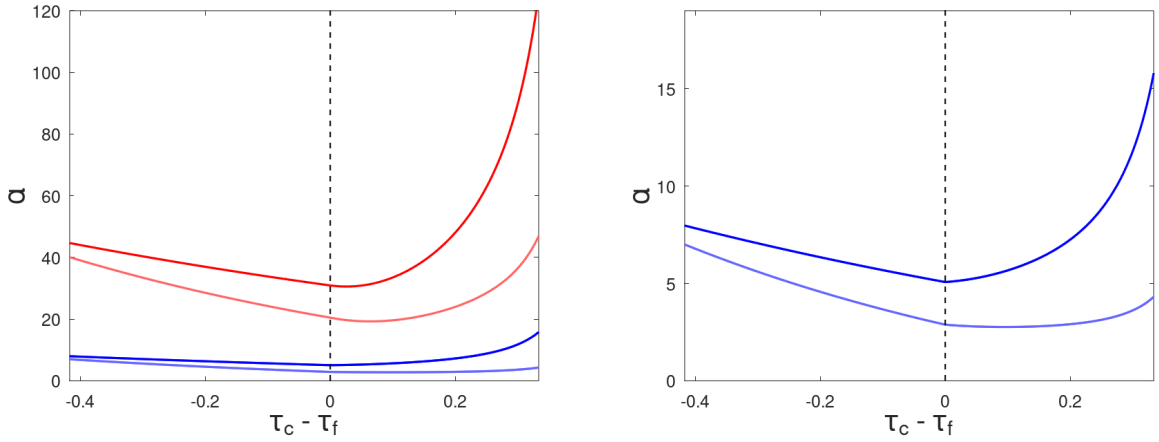

Figure 5.5: Bifurcation diagram in terms of the amount of phenological asynchrony. For descriptions of the red and blue curves, see Figure 5.2. The consumer-extinction boundaries from the left plot are enlarged on the right. The two sets of curves correspond to $\gamma_c = 0.19375, 0.775$. Darker colours indicate increasing values of γ_c. All other parameters are listed in (5.3.1).

consumer emergence increases the amount of resource per consumer, while maintaining the maximum active season length. When α is large, the remaining consumers reproduce in high quantities, making up for the consumer deaths that occurred before the resource emerged.

We checked our results for different values of μ that Pachepsky et al. [35] considered biologically reasonable, with γ_c remaining equal to $\frac{\mu}{2}$. We observe the same qualitative results for adjusted values of α. More specifically, when the consumer density is larger (smaller μ), each consumer must consume less resource (smaller α) to maintain the qualitative behaviour. Therefore, our results are robust with respect to changes in μ.

5.3.2 Lower Consumer Winter Mortality

We consider a consumer that has relatively low winter mortality ($\gamma_c = \frac{\mu}{8}$). The bifurcation diagram in Figure 5.5 displays the stability boundaries of the coexistence state for both lower and higher consumer winter mortality. The darker curves are the same as those in Figure 5.2. In the given parameter ranges, there is no overcompensation-cycles boundary for either value of γ_c.

Independent of consumer winter mortality, the stability boundaries are maximized for high phenological asynchrony and minimized for low asynchrony. We explained the mechanism behind this observation in Subsection 5.3.1. However, as the value of γ_c decreases, both stability boundaries decrease. The mechanism behind these observations is that decreasing the value of γ_c increases the consumer lifespan, resulting in more consumer–resource interactions. Hence, when there is lower consumer winter mortality, smaller values of α are required to destabilize the system and to avoid consumer extinction.

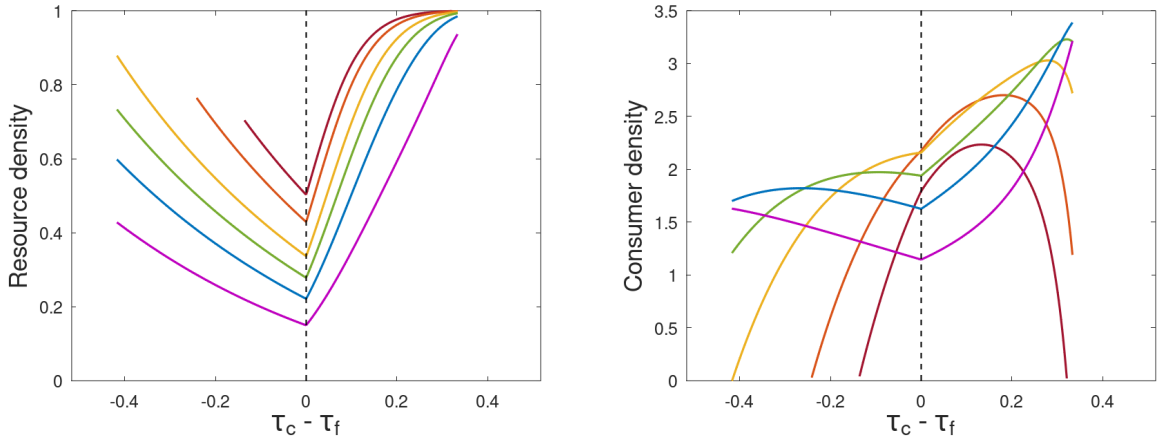

Figure 5.6: Asymptotic densities in terms of the amount of phenological asynchrony. The six curves correspond to $\alpha = 4, 5, 7, 9, 12, 19$. The order of the colours in the rainbow indicate increasing values of α (red is the minimum value and purple is the maximum). The other parameters are $\gamma_c = 0.19375$ and those listed in (5.3.1).

As we did in Subsection 5.3.1, we select increasing values of α that are above the consumer-extinction boundary and plot the asymptotic density of the resource (left) and consumer (right) in terms of the amount of asynchrony; see Figure 5.6. In Subsection 5.3.1, we demonstrated that for higher consumer winter mortality, the distributions of the average consumer and resource densities do not change qualitatively as the value of α crosses the consumer–resource cycles boundary; see Figure 5.4. The same is true for lower consumer winter mortality, so we chose to only select values of α that ensure that all equilibrium points shown in Figure 5.6 are locally asymptotically stable.

We observe the same qualitative results for the resource for lower (Figure 5.6) and higher (Figure 5.3) consumer winter mortality. The same is not entirely true for the consumer. As the value of α increases from the consumer-extinction boundary, the consumer distributions in both Figures 5.3 and 5.6 begin unimodal; they increase, transition into a bimodal distribution and then decrease again. Additionally, increasing the value of α results in the optimal consumer density occurring at increasing degrees of asynchrony. In other words, the local maximums of the consumer distributions in both Figures 5.3 and 5.6 that exist when there is positive (negative) asynchrony, shift further to the right (left) as the value of α increases. However, for lower consumer winter mortality, the consumer density is always globally maximized when there is positive asynchrony. As previously explained and illustrated by Figure 5.3, this is not always true when there is higher consumer winter mortality.

To explain the reasoning behind our observations, we provide an example that illustrates the effects of phenological asynchrony on the within-year dynamics for lower (top row) and higher (bottom row) consumer winter mortality; see Figure 5.7. For both values of γ_c, as the positive phenological asynchrony increases, the resource density at the end of the pink period increases towards its carrying capacity. This is because higher positive asynchrony increases the length of the consumer WRP, thereby increasing the time that the resource

has to grow independently. For the lower consumer winter mortality, as the positive asynchrony increases, the consumer density directly following the consumer birth pulse increases, whereas it decreases for the higher consumer winter mortality. The explanation behind this observation is that increasing the consumer WRP less severely affects the consumer when its winter mortality is lower. Therefore, the optimal consumer density occurs for higher positive asynchrony when the consumer winter mortality is lower. As we did in Subsection 5.3.1, we selected different biologically reasonable values of μ, with $\gamma_c = \frac{\mu}{8}$, and verified that our results are robust with respect to changes in μ.

5.4 Comparison of Results

The MMH suggests that phenological synchrony between consumer reproduction and peak resource availability is optimal for the consumer [8], but it overlooks the long-term consequences of overexploitation [39]. As demonstrated by the Revilla model and our model, the asymptotic resource density displays an exploitation valley, meaning that the greatest risk of overexploitation occurs when there is synchrony and that asynchrony decreases the risk. As a result, Revilla et al. [39] observed that the optimal asymptotic consumer density occurs when there is intermediate (specifically negative) asynchrony, which partially contradicts the MMH.

In contrast to Revilla et al., we show that the optimal amount of asynchrony depends on the selected parameter values. In particular, as the consumer consumption rate (α) increases, the risk of overexploitation increases, so the optimal amount of asynchrony increases as well. We show that synchrony is optimal when the consumer has higher winter mortality (γ_c) and the value of α is low. Whether or not this supports the MMH depends on how we define synchrony. If we consider resource availability as the length of time that the resource is available to the consumer, rather than the actual resource density, then our definition of synchrony, which is that the emergence times are equal, is the same as that of the MMH. As we increase the value of α, our results become consistent with those of Revilla et al.; i.e., that intermediate asynchrony is optimal. In our model, it is not always true that negative, rather than positive, intermediate asynchrony is best for the consumer. This is especially obvious when the consumer winter mortality is lower. In contrast to Revilla et al., we observe that high asynchrony can be optimal for the consumer, specifically for large values of α.

The differences between our results and Revilla et al.'s are attributed to our differing model formulations and selected parameter values. More specifically, as the amount of positive asynchrony increases, the resource density at the consumer emergence time increases in our model, but it decreases in the Revilla model. As a result, high positive asynchrony can be optimal for the consumer in our model, but it is not in the Revilla model. Additionally, the Revilla model uses parameter values that ensure that high negative asynchrony results in the consumer going extinct before the resource emerges and that synchrony results in overexploitation. In our model, we vary parameter values so that this is not always the case.

Overall, our results demonstrate that whether synchrony (as suggested by the MMH) or asynchrony (as suggested by Revilla et al.) is optimal for the consumer depends on the

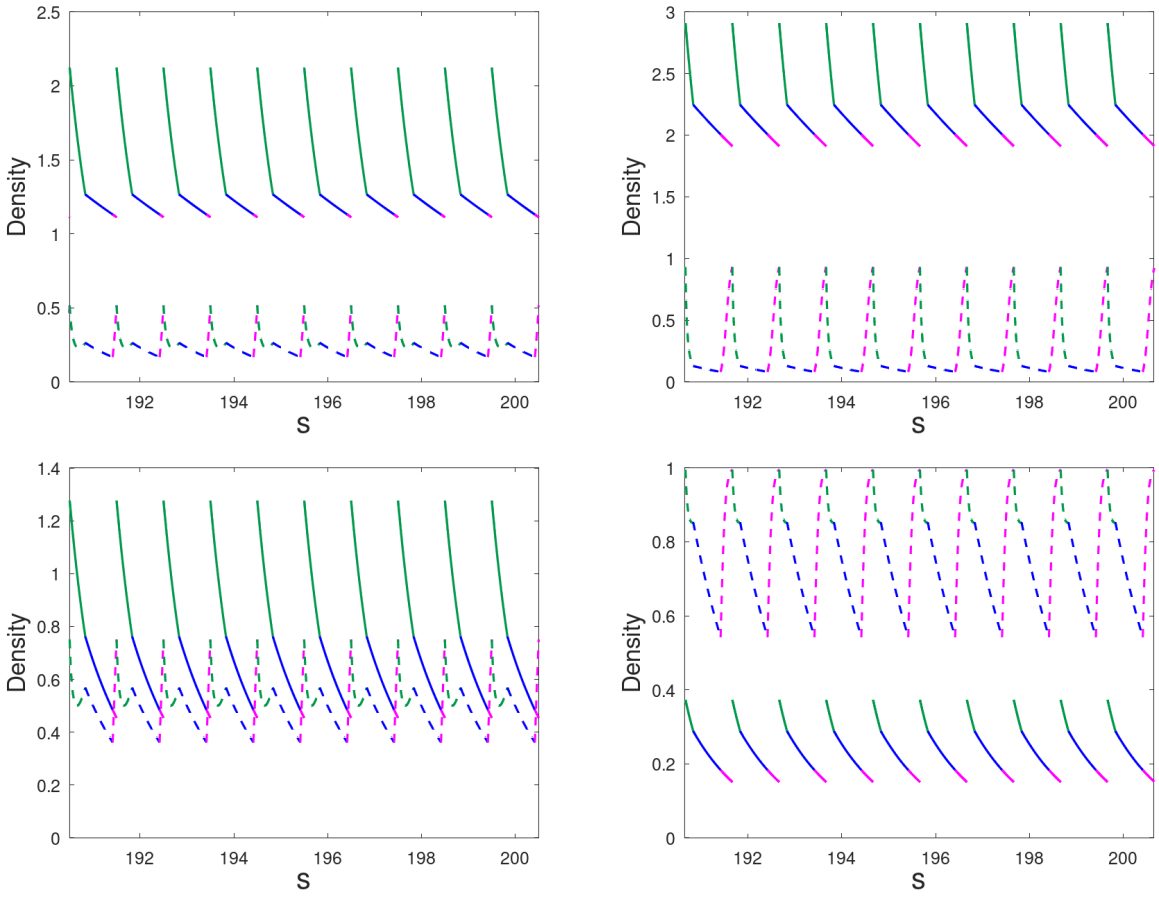

Figure 5.7: Example of a solution for different degrees of phenological asynchrony and consumer winter mortality. The green period indicates the time when both the consumer and resource are active. The blue period indicates when both are dormant. The pink period indicates when only the resource is active. The dashed (solid) line represents the resource (consumer) density. In the top row, $\gamma_c = 0.19375$ and in the bottom row, $\gamma_c = 0.775$. In the first column, $\tau_c = \frac{6}{12}$ and in the second column, $\tau_c = \frac{8}{12}$. The remaining parameters are $\alpha = 10$ and those listed in (5.3.1).

specific consumer species. Our results only align with the MMH when overexploitation is unlikely, which is understandable, given that the MMH does not consider overexploitation. As the risk of overexploitation increases, our results more closely align with the results of Revilla et al. Both of our results illustrate that the amount of asynchrony that is optimal for the consumer is highly dependent on the risk of overexploitation.

Chapter 6

Discussion

In this thesis, we created a novel "semi-discrete" consumer–resource model, which we used to study the dynamic consequences of phenological asynchrony. We were specifically interested in modelling a specialist consumer and its resource that both overwinter in a dormant state. We explicitly incorporated phenology into our model by including parameters for each species' emergence and immergence times. To be able to study the effects of phenological asynchrony, we allowed the active and dormant periods to differ between the two species. We measured phenological asynchrony as the difference between the consumer and resource emergence times. Thus, phenological synchrony corresponds to when they have equal emergence times. We considered a total of four possible yearly scenarios; see Figure 3.1.

Our impulsive ODE model was inspired by the model by Pachepsky et al. [35]. In our model, the consumer reproduces annually, at the end of their winter resting period (WRP), and the resource reproduces continuously while active. We transformed our model into a fully discrete model for each of the four yearly scenarios. We decided to focus our attention on the emergence times, so we simplified our model such that the two species have equal immergence times. As a result, we only had two possible yearly scenarios to consider: (i) the consumer emerges earliest or at the same time as the resource ($\tau_c \leq \tau_f$), or (ii) the resource emerges earliest ($\tau_c > \tau_f$). We calculated all possible equilibrium points of the resulting model and analyzed their stability. To study the effects of phenological shifts on the stability of the coexistence state, we created two-parameter bifurcation diagrams and observed any qualitative changes in the results. To analyze its effects on the asymptotic densities, we instead created orbit diagrams.

Our Main Findings

Our model is capable of displaying the same range of dynamical behaviour as the model by Pachepsky et al. [35]. There exist three types of equilibrium points: the extinction state, the resource-only state and the coexistence state. When the consumer and its resource coexist, we can observe stable coexistence, consumer–resource cycles, overcompensation cycles or

chaos. We chose not to explore chaotic behaviour in this thesis.

Our main focus was to study how phenological asynchrony affects the consumer–resource dynamics in our model. Before doing so, we imposed phenological synchrony, while shifting the shared immergence time, to better understand the effects of the active season length; i.e., the period when both species are active. We found that longer active season lengths decrease the stability of the coexistence state but increase on average the asymptotic consumer and resource densities; see Figures 4.1, 4.3 and 4.4.

To study phenological asynchrony, we began with investigating its effects on the stability of the coexistence state. We observed that higher negative asynchrony ($\tau_c < \tau_f$) increases stability; see Figure 4.5 (left). The effects of positive asynchrony ($\tau_c > \tau_f$) depend on the active season length. With a long fixed active season length, higher positive asynchrony reduces our model to essentially a single-species model for the consumer. As a result, the system only partially stabilizes, since consumer–resource cycles become less likely, but overcompensation cycles become more likely; see Figure 4.5 (right). When higher positive asynchrony decreases the active season length, we observed increases in stability; see Figure 4.8 (left). Unlike before, overcompensation cycles become less likely as positive asynchrony increases, since the consumer must consume and die quicker when the active season length is shorter. Throughout the rest of the thesis, we fixed τ_f and varied τ_c. In this case, higher asynchrony in either direction stabilizes the system; see Figure 4.9.

We then investigated the amount of asynchrony required to maximize the asymptotic consumer density for varying consumer consumption rates (α) and consumer winter mortality (γ_c). For increasing values of α, the consumer distribution transitions from a unimodal pattern that is maximized for low asynchrony to a bimodal pattern that is maximized for increasing asynchrony and minimized for low asynchrony; see Figures 5.3 and 5.6 (both right). Independent of the value of α, the resource distribution displays an "exploitation valley" pattern, where the asymptotic density decreases as the asynchrony decreases; see Figures 5.3 and 5.6 (both left). These results indicate that the qualitative changes in the consumer distributions occur as a result of consumer interactions with one another, rather than with the resource. In particular, the key mechanism that determines the optimal amount of asynchrony for the consumer is overexploitation. As the value of α increases, the risk of overexploitation increases, resulting in higher asynchrony being optimal for the consumer and lower asynchrony being suboptimal. For higher consumer winter mortality and large values of α, negative asynchrony is optimal for the consumer, as it reduces the risk of overexploitation while maintaining the maximum active season length; see Figure 5.3 (right). In contrast, the optimal amount of asynchrony for consumer species with lower winter mortality is always positive, as they are less severely affected by longer WRPs; see Figure 5.6 (right). Thus, they benefit from providing the resource with time to grow independently of the consumer.

We ended this thesis by comparing our results with the results by Revilla et al. [39], within the context of the match–mismatch hypothesis (MMH). The MMH proposes that phenological synchrony is optimal for the consumer [8], but it fails to consider the long-term consequences of overexploitation [39]. Due to the MMH overlooking overexploitation, our results only agree with it when the risk of overexploitation is negligible (low α). If the risk of

overexploitation exists but is not too high, then our results agree with Revilla et al.'s, which is that intermediate asynchrony is optimal for the consumer and synchrony is suboptimal.

Mathematical Achievements

Our main mathematical achievement is that we constructed a novel phenologically explicit consumer–resource model that can be used to study the effects of phenological asynchrony on the population dynamics. An advantage of our model is that it is explicitly solvable, which is not the case for many other phenologically explicit models that were also used to study phenological asynchrony [31, 39, 42]. More specifically, using our nondimensional model, we determined solution maps that relate the densities from consecutive years for each of the four possible yearly scenarios. In our analysis, we made the simplifying assumption that the consumer and its resource share an immergence time, but in theory, we could determine the equilibrium points and analyze their stability for all four yearly scenarios.

No matter which species emerges first, we determined an explicit expression for the resource-only state and a condition under which the resource density is positive. When the consumer emerges first or at the same time as the resource, we determined an explicit expression for the coexistence state (v_c, w_c). When the resource emerges first, an explicit expression for the coexistence state (v_f, w_f) does not exist. However, we were able to determine an expression for v_f in terms of w_f, which we used to numerically solve for the coexistence state. No matter which species emerges first, we determined an explicit expression for the transcritical bifurcation of the coexistence state and resource-only state. Using numerical methods to perform the Jury test, we generated two-parameter bifurcation diagrams for the coexistence state, which illustrate the transcritical, Naimark–Sacker (Hopf) and flip bifurcations. Following the analysis by Pachepsky et al. [35], we determined an explicit expression for the cycle period at the Naimark–Sacker bifurcation.

Since we have an explicit expression for w_c as a function of τ_c, we calculated the local and global extrema, the intervals of increase/decrease and the concavity of the asymptotic consumer density distributions in Figures 5.3 and 5.6 (both right) on the interval $\tau_c - \tau_f \in [-\tau_f, 0]$. Although we did not show these calculations in this thesis, we used the Extreme Value Theorem, as well as the first and second derivative tests. We chose not to show this analysis, as the techniques used are covered in introductory undergraduate calculus courses, and we only used our results to verify to ourselves that our code was working properly.

Ecological Insights

Our results demonstrate possible long-term dynamical consequences of phenological shifts for a specialist consumer and its resource. It is well documented that climate change has triggered phenological shifts in the past [10, 17], and it is expected to continue to do so in the future [21]. We now analyze our results within the context of climate change.

Longer summers and shorter winters are associated with climate change. Our results

suggest that if phenological synchrony is maintained but climate change extends the active season length (the "summer"), then we expect to observe cycles between consumer density "explosions" (due to consecutive years of favourable conditions; i.e., high resource availability) and consumer crashes (due to overexploitation of the resource). Consumer populations are at their most vulnerable directly before a crash, when the resource density is low, or after a crash, when the consumer density is low. Climate change is expected to increase environmental stochasticity, which can be detrimental to populations and can potentially lead to extinction, especially in already-vulnerable populations.

The St. Matthew Island reindeer (*Rangifer tarandus*) study [24] illustrates the concepts described above. In 1944, 29 reindeer were introduced to the island. Due to consecutive years of high food availability and low reindeer mortality, the reindeer population grew to about 6000 individuals by the summer of 1963. Researchers anticipated and observed a crash in the reindeer population due to overexploitation. However, environmental stochasticity was also partially responsible for the crash. The particularly cold and snowy winter of 1963–1964 decimated the already-vulnerable reindeer population to under 50 individuals.

When we analyzed the consequences of phenological asynchrony on the asymptotic consumer density, we observed differing optimal asynchrony depending on the consumer species considered. Hence, the consequences of climate change–induced phenological shifts are species dependent. We observed that the optimal asynchrony is highly influenced by the risk of overexploitation. For consumer species with low risk of overexploiting their resource, we expect consumer growth to be optimized if there is synchrony between its timing of reproduction and the timing of peak resource availability, as suggested by the MMH [8]. Thus, when climate change shifts the phenology of the resource, we expect the consumer to shift its phenology as well, in order to maintain synchrony. This behaviour has been observed in many bird species [7]. It is expected that climate change will make phenological asynchrony more prevalent [21]. In cases where synchrony is optimal but climate change results in phenological asynchrony, we expect the consumer to suffer. This situation was observed in nature for a Dutch population of the great tit (*Parus major*) [46].

Consumer species that are capable of overexploitation can suffer in the long term from synchrony, as illustrated by the previous reindeer example. If climate change increases asynchrony as expected, the risk of overexploitation decreases, thus generally benefiting these consumer species. In our model, the active season length remains maximized when there is negative asynchrony ($\tau_c < \tau_f$), whereas it shortens when there is positive asynchrony ($\tau_c > \tau_f$). There exists evidence that consumer species can benefit from emerging earlier, since it increases their active season length. For example, earlier consumer emergence times, resulting in longer active season lengths, decreased the mortality of yellow-bellied marmot (*Marmota flaviventris*) for a population in the USA [34]. However, our results illustrate that positive asynchrony tends to be optimal for consumer species with lower winter mortality. If climate change causes high asynchrony in either direction, then there is risk of consumer extinction as a result of starvation. The risk of extinction is highest for consumer species with a low consumption rate.

Interestingly, our results demonstrate that consumer species with a high consumption rate can benefit from high asynchrony. In particular, we observed that emerging up to five

months ahead of the resource can be optimal for the consumer. The following example demonstrates why we question whether this result would occur in nature. The spruce budworm (*Choristoneura fumiferana*) is the most damaging defoliator within North American boreal forests [11]. They have been shown to benefit from negative asynchrony with the balsam fir (*Abies balsamea*), but even they risk extinction if they emerge more than two weeks ahead of the balsam fir [37]. Furthermore, we observed that emerging up to four months after the resource can be optimal for the consumer. It is not uncommon to observe species in nature with long WRPs. For example, dormant bears can survive up to seven months without eating or drinking [16], and spruce budworms have a WRP of 8–9 months [37]. However, even if resources remain available, consumers that emerge too long after their resource have also been shown to be at risk of extinction [37]. These potentially unrealistic results arise due to our model formulation; see "Limitations" below.

Limitations

Models represent reality, but reality is so complex that this representation is never perfect. Due to the simplifying assumptions that models make, they have limitations. Our model assumes that all individuals within a population emerge at the same time. To reflect the heterogeneity of individuals within a population, we could have used time-dependent emergence distributions instead [3, 31, 39]. The same assumption applies to the immergence time; however, we have not seen time-dependent immergence distributions used in phenologically explicit models in the literature. If we let individuals emerge according to a normal distribution like Revilla et al. [39], then our model would not have been explicitly solvable. As a result, our mathematical analysis would have been limited, forcing us to rely more heavily on simulations.

Similar to the above assumption, our model also assumes that the consumer birth pulse is instantaneous. As explained in Subsection 2.3.2 for the Pachepsky model, by making this assumption, our model does not consider the heterogeneity of consumer individuals with respect to the time at which they reproduce annually. Instead, we essentially use an average or median birth pulse date for the consumer population. Our model is thus suitable for modelling consumer populations with individuals that reproduce within a short amount of time from one another. However, our model is not suitable for modelling consumer populations with high variability with regards to the timing of annual reproduction.

When constructing our model, we assumed that an active consumer does not have access to a dormant (not growing) resource. More specifically, we assumed that

$$\frac{\mathrm{d}B}{\mathrm{d}t} = 0, \tag{6.0.1}$$

in the orange period in Figure 3.1. Hence, our model is suitable for resources like small mammals that are protected from predators when they hibernate or for deciduous trees that do not have leaves in the winter. However, our model does not consider the case where a dormant resource remains available to the active consumer. For example, coniferous trees retain their old needles in the winter, even though they do not grow new needles until the

spring. Similarly, old grass remains available to active grazers in the winter. To reflect this case, we can adapt our model such that

$$\frac{\mathrm{d}B}{\mathrm{d}t} = aF, \tag{6.0.2}$$

in the orange period.

When formulating our model, we did not include a term for consumer starvation. We made this choice, as the starvation term would have depended on the resource density, resulting in our model no longer being explicitly solvable. If we had included consumer starvation explicitly into our model, then the consumer would be at risk of extinction if the negative asynchrony is too high.

Another simplifying assumption that we made is that the resource quality is fixed. In reality, the resource tends to become of poorer quality as time goes on. If we had included resource quality into our model, then the consumer would be at risk of extinction if the positive asynchrony is too high.

Lastly, when we studied the consequences of phenological shifts, we ran simulations using different emergence and immergence times, but we assumed that the selected values were fixed from year to year. Without this assumption, we would not have been able to calculate the equilibrium points, as none would have existed. We expect species' phenologies to change with climate change [21], so year-to-year variation is expected. We want to modify our model in the future to account for this variation; see "Future Directions" below.

Future Directions

Our model provides a way to study the consequences of phenological asynchrony on consumer–resource dynamics, but the phenology studied is the same each year. The phenologies of species living in temperate climates are affected by temperature [12, 36]. Temperatures are expected to continue to increase with climate change [18], so we expect to observe year-to-year variation in species' phenologies as a result. In the future, we want to include climate change more explicitly into our model by considering temperature variability. To do so, we plan to combine our population-dynamics model with the temperature-dependent model by Portalier et al. [37]. Their model is constructed so that throughout a species' WRP, they accumulate some quantity (i.e., heat) according to an accumulation rate function $\big(R(\cdot)\big)$ that depends on temperature $\big(x(\cdot)\big)$. Once the accumulated quantity reaches a specified threshold $(\bar{F})$, the species emerges from its WRP. If its immergence time $(\hat{\tau})$ is known, then Portalier et al.'s model can be used to solve for its emergence time (τ). Their model is

$$\int_{\hat{\tau}}^{\tau} R\big(x(s)\big)\,\mathrm{d}s = \bar{F}, \tag{6.0.3}$$

where s is the time. We will use a simple sinusoidal function for $x(\cdot)$, which we will fit to real temperature time series, as well as predicted temperature time series under different warming scenarios. Using (6.0.3), we will solve for the consumer and resource emergence times each

year, which we will then use in our model, and analyze the resulting consumer–resource dynamics.

In a separate future project, we want to consider the effects of evolution when analyzing the consumer emergence time. In Figures 5.3 and 5.6 (both right), we demonstrated that the asymptotic consumer density can be maximized by high asynchrony. We want to see if the consumer will evolve to have such high asynchrony with its resource. One way to study this question is to use adaptive dynamics [5, 9]. This approach has been used to study phenology before. For example, Johansson and Jonzén [19] used adaptive dynamics to study how arrival dates of migratory birds will evolve with climate change. We will introduce a mutant consumer that only differs from the resident consumer in its emergence time. The mutant first appears at a low density. We will update our nondimensional model (3.3.4)–(3.3.8) to include the mutant consumer. Each period of the year will now have five equations: $\frac{\mathrm{d}f}{\mathrm{d}s}$, $\frac{\mathrm{d}c}{\mathrm{d}s}$, $\frac{\mathrm{d}b}{\mathrm{d}s}$, $\frac{\mathrm{d}\bar{c}}{\mathrm{d}s}$, $\frac{\mathrm{d}\bar{b}}{\mathrm{d}s}$, where the latter two equations are for the mutant consumer. We will linearize the system and see whether the mutant can invade. If it can, then it becomes the new resident. We will repeat this process until we find the evolutionarily stable consumer emergence time.

Overall, this thesis has advanced our collective understanding of the consequences of phenological asynchrony on consumer–resource dynamics, and it has opened new doors for future discoveries within the context of climate change and evolution.

Bibliography

[1] P. A. Abrams. Predator–prey models. In A. Hastings and L. J. Gross, editors, *Encyclopedia of Theoretical Ecology*. University of California Press, 2012.

[2] R. J. H. Beverton and S. J. Holt. *On the dynamics of exploited fish populations*, volume 19. Fishery Investigations, Series II, 1957.

[3] S. Bewick, R. S. Cantrell, C. Cosner, and W. F Fagan. How resource phenology affects consumer population dynamics. *The American Naturalist*, 187(2):151–166, 2016.

[4] M. B. Bonsall and C. Dooley. Population ecology. In A. Hastings and L. J. Gross, editors, *Encyclopedia of Theoretical Ecology*. University of California Press, 2012.

[5] Å. Brännström, J. Johansson, and N. von Festenberg. The hitchhiker's guide to adaptive dynamics. *Games*, 4(3):304–328, 2013.

[6] C. A. Cobbold, J. Roland, and M. A. Lewis. The impact of parasitoid emergence time on host–parasitoid population dynamics. *Theoretical Population Biology*, 75:201–215, 2009.

[7] H. Q. P. Crick, C. Dudley, D. E. Glue, and D. L. Thomson. UK birds are laying eggs earlier. *Nature*, 388:526, 1997.

[8] D. H. Cushing. Plankton production and year-class strength in fish populations: an update of the match/mismatch hypothesis. In J.H.S. Blaxter and A.J. Southward, editors, *Advances in Marine Biology*, volume 26, pages 249–293. Academic Press, 1990.

[9] O. Diekmann. A beginner's guide to adaptive dynamics. *Banach Center Publications*, 63:47–86, 2004.

[10] R. Findlay-Robinson, V. B. Deecke, A. Weatherall, and D. L. Hill. Effects of climate change on life-history traits in hibernating mammals. *Mammal Review*, 53(2):84–98, 2023.

[11] R. A. Fleming. Climate change and insect disturbance regimes in Canada's boreal forests. *World Resource Review*, 12(3):521–548, 2000.

[12] J. Forrest and A. J. Miller-Rushing. Toward a synthetic understanding of the role of phenology in ecology and evolution. *Philosophical Transactions of the Royal Society B: Biological Sciences*, 365:3101–3112, 2010.

[13] F. Geiser. Hibernation. *Current Biology*, 23(5):R188–R193, 2013.

[14] Y. Geng and F. Lutscher. Competitive coexistence of seasonal breeders. *Journal of Mathematical Biology*, 83(38):1–35, 2021.

[15] Y. Geng, X. Wang, and F. Lutscher. Coexistence of competing consumers on a single resource in a hybrid model. *Discrete & Continuous Dynamical Systems - Series B*, 26(1):269–297, 2021.

[16] E. C. Hellgren. Physiology of hibernation in bears. *Ursus*, 10:467–477, 1998.

[17] A. M. Iler, P. J. CaraDonna, J. R. K. Forrest, and E. Post. Demographic consequences of phenological shifts in response to climate change. *Annual Review of Ecology, Evolution, and Systematics*, 52:221–245, 2021.

[18] IPCC. *Climate Change 2022: Impacts, Adaptation and Vulnerability. Contribution of Working Group II to the Sixth Assessment Report of the Intergovernmental Panel on Climate Change*. Cambridge University Press, Cambridge, UK and New York, NY, USA, 2022.

[19] J. Johansson and N. Jonzén. Game theory sheds new light on ecological responses to current climate change when phenology is historically mismatched. *Ecology Letters*, 15(8):881–888, 2012.

[20] E. I. Jury. On the roots of a real polynomial inside the unit circle and a stability criterion for linear discrete systems. *IFAC Proceedings Volumes*, 1(2):142–153, 1963.

[21] H. M. Kharouba, J. Ehrlén, A. Gelman, K. Bolmgren, J. M. Allen, S. E. Travers, and E. M. Wolkovich. Global shifts in the phenological synchrony of species interactions over recent decades. *Proceedings of the National Academy of Sciences*, 115(20):5211–5216, 2018.

[22] H. M. Kharouba and E. M. Wolkovich. Disconnects between ecological theory and data in phenological mismatch research. *Nature Climate Change*, 10:406–415, 2020.

[23] H. M. Kharouba and E. M. Wolkovich. Lack of evidence for the match-mismatch hypothesis across terrestrial trophic interactions. *Ecology Letters*, 26(6):955–964, 2023.

[24] D. R. Klein. The introduction, increase, and crash of reindeer on St. Matthew Island. *The Journal of Wildlife Management*, 32(2):350–367, 1968.

[25] M. Kot. *Elements of Mathematical Ecology*. Cambridge University Press, 2001.

[26] J. E. Lane, L. E. B. Kruuk, A. Charmantier, J. O. Murie, and F. S. Dobson. Delayed phenology and reduced fitness associated with climate change in a wild hibernator. *Nature*, 489:554–557, 2012.

[27] A. J. Lotka. Analytical note on certain rhythmic relations in organic systems. *Proceedings of the National Academy of Sciences of the United States of America*, 6(7):410–415, 1920.

[28] F. Lutscher and S. V. Petrovskii. The importance of census times in discrete-time growth-dispersal models. *Journal of Biological Dynamics*, 2(1):55–63, 2008.

[29] R. M. May. Biological populations with nonoverlapping generations: stable points, stable cycles, and chaos. *Science*, 186(4164):645–647, 1974.

[30] K. McCann and G. Gellner. Food chains and food web modules. In A. Hastings and L. J. Gross, editors, *Encyclopedia of Theoretical Ecology*. University of California Press, 2012.

[31] T. Nakazawa and H. Doi. A perspective on match/mismatch of phenology in community contexts. *Oikos*, 121(4):489–495, 2012.

[32] A. J. Nicholson. The balance of animal populations. *Journal of Animal Ecology*, 2(1):132–178, 1933.

[33] A. J. Nicholson and V. A. Bailey. The balance of animal populations. Part I. *Proceedings of the Zoological Society of London*, 105(3):551–598, 1935.

[34] A. Ozgul, D. Z. Childs, M. K. Oli, K. B. Armitage, D. T. Blumstein, L. E. Olson, S. Tuljapurkar, and T. Coulson. Coupled dynamics of body mass and population growth in response to environmental change. *Nature*, 466:482–485, 2010.

[35] E. Pachepsky, R. M. Nisbet, and W. W. Murdoch. Between discrete and continuous: consumer–resource dynamics with synchronized reproduction. *Ecology*, 89(1):280–288, 2008.

[36] S. Pau, E. M. Wolkovich, B. I. Cook, T. J. Davies, N. J. B. Kraft, K. Bolmgren, J. L. Betancourt, and E. E. Cleland. Predicting phenology by integrating ecology, evolution and climate science. *Global Change Biology*, 17(12):3633–3643, 2011.

[37] S. M. J. Portalier, J. N. Candau, and F. Lutscher. A temperature-driven model of phenological mismatch provides insights into the potential impacts of climate change on consumer–resource interactions. *Ecography*, 2022(8):e06259, 2022.

[38] S. L. Rasmussen, T. B. Berg, T. Dabelsteen, and O. R. Jones. The ecology of suburban juvenile European hedgehogs (*Erinaceus europaeus*) in Denmark. *Ecology and Evolution*, 9(23):13174–13187, 2019.

[39] T. A. Revilla, F. Encinas-Viso, and M. Loreau. (A bit) Earlier or later is always better: Phenological shifts in consumer–resource interactions. *Theoretical Ecology*, 7:149–162, 2014.

[40] W. E. Ricker. Stock and recruitment. *Journal of the Fisheries Research Board of Canada*, 11(5):559–623, 1954.

[41] M. L. Rosenzweig and R. H. MacArthur. Graphical representation and stability conditions of predator–prey interactions. *The American Naturalist*, 97(895):209–223, 1963.

[42] E. G. Simmonds, E. F. Cole, B. C. Sheldon, and T. Coulson. Phenological asynchrony: a ticking time-bomb for seemingly stable populations? *Ecology Letters*, 23(12):1766–1775, 2020.

[43] S. Stålhandske, M. Olofsson, K. Gotthard, J. Ehrlén, C. Wiklund, and O. Leimar. Phenological matching rather than genetic variation in host preference underlies geographical variation in host plants used by orange tip butterflies. *Biological Journal of the Linnean Society*, 119(4):1060–1067, 2016.

[44] N. Toupoint, L. Gilmore-Solomon, F. Bourque, B. Myrand, F. Pernet, F. Olivier, and R. Tremblay. Match/mismatch between the *Mytilus edulis* larval supply and seston quality: effect on recruitment. *Ecology*, 93(8):1922–1934, 2012.

[45] C. Turbill, C. Bieber, and T. Ruf. Hibernation is associated with increased survival and the evolution of slow life histories among mammals. *Proceedings of the Royal Society B: Biological Sciences*, 278(1723):3355–3363, 2011.

[46] M. E. Visser, A. J. van Noordwijk, J. M. Tinbergen, and C. M. Lessells. Warmer springs lead to mistimed reproduction in great tits (*Parus major*). *Proceedings of the Royal Society of London. Series B: Biological Sciences*, 265(1408):1867–1870, 1998.

[47] V. Volterra. Variations and fluctuations of the number of individuals in animal species living together. *Journal du Conseil*, 3(1):3–51, 1928.